QUANTITATIVE DETERMINATION OF CHEMICAL PROCESSES BY DYNAMIC NUCLEAR POLARIZATION ENHANCED NUCLEAR MAGNETIC RESONANCE SPECTROSCOPY

A Dissertation

by

HAIFENG ZENG

Submitted to the Office of Graduate Studies of
Texas A&M University
in partial fulfillment of the requirements for the degree of

DOCTOR OF PHILOSOPHY

May 2012

Major Subject: Chemistry

QUANTITATIVE DETERMINATION OF CHEMICAL PROCESSES BY DYNAMIC NUCLEAR POLARIZATION ENHANCED NUCLEAR MAGNETIC RESONANCE SPECTROSCOPY

QUANTITATIVE DETERMINATION OF CHEMICAL PROCESSES BY DYNAMIC NUCLEAR POLARIZATION ENHANCED NUCLEAR MAGNETIC RESONANCE SPECTROSCOPY

A Dissertation

by

HAIFENG ZENG

Submitted to the Office of Graduate Studies of
Texas A&M University
in partial fulfillment of the requirements for the degree of

DOCTOR OF PHILOSOPHY

Approved by:

Chair of Committee,	Christian Hilty
Committee Members,	Paul A. Lindahl
	Robert R. Lucchese
	Jim(Xiuquan) Ji
Head of Department,	David H. Russell

May 2012

Major Subject: Chemistry

ABSTRACT

Quantitative Determination of Chemical Processes by Dynamic Nuclear Polarization Enhanced Nuclear Magnetic Resonance Spectroscopy. (May 2012)

Haifeng Zeng, B.S, Peking University, China P.R.

Chair of Advisory Committee: Dr. Christian Hilty

Dissolution dynamic nuclear polarization (DNP) provides several orders of magnitude of NMR signal enhancement by converting the much larger electron spin polarization to nuclear spin polarization. Polarization occurs at low temperature (1.4K) and is followed by quickly dissolving the sample for room temperature NMR detection. DNP is generally applicable to almost any small molecules and can polarize various nuclei including ^{1}H, ^{19}F and ^{13}C. The large signal from DNP enhancement reduces the limit of detection to micromolar or sub-micromolar concentration in a single scan. Since DNP enhancement often provides the only source for the observable signal, it enables tracking of the polarization flow. Therefore, DNP is ideal for studying chemical processes. Here, quantitative tools are developed to separate kinetics and spin relaxation, as well as to obtain structural information from these measurements. Techniques needed for analyzing DNP polarized sample are different from those used in conventional NMR because a large, yet non-renewable hyperpolarization is available. Using small flip angle pulse excitation, the hyperpolarization can still be divided into multiple scans. Based on this principle, a scheme is presented that allows reconstruction of indirect spectral

dimensions similarly to conventional 2D NMR. Additionally, small flip angle pulses can be used to obtain a succession of scans separated in time. A model describing the combined effects of the evolution of a chemical process and of spin-lattice relaxation is shown. Applied to a Diels-Alder reaction, it permitted measuring kinetics along with the effects of auto- and cross-relaxation. DNP polarization of small molecules also shows significant promise for studying protein-ligand interaction. The binding of fluorinated ligands to the protease trypsin was studied through the observation of various NMR parameter changes, such as line width, signal intensity and chemical shift of the ligands. Intermolecular polarization transfer from hyperpolarized ligand to protein can further provide information about the binding pocket of the protein. As an alternative to direct observation of protein signal, a model is presented to describe a two-step intermolecular polarization transfer between competitively binding ligands mediated through the common binding pocket of the protein. The solutions of this model relate the evolution of signal intensities to the intermolecular cross relaxation rates, which depend on individual distances in the binding epitope. In summary, DNP provides incomparable sensitivity, speed and selectivity to NMR. Quantitative models such as those discussed here enable taking full advantage of these benefits for the study of chemical processes.

DEDICATION

To my parents

ACKNOWLEDGEMENTS

First I would like to show my highest regards and gratitude to my research advisor Dr. Christian Hilty. Thanks for his smart guidance during my Ph.D. study. Thanks for his patience lead me the way to scientific research. His discussion and advice helps me to solve the questions in research.

I sincerely thank my fellow group members, Soyoun Hwang, Giridhar Sekar, Mukundan Ragavan, Hsueh-ying Chen. Especially thank Youngbok Lee for the collaboration.

I would like to thank my committee members, Dr. Paul A. Lindahl, Dr. Robert R. Lucchese, Dr. Jim(Xiuquan) Ji. Also I would like to thank Dr. Yi-Qin Gao for his help.

Many thanks for the collaborator in some of the projects. Thank Dr. Donghan Lee and Dr. Christian Griesinger for providing the sample useful discussion about the polarization transfer between competitive binding ligands. Thank Dr. Alvar Gossert for providing some sample for the fluorinated ligand binding experiment and useful discussion.

Finally, I would like to thank my family for their support.

NOMENCLATURE

1D	One Dimensional
2D	Two Dimensional
3D	Three Dimensional
BDPA	α,γ-bisdiphenylene-β-phenylallyl
CIDNP	Chemically Induced Dynamic Nuclear Polarization
CPD	Composite Pulse Decoupling
CW	Continuous Wave
DMSO	Dimethyl sulfoxide
DNP	Dynamic Nuclear Polarization
DPBD	1,4-dipheneylbutadiene
DQ	Double-Quantum
ESR	Electron Spin Resonance
FID	Free Induction Decay
HMQC	Heteronuclear Multiple-Quantum Correlation
HPLC	High-Performance Liquid Chromatography
HSQC	Heteronuclear Single Quantum Correlation
INPHARMA	Interligand Polarization Transfer for Pharmacophore Mapping
MRI	Magnetic Resonance Imaging
MRS	Magnetic Resonance Spectroscopy
MW	Microwave

NMR	Nuclear Magnetic Resonance
NOE	Nuclear Overhauser Effect
pCBA	p-chlorobenzaldehyde
ppm	Parts per million
PTD	4-phenyl-1,2,4-triazole-3,5-dione
RF	Radio Frequency
RMSD	Root Mean Square Deviation
S.I.	Selective Inversion
SPINOE	Spin Polarization–Induced Nuclear Overhauser Effect
STD	Saturation Transfer Difference
TEMPO	(2,2,6,6-Tetramethylpiperidin-1-yl)oxyl
TEMPOL	4-Hydroxy-2,2,6,6-tetramethylpiperidine-1-oxyl
TFA	Sodium trifluoroacetate
TFBC	4-(Trifluoromethyl)benzene-1-carboximidamide hydrochloride
TPPI	Time Proportional Phase Incrementation
UV-VIS	Ultraviolet-Visible
ZQ	Zero-Quantum

TABLE OF CONTENTS

CHAPTER Page

LIST OF FIGURES

FIGURE Page

FIGURE Page

FIGURE Page

LIST OF TABLES

CHAPTER I

INTRODUCTION

Liquid state nuclear magnetic resonance (NMR) spectroscopy is a powerful technique for studying molecular structure, dynamics and interactions. NMR acts on the nuclear spin, which is sensitive to the chemical environment, yet changes in spin state are unlikely to perturb molecular properties. The narrow line width in liquid state NMR spectra, often in the sub-Hertz range, permits the resolution of most chemical sites in a small molecule through their individual chemical shift. By spreading signals along more than one frequency axis, multidimensional NMR further reduces overlap, enabling the study of complex molecules with thousands of nuclei.[1] Apart from chemical shift, various interactions between nuclear spins or their environment give rise to measurable NMR parameters that contain molecular information. Scalar coupling, an indirect interaction between two nuclear spins mediated by electrons, can be used to transfer coherence between spins. It yields information on chemical bond connectivity and dihedral angle. Dipole-dipole coupling, a direct interaction between two spins, gives rise to the nuclear Overhauser effect (NOE),[2-3] which depends on the distance between the two spins as $NOE_{ij} \propto 1/r_{ij}^6$. Distances obtained from NOE measurement and dihedral angles from scalar couplings provide geometrical constrains that can be used to reconstruct the three-dimensional molecular structure.[4] Other constrains such as paramagnetic relaxation enhancement[5] and residual dipolar coupling[6] can further be used to refine NMR structures. Interactions between nuclear spins are the source of various

---

This dissertation follows the style of *Analytical Chemistry*.

spin relaxation mechanisms. In addition to structural information available through NMR, measurements of spin relaxation are often used to probe the local and global dynamics of a molecule.[7]

These different types of information available from liquid state NMR spectroscopy have prompted its application in various fields. NMR is routinely used to characterize the structure of small molecules in organic synthesis and to analyze natural products.[8-13] It also provides for the structure determination of biological macromolecules with atomic resolution.[4, 14] In the liquid state, close to physiological sample conditions can be chosen. Therefore, NMR spectroscopy can further be used to study interactions between biological molecules,[15-17] for example for drug discovery.[18-21]

Sensitivity of NMR

The sensitivity is the most limiting factor of many NMR experiments.[22] Relative to optical spectroscopy, a comparably large amount of sample or a long averaging time is required to distinguish the NMR signal from noise. A typical concentration of 1 mM is required to obtain a proton spectrum in a single scan with the 400 MHz spectrometer used in present dissertation. Protons are the most sensitive NMR active nuclei that are commonly encountered. Carbon, on the other hand, is the central element in organic chemistry, making ^{13}C NMR a widely used technique. ^{13}C NMR spectra are particularly well amenable to interpretation because of the large chemical shift range of this nucleus. However, its low gyromagnetic ratio (0.25, relative to ^{1}H) and low natural abundance (1.1%) reduces the signal intensity.

Techniques for increasing the NMR sensitivity allow the application of NMR in cases where high sample concentrations are not achievable, either due to low solubility or low availability of the sample. Orthogonally to these applications, sensitivity enhancement techniques can increase the time resolution of NMR, by reducing or removing the need for signal averaging.

One of the reasons for the low sensitivity of NMR is the weak interaction of the nuclear spin with an externally applied magnetic field. This interaction, termed the Zeeman effect, results in a splitting of energy levels for different spin states. The transitions between these energy levels form the basis for NMR spectroscopy. In the present dissertation, the discussion is limited to spin-1/2 nuclei, which have two energy eigenstates denoted as α and β. The populations of the two corresponding energy levels are given by the Boltzmann distribution. The two spin states give rise to opposite magnetization, and the net magnetization determines the NMR signal intensities. The fraction of population excess of the lower energy state, called polarization, is defined as following,

$$P = \frac{n_\alpha - n_\beta}{n_\alpha + n_\beta} = \frac{1 - e^{-\Delta E/kT}}{1 + e^{-\Delta E/kT}} = \tanh\left(\frac{\Delta E}{2kT}\right) = \tanh\left(\frac{\hbar\gamma B_0}{2kT}\right) \qquad \text{(I-1)}$$

in which $\hbar = h/2\pi$ is the reduced Planck constant, γ is the gyromagnetic ratio, B_0 is the strength of externally applied magnetic field, k is the Boltzmann constant, and T is the temperature. The gyromagnetic ratios of some commonly used nuclei are listed in Table I-1. For comparison, the gyromagnetic ratio of a free electron is also listed.

Table I-1: Gyromagnetic ratios of common spins**.**

Species	free electron	^{1}H	^{2}D	^{13}C	^{15}N	^{19}F	^{31}P	^{129}Xe
$\gamma / 2\pi$ (MHz/T)	2.8025×10^{4}	42.576	6.53593	10.705	-4.3156	40.0593	17.235	-11.777

From Equation (I-1), it can be seen that at room temperature, the polarization is approximately proportional to the magnetic field strength and gyromagnetic ratio. Efforts are continuously made to increase the static magnetic fields of modern NMR spectrometers. For a 400 MHz spectrometer, the thermal polarization of ^{1}H is only 3×10^{-5} at room temperature. Up to now, the highest field commercialized NMR spectrometer, installed in 2009, has a magnetic field strength of 23.5 T.[23] The corresponding ^{1}H resonance frequency of this spectrometer is 1000 MHz, and the ^{1}H polarization at room temperature is 8×10^{-5}. Due to technical challenges in the construction of superconducting magnets, the cost of an NMR instrument increases non-linearly with the magnetic field. Therefore, it is of significant interest to explore other, complementary strategies for increasing nuclear spin polarization in NMR experiments.

Hyperpolarization

Hyperpolarization affords signal enhancement in NMR spectra by generating a highly polarized, non-equilibrium nuclear spin state through polarization transfer from a more ordered quantum system. In the following, common hyperpolarization approaches are discussed.

Chemically Induced Dynamic Nuclear Polarization (CIDNP)

Chemically induced dynamic nuclear polarization (CIDNP) refers to the hyperpolarized state produced during a thermal or photochemical reaction involving free radicals. These reactions proceed through radical pair intermediate states with correlated electron spins. Depending on the electron spin states, different products are formed. The singlet-radical pair tends to recombine, while the triplet one tends to diffuse apart. The fast exchange (life time of 10^{-8} to 10^{-3} s)[24] between the singlet- and the triplet-state of the radical pairs is affected by the nuclear spin state in a magnetic field. Different nuclear spin states are enriched in products that recombine vs. those that diffuse apart, resulting in a nuclear spin polarization enhancement.[25-27] In a typical photo-CIDNP experiment aimed at investigating a protein, the sample is doped with a small amount of dye, which is then photolyzed. The photon excited dye reacts with the side chains of certain amino acid residues, and selectively enhances their NMR signal. The selective enhancement distinguishes between surface residues and buried residues, providing information about protein structure.[28] The enhancements of different chemical sites in the same molecule are also dependent on their distances to the radical center, which yields information about the structure of the radical intermediate of the reaction.[29] CIDNP can further be used to study reaction mechanisms of electron transfers, hydrogen abstractions, photoinitiator fragmentations, isomerizations and cycloadditions.[26, 30-38] However, CIDNP is limited to enhance the NMR signal intensities of the products of chemical reactions involving free radicals.

Optical Pumping

Optical pumping transfers the polarization from photon to nuclear spin. It requires circularly polarized light, alkali metal vapor and a noble gas in a low magnetic field. The circularly polarized light excites an electron in an alkali metal atom from the ground state to the first excited state. In this process, one of the electron spin states of the alkali metal atom is enriched. Collisions between the alkali metal atoms with noble gas atoms transfers some of the electron spin polarization to the nuclear spins of the noble gas.[39] In the most common application, optical pumping of rubidium is used to hyperpolarize xenon gas.[40] Hyperpolarized ^{129}Xe has been used for biomedical applications, such as magnetic resonance imaging (MRI) of the lung *in vivo*,[41] and observation of xenon penetrating human red blood cells.[42] It has also been proposed for imaging of the distribution of receptor proteins with specially designed xenon biosensors.[43-45] Combined with spin polarization–induced nuclear Overhauser effect (SPINOE), other nuclei such as ^{1}H and ^{13}C can be selectively enhanced by hyperpolarized ^{129}Xe.[40, 46-47] This selective enhancement can be used to study the surface of porous materials,[48-50] lipid membranes,[51] and proteins.[52-53] This technique of optical pumping is specialized towards enhancing the NMR signal of noble gases.

Parahydrogen Induced Polarization

Parahydrogen induced polarization is based on a highly ordered spin configuration of the H_2 molecule. In parahydrogen, the two proton spins are in an anti-symmetric configuration. Expressed in terms of the basis states α and β, the spin state of

parahydrogen is the singlet state, $1/\sqrt{2}(\alpha_1\beta_2 - \beta_1\alpha_2)$. Due to the equivalence of the two protons, this state does not produce an NMR signal. Observation of the hyperpolarized NMR signal requires a hydrogen molecule in the para spin state to react with an unsaturated, asymmetric compound. In the reaction product, these two scalar coupled hydrogen atoms are in different chemical environments. The symmetry is broken, and the possible eigenstates of this two-spin system are $\alpha_1\alpha_2$, $\alpha_1\beta_2$, $\beta_1\alpha_2$ and $\beta_1\beta_2$. If the hydrogenation reaction is performed inside of a magnetic field, the spins are only populated in the $\alpha_1\beta_2$ and $\beta_1\alpha_2$ states in the products. The NMR signal is observed by the transition between these two populated spin states and their almost unpopulated counterparts. Comparing to the nearly equal populations at thermal equilibrium, a large enhancement is obtained.[54] For spin 1, the transition $\alpha_1\beta_2 \rightarrow \beta_1\beta_2$ is absorption; while the transition $\beta_1\alpha_2 \rightarrow \alpha_1\alpha_2$ is emission (spin 2 behaves in the same way). Therefore, antiphase doublets are expected.[55-56] In a variation of this experiment, the hydrogenation reaction is preformed outside of the magnet followed by transport of the product into the NMR magnet through an adiabatic process. Through this process, only one spin state, $\alpha_1\beta_2$ or $\beta_1\alpha_2$, is populated, resulting in a simpler in-phase spectrum.[54, 57] Apart from direct observation of the proton in the products originating from the reaction, when a hydrogen molecule and other ligands form a coordination complex compound with a common diamagnetic metal center, the polarization of the parahydrogen can be transferred to other ligands.[58] In this scheme, polarizable compounds are not limited to unsaturated chemicals.[59] Parahydrogen enhanced NMR is well suited to study the mechanisms of inorganic reactions.[60] In another application, parahydrogen induced polarization

combined with MRI was used to directly visualize hydrogenation products in the gas-phase, as an indicator of the density of catalyst activities.[61] The parahydrogen induced polarization can be converted into net hyperpolarization of a nearby ^{13}C.[62-63] Using [^{13}C]-2-hydroxyethylpropionate hyperpolarized by this technique, a pig chest angiography was acquired by ^{13}C MRI.[64]

Dynamic Nuclear Polarization (DNP)

Theory

DNP refers to the transfer of spin polarization from electrons to nuclei by means of electromagnetic wave irradiation.[65] Based on the electron's higher gyromagnetic ratio compared to that of protons ($\gamma_e/\gamma_{1H} = 658$), a maximum enhancement of a factor of more than 600 is potentially achievable. Different from most other hyperpolarization techniques, DNP is able to polarize almost any small molecule. A primary requirement is that the sample contains unpaired electron spins, which however do not need to be part of the molecule of interest. The main mechanisms for DNP enhancement are discussed in the following.

In free radical solution or in metals, the polarization of nuclear spin can be enhanced by microwave irradiation at electron spin resonance (ESR) frequency. This is the Overhauser effect, which was predicted[66] and experimentally demonstrated[2-3] in the early days of NMR in the 1950s. Overhauser DNP enhancement relies on the polarization transfer caused by cross relaxation between the electron spin and the nuclear spin. This relaxation requires time dependent dipolar or scalar interactions between the electron spins and the nuclear spins. In the liquid state, molecular tumbling provides the

time-dependence of the interactions, while in the solid state, the mobility of electrons in a metal is required. The efficiency of this polarization transfer by dipolar interaction is dependent on the spectral density of the zero- or double-quantum transition. The spectral density is a function of the correlation time for molecular tumbling (τ_c) and of the ESR frequency (ω_e):

$$J(\omega) = \frac{2\tau_C}{5(1+\omega^2\tau_C^2)}, \omega = \omega_e \pm \omega_n \approx \omega_e \quad \text{(I-2)}$$

The efficiency drops sharply when the ESR frequency increases as the magnetic field increases because, as can be seen from Equation (I-2), the spectral density is close to zero at a high electron Larmor frequency.[67-69] In other words, this process is more efficient in a low magnetic field.

On the other hand, the Overhauser DNP enhancement due to scalar couplings has a different magnetic field dependence and can lead to substantial NMR signal enhancements at high magnetic fields.[70]

In the solid state, in the absence of motions, the Overhauser effect is not active. The DNP effect still occurs due to the hyperfine interactions. Depending on the ESR line width and the nuclear Larmor frequency, three different cases can be distinguished. These include the solid effect, cross effect and thermal mixing.

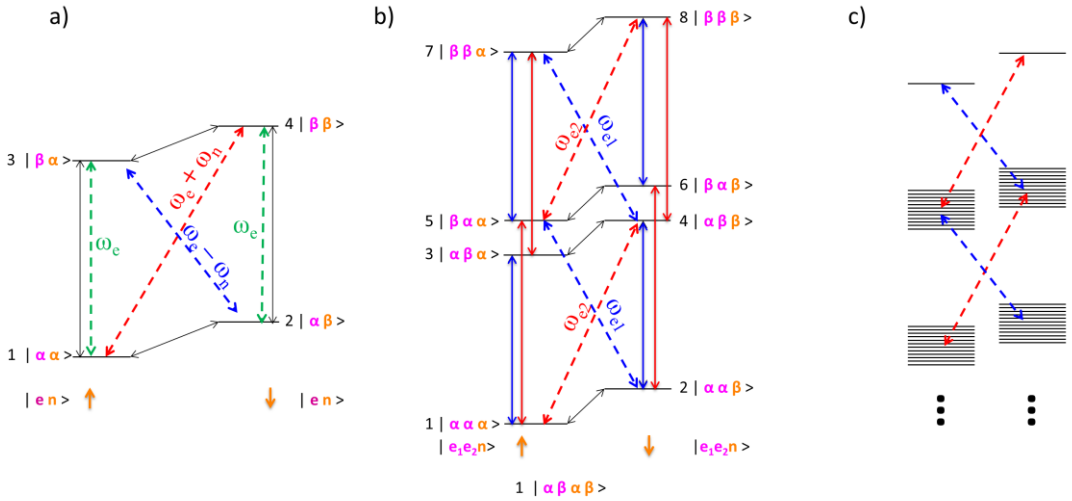

Figure I-1 : Energy diagrams of electron-nuclear spin systems for DNP mechanisms in the solid state, a): solid effect, one electron spin (e) and one nuclear spin (n); b): cross effect, two electron spins and one nuclear spin; c): thermal mixing, multiple electron spins and one nuclear spin. These energy states are grouped according to the two nuclear spin states, i.e. left and right sides of each panel. Possible microwave transitions that cause enhancements (red: negative; blue: positive) are indicated with dashed lines.[71-72]

The solid effect is a two-spin process. Figure I-1a shows the energy diagram of such an electron-nuclear spin system.[73] The left and right sides correspond to α and β nuclear spin states. Therefore, any transition that changes the relative population between the two sides will enhance the nuclear polarization. The hyperfine interaction between the electron spin and the nuclear spin mixes the states, enabling the forbidden double-quantum and zero-quantum transitions. As a result, irradiation at the frequency of $\omega_e + \omega_n$ leads to a transition between |1> and |4>. At thermal equilibrium, the population of |1> is larger than |4>, since they differ in electron spin states, which are corresponding to a large energy separation. Through the radio-frequency irradiation, population is transferred from |1> to |4>. Since the electron spin relaxation rate is much faster than the nuclear spin relaxation rate, the population in |4> relaxes to |2>. The net effect is a

pumping of the population from |1> to |2>, resulting in negative DNP enhancements. Similarly, irradiation at the frequency of $\omega_e - \omega_n$ leads to positive DNP enhancement. The effects of irradiation at the frequency of $\omega_e - \omega_n$ (zero-quantum transition) and $\omega_e + \omega_n$ (double-quantum transition) are opposite. Thus, in order to prevent (partial) cancellation, the two lines must be resolved. At high magnetic fields, ESR lines are inhomogeneously broadened due to the g-anisotropy. Therefore, many radicals such as (2,2,6,6-tetramethylpiperidin-1-yl)oxyl (TEMPO) derivatives do not satisfy this condition.[73]

The cross effect is a process that flip-flops two electron spins and one nuclear spin.[74-76] The resonance frequencies of the electron spins depend on their relative orientation to the static magnetic field due to g-anisotropy. The cross effect requires that the ESR frequencies of the two dipole-coupled electron spins differ by the nuclear Larmor frequency ($\omega_{e2} - \omega_{e1} = \omega_n$). The energy diagram for this process is shown in Figure I-1b. Possible transitions are indicated with red lines in Figure I-1b, in which dashed lines lead to effective DNP enhancement. Similar to the solid effect, population is transferred from |1> to |4> (and from |5> to |8>) through irradiation at the frequency of ω_{e2}. It is then transferred to |2> due to the fast electron spin relaxation, resulting in negative DNP enhancement compared to the thermal polarization. When the frequency is ω_{e1}, the process involving the complementary set of spin states yields a positive enhancement. Because of the condition $\omega_{e2} - \omega_{e1} = \omega_n$, the cross effect works when the inhomogeneously broadened ESR line width Δ is larger than the nuclear Larmor frequency ω_n.[73]

Thermal mixing, which also involves a three-spin process, can be treated as an extension of the cross effect.[77] In the case of multiple coupled electron spins, the strong dipole-dipole interactions among the electron spins leads to a homogeneously broadened ESR spectrum, as illustrated in Figure I-1c. Thermal mixing is described using three reservoirs, the electron Zeeman system, the electron dipolar system, and the nuclear Zeeman system, which are thermally coupled.[78] Off-resonance irradiation of the ESR transition produces an unequal polarization across the ESR line, cooling down the electron dipolar system. Through an energy conservation process similar to the cross effect, an electron spin pair and the nuclear spin are mutually flip-flopped if $|\omega_{e2} - \omega_{e1}| = \omega_n$. The nuclear spin ensemble is cooled, resulting in DNP enhancement.[73, 79]

The conditions for the three solid-state DNP mechanisms are listed in Table I-2.

Table I-2 : DNP mechanism and requirements of EPR line width. ω_n : Larmor frequency of nuclear spin; δ: EPR homogeneous line broadening; Δ: EPR inhomogeneous line broadening.

Mechanism	solid effect	cross effect	thermal mixing
Linewidth requirement	$\delta, \Delta < \omega_n$	$\delta < \omega_n < \Delta$	$\omega_n < \delta, \Delta$

Applications

DNP was used to enhance the solid state NMR signal of charcoal, diamonds and organic crystals in the 1980s.[77, 80-81] Combined with magic-angle spinning, using a magnetic field of 1.4T (40 GHz ESR and 60 MHz ^{1}H), polymers were studied.[82-84] Starting from the 1990s, Griffin's group pioneered the use of high-field DNP.[85] At high magnetic fields, microwave radiation is needed to transfer the polarization from electron

spins to nuclear spins. Gyrotrons, vacuum electronic devices based on the stimulated cyclotron radiation of electrons oscillating in a strong magnetic field, were used to generate microwaves of sufficiently high power. The gyrotrons developed in Griffin's group are capable of generating up to 460 GHz microwave at watt range power,[86-91] allowing direct DNP enhancement of the NMR signal of a 700 MHz (corresponding magnetic field: 16.4 T) spectrometer. Waveguides were designed to transmit the microwaves to the sample with less than 1-2 dB total losses.[92-94] Experiments in the solid state need to be carried out at low temperatures, and also require specialized NMR hardware. Low temperature NMR probes were developed for simultaneous application of microwave radiation, radio frequency pulses and magic angle spinning.

The free electron centers required by the DNP mechanism are provided by stable free organic radicals. The structures of some typical free radicals for DNP are shown in Figure I-2. For example, TEMPO, a nitroxide radical, is frequently used to polarize ^{1}H. The DNP efficiency depends on the properties of the radicals. For the cross effect to occur, it is necessary that the two dipolar coupled electron spins have the appropriate resonance frequency difference. For this purpose, biradicals consisting of two tethered TEMPO radicals[95-98] were developed. In some cases, mixtures of TEMPO and trityl radicals[99] also showed improved enhancements. Under optimum conditions, up to 290 fold enhancement of ^{1}H was obtained at 90 K in a magnetic field of 5 T.[96, 100]

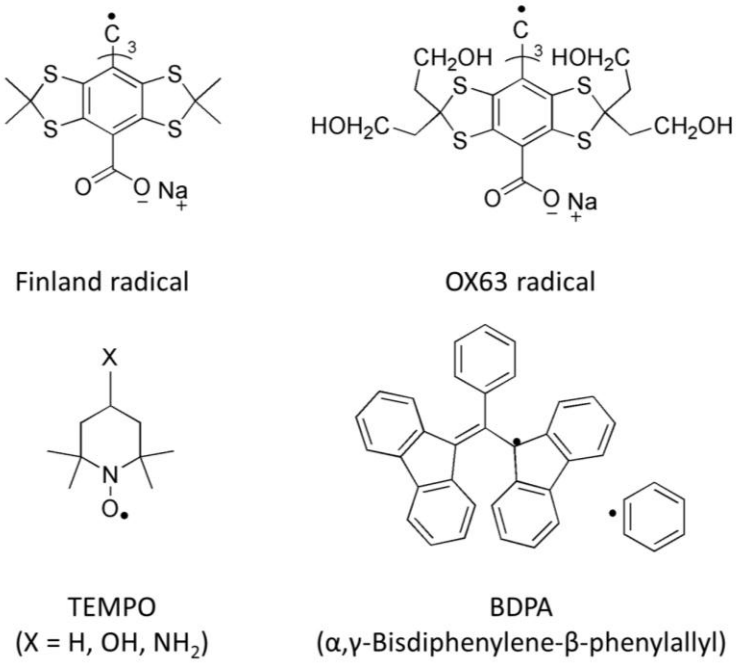

Figure I-2 : Structures of the free radical used for DNP polarization. Finland radical: tris[8-carboxy-2,2,6,6-tetramethylbenzo[1,2-d:4,5-d′]-bis(1,3)dithiol-4-yl]methyl sodium salt; OX63 radical: tris[8-carboxyl-2,2,6,6-tetra[2-(1-hydroxyethyl)]-benzo(1,2-d:4,5-d)bis(1,3)dithiole-4-yl]methyl sodium salt.

Using the signal enhancement from DNP, biological macromolecules such as membrane[101-102] and amyloid-forming peptides[103] were studied with solid state NMR. Hall et al. studied T4 lysozyme with ^{15}N polarization, using ^{15}N enrichment of alanine residues.[85] Improved stability of the DNP equipment further allowed for two dimensional solid state NMR experiments.[86, 104]

In the liquid state, the Overhauser effect is the only DNP mechanism that allows direct polarization. Overhauser DNP was used to enhance NMR signal intensities of various nuclei such as ^{1}H, ^{19}F, ^{31}P and ^{13}C in low magnetic fields (0.1–1T).[105-107] More recently, Overhauser DNP enhancement was used to probe local water mobility[108] and protein aggregation.[109] Water polarized through Overhauser DNP can further be used as

an imaging contrast agent.[110] For high field spectroscopy of various molecules, Reese and Krahn et al. polarized samples in a 0.35 T magnet, and then pneumatically shuttled them to a 600 MHz (14 T) spectrometer, resulting in up to 15 times NMR signal enhancement.[111-112] It is further possible to perform Overhauser DNP directly at high magnetic fields by using scalar coupling induced cross relaxation. Signal enhancement of more than 10-fold was achieved in liquid samples at room temperature and magnetic fields of 9.2 T (ν_{1H} = 400 MHz, ν_e = 260 GHz).[69, 92]

Another strategy to obtain high polarization in the liquid state is to first polarize the sample in the solid state at a low temperature, and then carry out a temperature jump to dissolve the sample. According to Equation (I-1), the polarization is higher at lower temperature due to the smaller Boltzmann factor. Compared to the thermal nuclear polarization at a higher temperature, these solid-to-liquid-state experiments benefit from additional enhancement besides gyromagnetic ratio contribution, due to the temperature effect. A temperature jump DNP experiment can be carried out using similar equipment as in the solid state DNP experiments.[113-114]

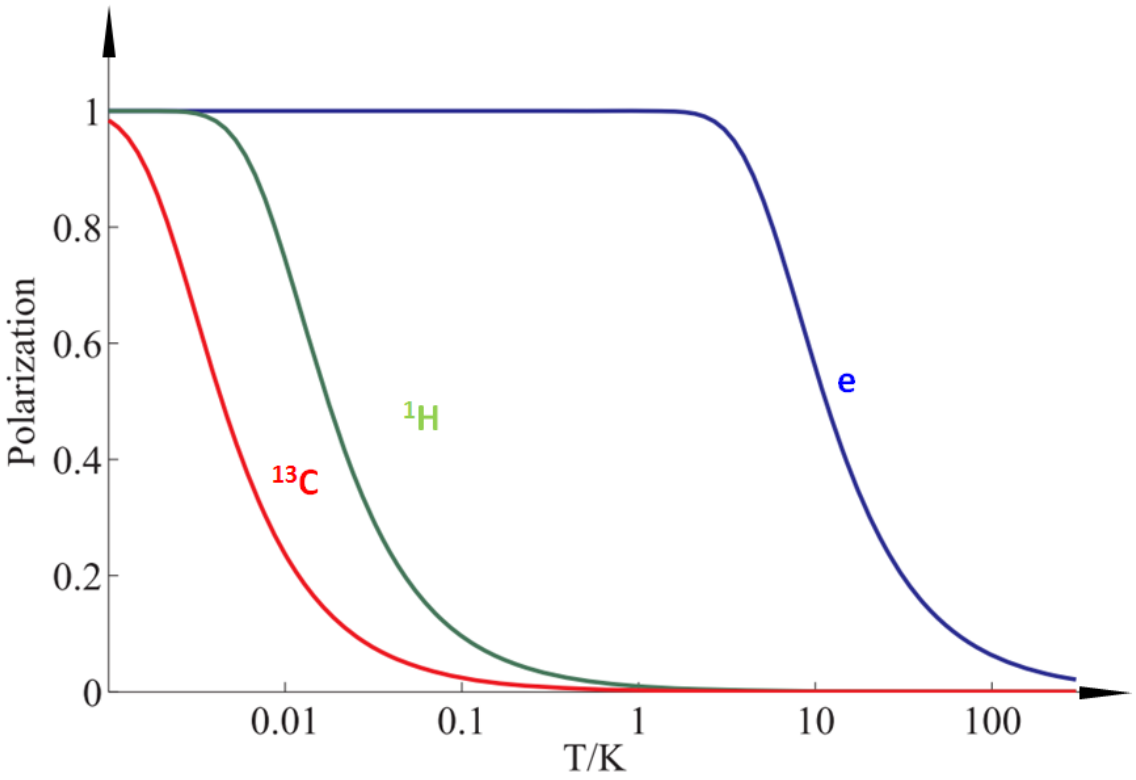

Figure I-3 : The polarization of free electron, ^{1}H and ^{13}C as a function of temperature in a 9.4 T magnet. The polarization is defined in Equation (I-1) and the values of gyromagnetic ratios are from Table I-1.

In Figure I-3, the absolute polarization of free electron, ^{1}H and ^{13}C as a function of temperature in a 9.4 T magnet is plotted. At liquid helium temperature, the polarization of electron spins is close to 100%. Highest liquid state enhancements have been obtained using DNP polarization at even lower than liquid helium temperature. Ardenkjaer-Larsen et al. carried out DNP polarization at 1.2 K, in a field of 3.35 T. Samples were subsequently heated to room temperature and injected to a high resolution spectrometer for NMR measurement. An enhancement of up to 44,000 compared to room temperature polarization was obtained.[115] At the low temperature, the spin relaxation is slow, and low power microwave radiation is sufficient to saturate the ESR transitions. Inexpensive

semiconductor based microwave sources with ~100 mW power can be used for DNP polarization under this condition.[116]

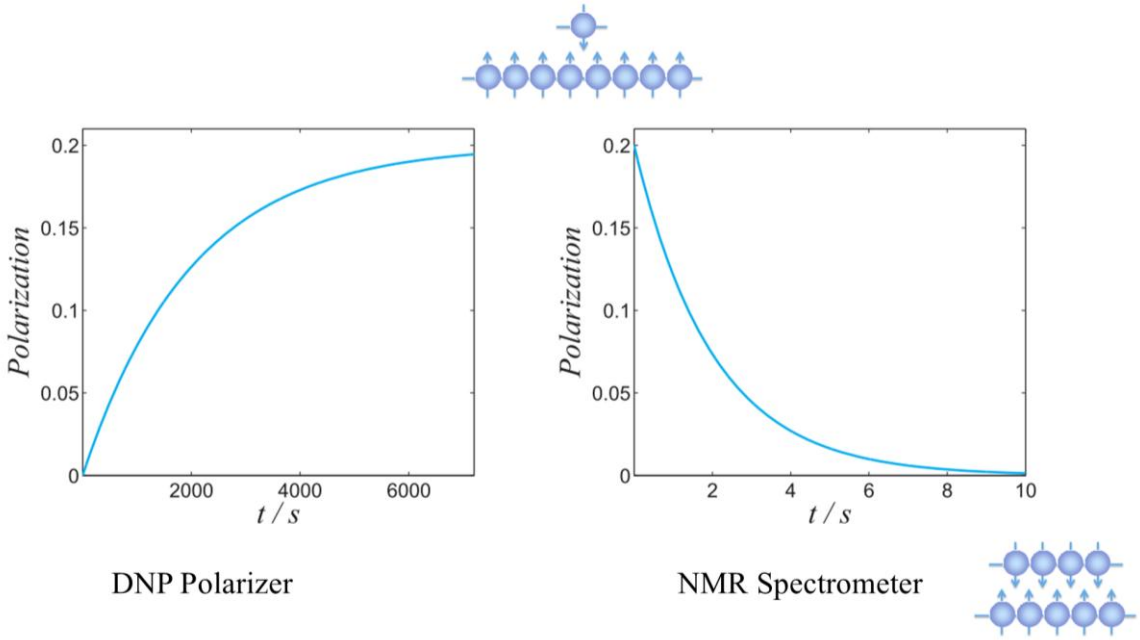

Figure I-4 : Typical time scale and polarization levels of a dissolution DNP experiment. The left panel is the polarization buildup curve in the solid state. The parameters are: maximum polarization p_{max} = 20%; buildup time constant τ = 2000 s. The equation of the curve is $p = p_{\max} \bullet (1 - \exp(-t/\tau))$. The right panel shows the spin relaxation in the liquid state. T_1 is 2 s, and the thermal polarization is ignored. The equation is $p = p_{\max} \bullet \exp(-t/T_1)$.

A commercialized dissolution DNP instrument implementing this technique was released by Oxford Instruments in 2006. The typical time scale of this DNP experiment is illustrated in Figure I-4. In the DNP polarizer, the polarization is built up over a time of minutes to hours. The signal obtained from the sample after dissolution can be equivalent to that obtained from months signal averaging without DNP enhancement. However, this hyperpolarization relaxes to a thermal polarization on the time scale of the spin-lattice relaxation time in the liquid state, which is typically on the order of seconds.

In most applications of dissolution DNP, the molecules to study are chosen such that they have relatively long relaxation times. For example, the carbonyl carbon in pyruvate and acetic anhydrate or the nitrogen atom in choline is subject to reduced dipole-dipole relaxation due to the absence of a nearby ^{1}H. In some cases, deuteration can be used to reduce the relaxation rate. In order to minimize the signal loss prior to NMR measurement for molecules with short relaxation time, it is of particular importance to reduce the sample transport time.[117]

Various applications of dissolution DNP both in spectroscopy and imaging have been developed.[118-122] Golman et al. initially aimed to apply the DNP polarized small molecules for ^{13}C MRI.[118-122] Compared to observation of ^{1}H in traditional MRI, ^{13}C provides more molecular information due to its wide chemical shift range. DNP enhancement and ^{13}C enrichment provide molecular contrast, allowing to distinguish the polarized chemical species and their metabolic products from the background. DNP enhanced 1-^{13}C pyruvate was injected *in vivo* and images of the spatial distribution of its conversion to lactate were acquired.[118] The conversion rate in this process provides a measurement of the malignancy of tumors because aggressive cancer shows upregulated metabolism. The conversion rate can either be obtained by measuring the lactate-pyruvate ratio[123-124] or by fit to a kinetic model describing the kinetic process together with spin relaxation.[125-126] Besides metabolic differences, tumors often show lower extracellular pH than in normal tissue. With injected hyperpolarized bicarbonate, pH *in vivo* was mapped by magnetic resonance spectroscopy (MRS) measurement of the bicarbonate : carbon dioxide ratio.[127] In another application, Merritt[128] et al. polarized

several chelated Y^{3+} compounds, obtaining up to 3000 times enhancement. Chelated Y^{3+} could potentially be used for pH imaging since its chemical shift is sensitive to the pH over a wide range.[129]

The high signal intensities obtained by dissolution DNP also can provide significant benefits for high-resolution NMR spectroscopy. The ^{15}N of isotope enriched choline, a precursor of cellular phospholipid metabolism, was polarized with an enhancement of 14000.[130-131] Small molecules are efficiently DNP polarized on ^{13}C; for glycine an enhancement of up to 15000 times was reported.[132] In another example, an amino acid mixture was acetylated with DNP polarized acetic anhydride for analysis.[133] More complex natural products with molecular weights of several hundred Da were polarized.[134-135] Reducing the spin-lattice relaxation by deuteration, ^{13}C of a 10 kDa protein was polarized, yielding up to 2000 fold signal enhancements.[136]

For more complicated experiments, techniques different from those used in conventional NMR need to be developed, since polarization from dissolution DNP is not renewable. Experiments requiring multiple scans, such as two-dimensional pulse sequences can not be directly applied. Two-dimensional spectra can still be acquired in a single scan using an ultrafast pulse scheme. By a series of selective excitations in different positions of the sample, different time points for indirect chemical shift evolution are encoded spatially.[137-138] A ^{1}H-^{15}N HSQC spectrum of a 200 nM sample of ^{15}N enriched urea was obtained in 0.13 s in this way.[139] Using the same technique, two 2D NMR spectra were measured through ^{15}N-^{1}H and ^{13}C-^{15}N-^{1}H transfer from a single sample of 180 μM of ^{13}C and ^{15}N enriched urea.[140] Heteronuclear correlations of DNP

polarized samples can also be indirectly obtained by a technique employing off-resonance decoupling. Chemical shifts of directly bonded nuclei can be reconstructed from observation of differential scaling of J-coupling splitting in function of the frequency of a low-power continuous wave decoupling field.[141]

In addition to NMR experiments at chemical equilibrium, DNP enhancement presents significant benefits to monitor non-equilibrium process, since signal averaging is not required. Hilty's group studied trypsin catalyzed hydrolysis of N-benzoyl-L-arginine ethyl ester with DNP enhancement. The depletion of reactant and formation of product were monitored and the kinetics of the reaction was measured.[142] Other kinetic studies include phosphorylation of choline,[130] and hydrolysis of acetic choline[143] with ^{15}N polarization. In all of these experiments, the spin-lattice relaxation time determines the time window that is accessible to the NMR experiments (see Figure I-4).

Reaction mechanisms can potentially be studied by tracking the flow of polarization from reactant to product. A chemical group of the reactant can be labeled by selective inversion of its spin polarization. The same chemical group in the product will then show opposite signals, correlating reactant and product.[144] Besides reactants and products, reaction intermediates with low population can be observed using DNP polarization, as is demonstrated by the synthesis of acetyl coenzyme-A.[145]

Relaxation processes in DNP polarized sample are based on the same principles as in conventional NMR. Nevertheless, relaxation phenomena in dissolution DNP experiments differ from those in thermally polarized sample in several aspects. Firstly, the process of relaxation of hyperpolarization to thermal equilibrium is irreversible;

while in a conventional NMR experiment, the polarization restores to the initial thermal equilibrium after each scan. Secondly, hyperpolarization is much larger than the thermal polarization. Thus, the thermal polarization is usually negligible when working with DNP polarized samples. As a result, relaxation processes such as cross relaxation can have different phenomenological effects on the evolution of polarization in DNP polarized sample.

An important focus in the present thesis lies in the quantification of such relaxation effects. Experiments include the application of two-dimensional NMR to DNP polarized samples, the determination of kinetics in non-equilibrium chemical reactions, as well as the use of hyperpolarized ligands to determine protein-ligand interactions. In 2D NMR experiments employing sequential scanning of a single hyperpolarized sample, the experimental conditions can be optimized when considering the combined effect of relaxation processes and the application of a series of small flip-angle pulses. When studying chemical reactions by real-time DNP-NMR, both the auto- and cross-relaxation rates contribute to the observed signal intensities in addition to the kinetic parameters. By separating the effects of spin relaxation from the observed signal, the reaction kinetics can be explored. At the same time, the relaxation rate constants contain additional information about the structure of the molecule. Protein-ligand interaction, a process of importance for example in drug discovery, presents a different situation. In this case, the sample is kinetically under equilibrium, and the relaxation and chemical exchange contribute to the observed signal intensities and line shape. Cross relaxation transfer of polarization from hyperpolarized ligand to protein further yields information

on binding kinetics and on the structure of the binding epitope. Benefitting from the high signal intensity of DNP, quantitative analysis of the NMR signal permits the study of chemical processes both on and off equilibrium.

CHAPTER II

SEQUENTIALLY ACQUIRED TWO-DIMENSIONAL NMR SPECTRA FROM HYPERPOLARIZED SAMPLE*

Introduction

Ex-situ dynamic nuclear polarization (DNP)[65, 115] is an emerging technology that allows the acquisition of liquid-state NMR spectra with greatly enhanced sensitivity.[139, 146-148] Using this technique, a sample aliquot is polarized in the solid state at low temperature, where the DNP process is the most efficient. The sample is subsequently dissolved in a stream of hot solvent, while maintaining polarization, and rapidly injected into an NMR spectrometer for acquisition of an NMR spectrum.

One of the potential drawbacks of using ex-situ DNP is that, once the polarization has been converted into an observable coherence, the spin system returns to the non-polarized state given by the Boltzmann population. While DNP makes available a high NMR signal level, the polarization provided by this technique can be used only once. In the most straight-forward application of ex-situ DNP, a single one-dimensional spectrum is acquired with high sensitivity. One-dimensional spectra however carry only a limited amount of information, and in many applications, including structural elucidation of organic molecules, two-dimensional NMR spectroscopy has long been a standard technique. Conventional 2D NMR experiments, where the spin system reaches an

---

* This chapter is reproduced with permission from Zeng, H., S. Bowen and C. Hilty (2009). "Sequentially acquired two-dimensional NMR spectra from hyperpolarized sample." *Journal of Magnetic Resonance* **199**(2): 159-165.

equilibrium state between successive scans, cannot be applied to such polarized samples. However, for these applications to benefit from the signal enhancement provided by DNP-NMR, it is necessary to find ways of making two-dimensional NMR spectroscopic techniques amenable to DNP polarized samples. Several strategies have been proposed towards this end. Firstly, in single-scan 2D NMR, pulsed field gradients are utilized to selectively address spatial regions; all of the "scans" necessary for a two-dimensional spectrum are acquired simultaneously from different regions of the sample.[137, 139] Secondly, in our own previous work, we proposed a scheme to derive two-dimensional chemical shift correlations using differential scaling of the observed scalar coupling by off-resonance decoupling, without explicitly acquiring a two-dimensional NMR spectrum.[141] As a third option, it is possible to acquire two-dimensional NMR spectra in sequential scans from one single hyperpolarized sample, using variable flip angles.[149-150] The technique employing off-resonance decoupling is particularly robust and easy to implement, however for larger molecules does not permit the resolution of overlapped resonances. The other two techniques both allow the acquisition of a true two-dimensional dataset. On one hand, single scan NMR is an elegant way of achieving this goal, and its application to hyperpolarized sample has been investigated.[139, 150] On the other hand, the simplicity of sequential acquisition of two-dimensional NMR spectra rivals that of the pseudo one-dimensional, off-resonance decoupling scheme. Additionally it gains the major advantage of two-dimensional NMR spectroscopy, its ability to resolve overlapped chemical shifts through dispersion in the second dimension. Although it is slower than single-scan 2D NMR, it is significantly easier to implement,

and is particularly robust against residual fluid motion in the sample caused by rapid injection of DNP polarized sample. For these reasons, its application to hyperpolarized sample in the context of structural elucidation of organic compounds merits investigation. Here, we compare heteronuclear correlation spectra[151-152] of hyperpolarized samples, using different strategies for sequential acquisition of the indirect chemical shift dimension. In addition, the effects of two different flip angle series for excitation are tested, and the consequences of the respective methods are discussed.

Experimental Section

Sample Preparation

(1) Sample for measurement of [^{13}C,^{1}H]-HMQC spectrum: 0.5 μL 3.6 M vanillin in a solution of 72% DMSO-d6 and 28% D_2O (Cambridge Isotope Laboratories, Andover, MA) with 15 mM 4-Hydroxy-2,2,6,6-tetramethylpiperidine-1-oxyl (TEMPOL) free radical (Sigma-Aldrich, St. Louis, MO). (2) Sample for testing the effect of variable flip angle series: 0.2 μL 3.6 M vanillin in a solution of 72% DMSO-d6 and 28% D_2O with 15 mM 4-Hydroxy-2,2,6,6-tetramethylpiperidine-1-oxyl (TEMPOL) free radical. (3) Sample for [^{1}H,^{13}C]-HMQC spectrum: 2.0 μL 3.6 M vanillin in a solution of 72% DMSO-d6 and 28% D_2O with 15 mM tris[8-carboxyl-2,2,6,6-tetramethyl-benzo(1,2-d:4,5-d')bis(1,3)dithiole-4-yl]methyl sodium salt free radical ("Finland"; Oxford Instruments, Tubney Woods, UK).

DNP Polarization

DNP polarization took place in an Oxford Instruments HyperSense DNP polarizer at a temperature of 1.3 K. For [^{13}C,^{1}H]-HMQC experiments and variable flip angle series test, 100 mW of microwave power was applied at a frequency of 94.270 GHz for a duration of 30 min. In [^{1}H,^{13}C]-HMQC experiments, the microwave power was 60 mW, the frequency 93.977 GHz and the polarization time 5.5 h. After polarization, samples were dissolved into acetonitrile, except for the flip angle test experiments shown in Figure II-5, where acetonitrile-d3 was used. For dissolution, 4 mL of solvent was heated until a pressure of 10 bar was achieved, flushed over the frozen sample, and injected into the NMR spectrometer using a homebuilt sample injector.[142] NMR spectra were acquired ca. 2.5 seconds after the start of dissolution. Post-dissolution sample concentrations were determined by HPLC following the NMR experiment. Typical final sample concentrations were in the low mM range (see below).

NMR Spectroscopy

Acquisition of the NMR spectrum was automatically triggered by a signal from the sample injector. Pulse sequences for [^{13}C,^{1}H]-HMQC and [^{1}H,^{13}C]-HMQC experiments are shown in Figure II-1. Raw NMR data was processed using the program TOPSPIN by Bruker. Fourier transformation was performed along the t_2 and t_1 dimension in the same way that a conventional NMR spectrum would be processed. Spectra obtained using [^{13}C,^{1}H]-HMQC pulse sequences without ^{1}H π pulses contain a ^{1}H chemical shift dependence in the ^{13}C dimension. These spectra were processed using the MATLAB

program, where this chemical shift dependence could be removed by multiplication with an offset dependent phase factor prior to Fourier transformation (see below).

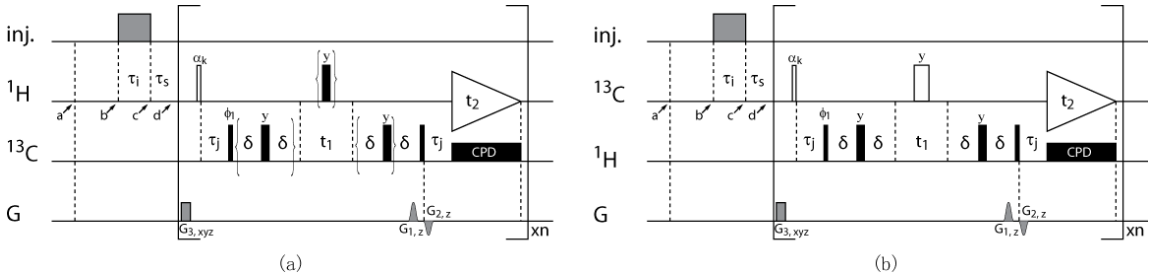

Figure II-1 : Pulse sequences for measurement of a 2D NMR spectrum of hyperpolarized sample, using (a) [^{13}C,^{1}H]-HMQC and (b) [^{1}H,^{13}C]-HMQC. An Oxford Instruments HyperSense DNP polarizer and a Bruker 400 MHz NMR spectrometer were used. Sample was delivered from the DNP polarizer to a home built sample injector between time points a and b. Sample injection into the NMR took place during τ_i=325 ms, and the NMR experiment was triggered after a stabilization time τ_s=200 ms at time point d. The two-dimensional dataset consists of *n*=32 transients, recorded by incrementing the evolution time t_1 and phase φ_1, using the States-TPPI (Time Proportional Phase Incrementation) method.[153-154] $G_{3,xyz}$ = (25..50;25..50;25..50 G/cm, 0.4 ms) removes unwanted coherence prior to the next acquisition. Its value was adjusted randomly within the indicated range, for each scan. The flip angles α_k of the excitation pulse (pulse strength γB_1=25 kHz) are adjusted to provide the same fraction of magnetization in each transient (see text). Narrow and wide black bars represent 90 ° and 180 ° pulses, and the phases are x unless indicated otherwise. Coherence selection is achieved by the pulsed field gradients $G_{1,z}$ and $G_{2,z}$. (a) [^{13}C,^{1}H]-HMQC spectra, $G_{1,z}$ = 50 G/cm and $G_{2,z}$ = -37.4 G/cm for zero-quantum version, $G_{1,z}$ = -40 G/cm and $G_{2,z}$ = 50 G/cm for double quantum version. The gradient time is 1 ms, and δ = 1.2 ms. $\tau_j = 1/(2J_{CH})$ = 3.12 ms. The delays and pulses in the brackets are deleted in the version without refocusing. During each acquisition period, 32768 points are acquired, using $t_{2,max}$ = 33 ms. ^{13}C composite pulse decoupling (CPD) is applied using GARP[155] at a field strength γB_1= 2.38 kHz. The carrier is set to 140 ppm on ^{13}C and 7 ppm on ^{1}H. The spectral width of ^{13}C is 250 ppm. (b) [^{1}H, ^{13}C]-HMQC spectra, $G_{1,z}$ and $G_{2,z}$ are 16.8 G/cm and 50 G/cm respectively. The gradient time is 500 μs, and δ = 700 μs. $\tau_j = 0.3/J_{CH}$ = 1.88 ms. During each acquisition period, 16384 points are acquired, and $t_{2,max}$ = 82 ms. ^{1}H CPD is applied at a field strength γB_1= 2.31 kHz. The carrier is set to 6.0 ppm on ^{1}H and 100 ppm on ^{13}C. The spectral width of ^{1}H is 12.0 ppm. The wide open bar on ^{13}C stands for a composite π pulse, which is ($3\pi/2_{-y}$, $2\pi_y$, $\pi/2_{-x}$, $3\pi/2_x$, $2\pi_{-x}$, $\pi/2_y$).[156]

Results and Discussion

Fast heteronuclear multi-quantum correlation experiments, [^{13}C,^{1}H]-HMQC and [^{1}H,^{13}C]-HMQC, were measured with the pulse sequences illustrated in Figure II-1, using DNP-polarized samples of vanillin. The indirect dimension was obtained from a Fourier transform of transients that were sequentially acquired from a single

hyperpolarized sample, with a total experimental duration of 1.4-3 seconds. Heteronuclear multi quantum coherence (HMQC) transfer ideally lends itself to the implementation of a multi transient experiment from hyperpolarized sample, because the small number of required pulses in a given scan allows the conservation of the remaining unused longitudinal magnetization for the subsequent scans. For excitation, a variable flip angle[149] was used to convert the same amount of longitudinal magnetization (polarization) into observable coherence in each scan.

[^{13}C,^{1}H]-HMQC Experiment

The pulse sequence in Figure II-1a represents the adaptation of an HMQC experiment[151, 157] for use with sample hyperpolarized on its 1H nuclei. This sequence contains only two pulses on the radio frequency channel corresponding to the polarized nuclei: the small flip angle pulse for excitation, and the π pulse for refocusing of chemical shift.[157] The resulting data can be processed using present-day NMR software without the need for additional scripts, and the resulting spectra can be presented in phase sensitive mode. The π pulse on the ^{1}H channel pulse does not alter the amount of the remaining polarization (*i.e.* longitudinal magnetization) after each transient, as it merely transforms the product operators I_z into $-I_z$. A spectrum acquired using this scheme is shown in Figure II-2. This experiment is most closely related to a conventional heteronuclear correlation experiment. Most importantly, it allows the resolution of chemical shifts that would otherwise be overlapped, or nearly overlapped, in a one-dimensional experiment (such as peaks B and D in Figure II-2). The number of points acquired in the ^{1}H dimension was 32768, and in the ^{13}C dimension was 32. The

large number of points in the ^{1}H dimension was selected to reduce the sampling interval, enabling the use of a digital filter in the relatively short duration (33 ms) of each of the free induction decays.[158] The data presented in Figure II-2 were acquired using a total acquisition time of 1.55 seconds of a sample at a concentration of 0.91 mM, corresponding to a concentration of 9.7 μM of the NMR active ^{13}C isotope.

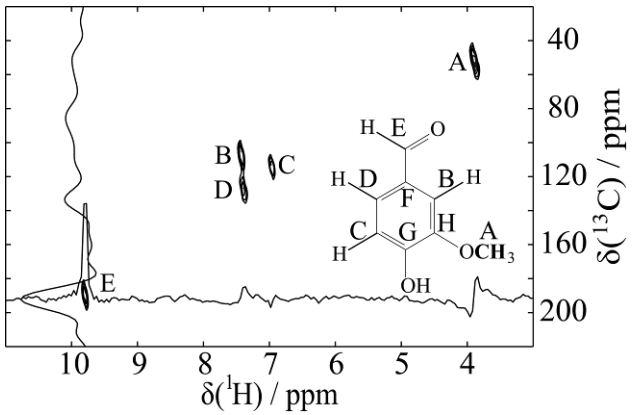

Figure II-2 : [^{13}C,^{1}H]-HMQC spectrum of vanillin with a total acquisition time of 1.55 s. The experiment shown in Figure II-1a was used, including the elements in the brackets. The acquisition parameters are in the caption of the pulse sequence. The data were zero filled to 128×32768 points, and processed with a 20 Hz line broadening exponential window function in the F2 dimension and Fourier transformed in both dimensions.

A spectrum acquired by this method may suffer from artifacts if the refocusing pulse is imperfect due to B_1 inhomogeneity, slight miscalibration of the pulse length, or off-resonance effects. These imperfections can influence the remaining polarization after each scan in a cumulative manner. Their effect is observable as small distortions of the baseline in the traces plotted through the spectrum in Figure II-2. An alternative option for recording this spectrum is by removing the refocusing π pulse on ^{1}H, leaving only the single variable flip angle pulse used for excitation of the coherence on this channel.

Figure II-3a and c show spectra acquired using a simplified scheme, where the bracketed pulse sequence elements in Figure II-1a have been removed. The experiment can be implemented either with double-quantum (DQ; Figure II-3a), or with zero-quantum coherence selection (ZQ; Figure II-3c). Due to the absence of a refocusing pulse, however, the chemical shifts of proton and carbon nuclei evolve concurrently during the evolution time t_1. The resulting indirect spectral dimension corresponds to the sum or the difference of the two chemical shifts depending on the gradient selection of double quantum coherence or zero quantum coherence, respectively. Without loss of general applicability, however, the proton chemical shift dependence can be removed by applying an offset dependent shift to the dataset. In (a), zero-quantum coherence selection requires a cyclic permutation $\omega_C \rightarrow \omega_C + (\omega_H - \omega_H^0)$ in the spectrum, which can be achieved most conveniently by multiplying each column of the dataset with the offset dependent factor $e^{i(\omega_H - \omega_H^0)}$ prior to Fourier transformation of the indirect dimension. In (c) double quantum coherence selection requires the cyclic permutation $\omega_C \rightarrow \omega_C - (\omega_H - \omega_H^0)$ in the spectrum, which is achieved by multiplication with $e^{-i(\omega_H - \omega_H^0)}$ prior to Fourier transformation of the indirect dimension. Resulting from this operation are spectra with identical chemical shifts, shown in panels b and d of the Figure II-3. In contrast to the spectra in Figure II-2, the spectra in Figure II-3 need to be presented in absolute value mode. This contributes to a slight broadening of the resonances, which may however be negligible compared to the achievable spectral resolution. The stated disadvantages should be weighed against the cleaner appearance

of the baseline in these spectra, as evident from the traces in Figure II-3. For this reason, the modified experiment depicted in Figure II-3 may well be superior for the routine acquisition of heteronuclear 2D spectra of hyperpolarized sample.

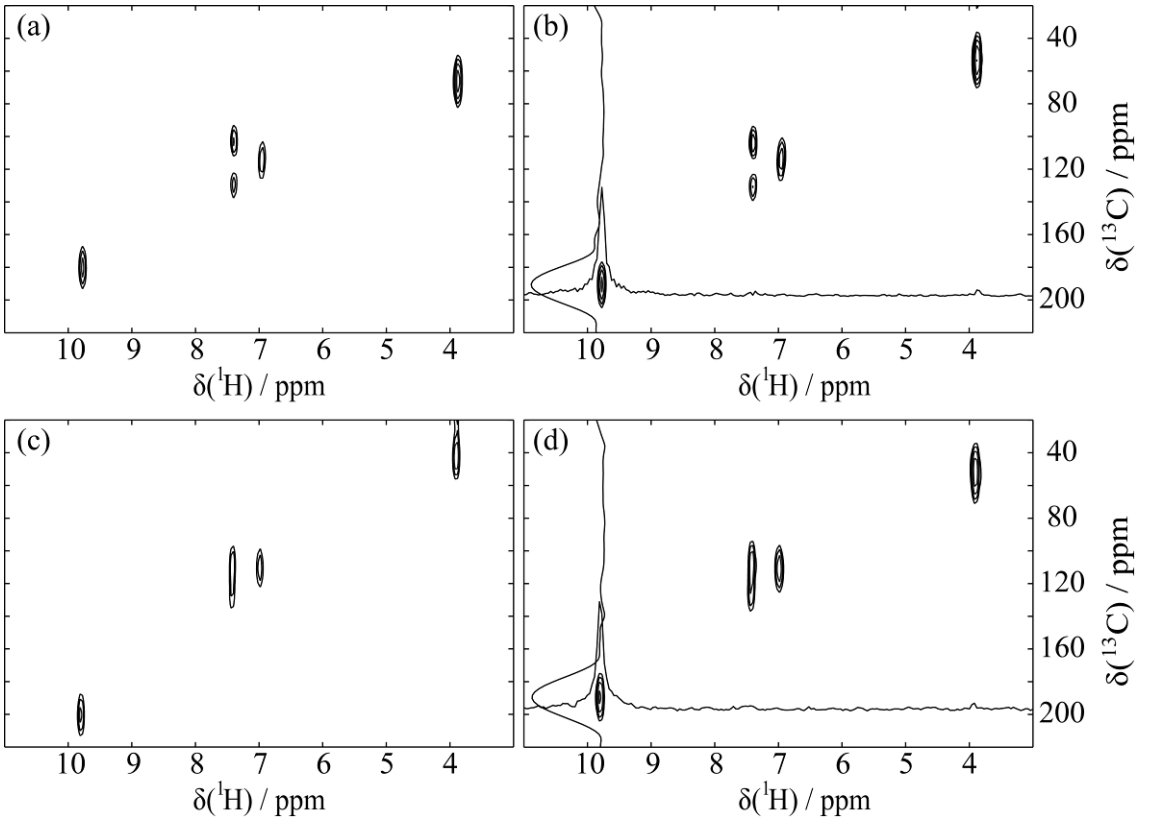

Figure II-3 : (a) Original Zero quantum (ZQ) coherence selection HMQC spectrum of vanillin. (b) Permutated ZQ HMQC spectrum. (c) Original Double quantum (DQ) coherence selection HMQC spectrum of vanillin. (d) Permutated DQ HMQC spectrum. The spectra were acquired using the pulse sequence shown in Figure II-1a, with the elements in brackets removed. The acquisition parameters are given in the caption of the pulse sequence. The total acquisition time was 1.44 s. The data was zero filled to 128×32768 points, and processed with an exponential window function using 20 Hz line broadening in the F2 dimension.

[^{1}H,^{13}C]-HMQC Experiment

The experiments presented in Figure II-2 and Figure II-3 make use of detection of hyperpolarized ^{1}H nuclei, and most closely resemble conventional [^{13}C,^{1}H]-HMQC

experiments. In our experience, typical signal enhancements for hyperpolarized carbon spins (~10,000×) are however higher than typical enhancements for protons (~1,000×). Certainly, part of this disadvantage is compensated for by the higher gyromagnetic ratio of protons, which increases the detection sensitivity by $(\gamma_{1H} / \gamma_{13C})^{3/2}$ =7.93.[159] Nevertheless, it may be interesting to consider the reverse [^{1}H,^{13}C]-HMQC experiment, where hyperpolarization as well as NMR signal acquisition is carried out on ^{13}C nuclei. The pulse sequence for this experiment is shown in Figure II-1b, and the resulting spectrum is presented in Figure II-4. Apart from an exchange of the two radio-frequency channels, it should be noted that in this case, the application of a refocusing pulse during the indirect chemical shift evolution is compulsory. In the absence of such a pulse, as a consequence of the large chemical shift range of ^{13}C, the indirectly detected sum or difference of chemical shifts, $\omega_H + (\omega_C - \omega_C^0)$ or $\omega_H - (\omega_C - \omega_C^0)$, would significantly exceed the ^{1}H spectral width. Increasing the spectral width of the indirect dimension to cover this broad range would have a detrimental effect on the spectral resolution that is achievable with a given number of scans. Even though the pure ω_H spectrum could still be reconstructed by the same cyclic permutation as described above, it is possible that, prior to permutation, some signal peaks would be shifted to the very edge of the spectrum, where noise is most significant. Again, because of the large chemical shift range of ^{13}C, we use a composite π pulse to minimize the off-resonance effects[156]. Finally, the [^{1}H,^{13}C]-HMQC experiment differs from the [^{13}C,^{1}H]-HMQC experiment in that the possibility exists for having n = 1..3 ^{1}H atoms attached to an originally excited ^{13}C atom. Each case would require a different time delay τ, for optimum coherence

transfer. A good compromise is, however, $\tau = 0.25/J_{CH}$ to $0.3/J_{CH}$. Since in all of these experiments, the spectral resolution in the indirect dimension is limited by the number of points that can be acquired (here, 32 points were used with an acquisition time of 82 ms per point), the choice of using the [^{1}H,^{13}C]-HMQC experiment in Figure II-4 over the [^{13}C,^{1}H]-HMQC experiment in Figure II-2 and Figure II-3 will largely depend on whether higher resolution is desired in the ^{1}H or the ^{13}C dimension.

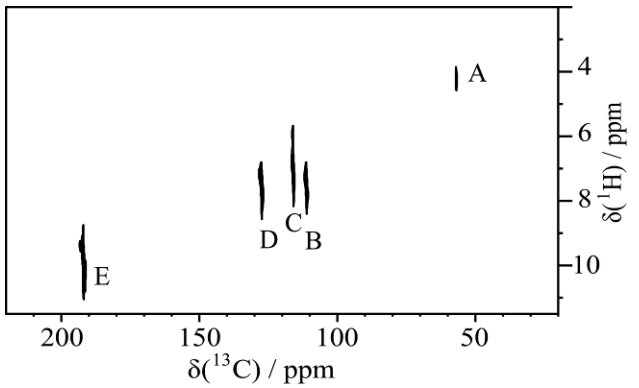

Figure II-4 : [^{1}H,^{13}C]-HMQC spectrum of vanillin with a total acquisition time 3.03 s, measured using the pulse sequence in Figure II-1b. The acquisition parameters are in the caption of the pulse sequence. The data was zero filled to 128×32768 points, and processed with an exponential window function using 20 Hz line broadening in the F2 dimension and a cosine window function in the F1 dimension. The letters correspond to those given in the drawing of vanillin in Figure II-2.

Variable Flip Angle

The experiments presented above make use of a variable flip angle so that every scan converts the same amount of polarization into observable coherence. In the absence of relaxation, the variable flip angle of the k^{th} scan is given by[141-142, 149]

$$\alpha_k = arcsin\sqrt{\frac{1}{n+1-k}} \qquad \text{(II-1)}$$

where n is total number of scans and k = 1...n. It should be noted that according to Equation (II-1), the flip angle for the last scan is always π/2, so that the last scan can make use of all of the remaining magnetization. The assumption that relaxation is insignificant is true when the experiment time is significantly shorter than the spin-lattice relaxation time (T_1). If this is not the case, later scans will give rise to less signal than earlier scans, and relaxation must be considered in the calculation of the flip angles.[149] A closed form of an equation for flip angles that compensate for relaxation effects can be derived as follows. Let α_k be the flip angle used for acquiring the k^{th} scan, and s_k be the polarization prior to the k^{th} scan. We require that each scan generates the same signal, and that the last scan utilizes all of the remaining polarization through the use of a π/2 pulse, so that

$$s_n = s_k \sin(\alpha_k). \tag{II-2}$$

Taking relaxation into account,

$$s_{k+1} = \beta s_k \cos(\alpha_k). \tag{II-3}$$

where $\beta = e^{-t/T_1} = e^{-t/T_1}$, is the time between scans and T_1 is the relaxation time.

Eliminating α_k by combining Equation (II-2) and Equation (II-3),

$$s_n^2 + \frac{s_{k+1}^2}{\beta^2} = s_k^2 \tag{II-4}$$

Equation (II-4) can be expanded into

$$s_{k+1}^2 + \frac{\beta^2 s_n^2}{1-\beta^2} = \beta^2 \left(s_k^2 + \frac{\beta^2 s_n^2}{1-\beta^2} \right). \tag{II-5}$$

Defining

$$f_k = s_k^2 + \frac{\beta^2 s_n^2}{1-\beta^2} \tag{II-6}$$

yields

$$f_{k+1} = \beta^2 f_k . \tag{II-7}$$

This is a geometric sequence, and

$$f_k = \beta^{2(k-n)} f_n . \tag{II-8}$$

Using

$$f_n = \frac{s_n^2}{1-\beta^2} \tag{II-9}$$

together with Equations (II-2) and (II-8),

$$\alpha_k = arcsin\sqrt{\frac{1-\beta^2}{\beta^{2(k-n)}-\beta^2}} , \tag{II-10}$$

which defines the flip angle series that takes relaxation into consideration. It should be noted that Equation (II-10) reduces to Equation (II-1) in the limit of $T_1 \to \infty$.

The difference between these two flip angle series in a case where relaxation cannot be neglected can be seen in the experimental data shown in Figure II-5. In Figure II-5a, peak integrals from a series of 1D ^{1}H spectra acquired of a hyperpolarized vanillin sample using the flip angles of Equation (II-1) are plotted. The delay between scans was chosen to be 200 ms, yielding a total experimental time of 6.4 seconds. This time is large compared to the relaxation time of vanillin (2.5 s for proton A, and from 5.0 to 5.7 s for protons B-E). Consequently, there is a sharp decrease in signal intensity for all nuclei. On the other hand, the flip angles used to obtain the data shown in Figure II-5b were

calculated using Equation (II-4), assuming a value of 5 seconds for the relaxation time T_1. It can be seen that in this case, the signals for protons B-E, which have matching relaxation times, remain virtually constant. The signal of proton A decays, albeit at a lower rate, because the relaxation time of this proton is shorter than the relaxation time used to calculate the flip angles.

We attribute the slight increase in signal in the last scan to the cumulative effect of imperfections in the preceding small-flip angle excitation pulses or sample movement, leaving slightly more than the calculated amount of polarization for the final $\pi/2$ excitation pulse. Furthermore, variations of signal intensities throughout the experiment due to cross-relaxation are possible.

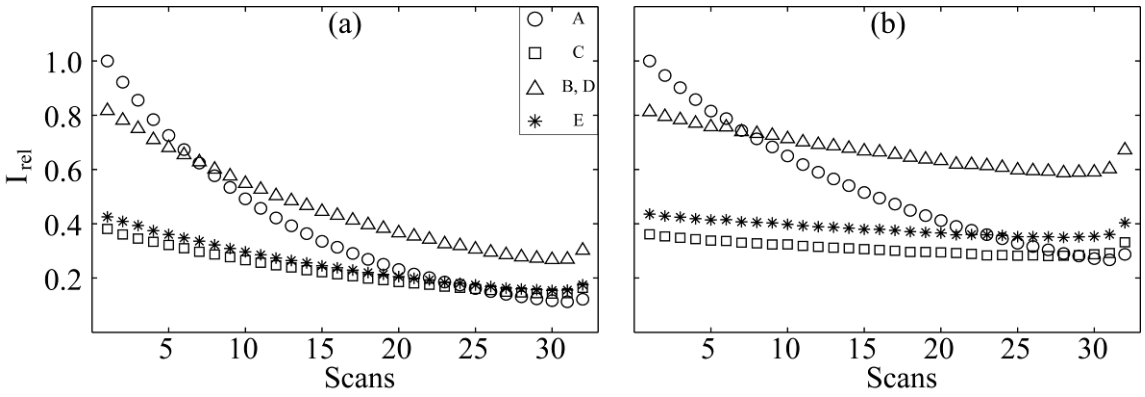

Figure II-5 : Signal intensities of successive scans in variable flip angle experiments using hyperpolarized vanillin. The integrals of each of the four peaks are plotted vs. the number of scan. In (a), the flip angle series is calculated using Equation (II-1); in (b), the flip angle series is calculated using Equation (II-10). After dissolution, 32 small flip angle 1D ^{1}H spectra were acquired at an offset of 7 ppm, with an acquisition time of 138 ms for each spectrum. The total duration between adjacent small flip angle pulses was t = 200 ms, yielding a total NMR experiment time of 6.4 s. The relaxation time in formula 10 takes a value of 5 s. The letters in the legend correspond to the structure of vanillin in Figure II-2. In a and b, the largest respective intensity has been assigned a relative intensity I_{rel} = 1.

It should be noted that because of the relatively long relaxation times of spins in the vanillin molecule, to accentuate the relaxation effect the delay time between scans for the data in Figure II-5 (200 ms) is larger than the delay time that was used for acquisition of the spectra in Figure II-2–Figure II-4 (45-95 ms). Under the conditions used for the 2D spectra, relaxation was negligible for the vanillin molecule, and consequently, Equation (II-1) was used for calculating the flip angle.

With flip angles calculated by Equation (II-1), the reduction in signal intensity with increasing scan number is more pronounced if a longer experiment time is used (see Figure II-5a), or if the spin-lattice relaxation time is shorter. In these cases, the effect on the spectra is a broadening of peaks in the indirect dimension similar to the application of a window function prior to Fourier transformation.[160] It may then be advantageous to use flip angles calculated by Equation (II-10) to obtain a narrower line shape. If flip angles are calculated using an assumed relaxation time $T_{1,assumed}$, which may be different from the actual relaxation time $T_{1,actual}$, the envelope of the signal in the indirect dimension is

$$I_{rel}(k) = e^{-\frac{(k-1)t}{T_{1,actual}} + \frac{(k-1)t}{T_{1,assumed}}} \qquad \text{(II-11)}$$

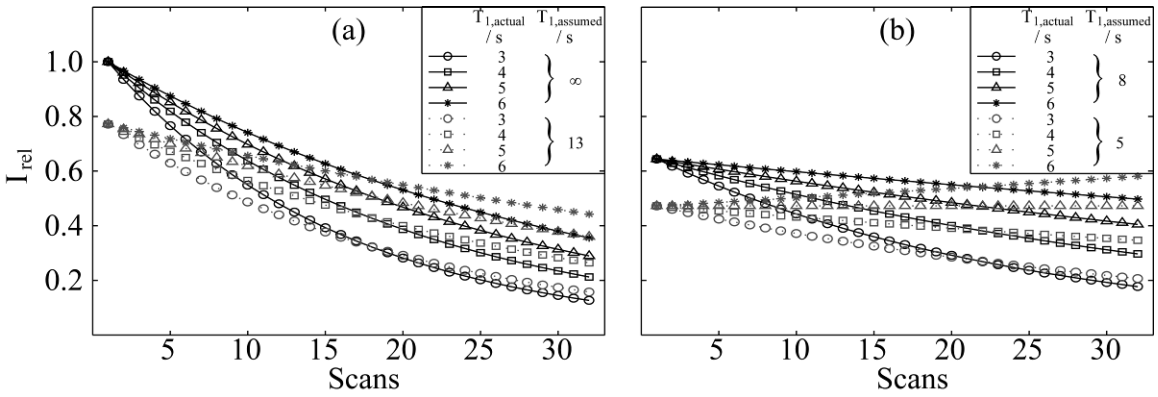

Figure II-6 : Simulated intensities for successive scans in variable flip angle experiments. Each group of curves represents the intensities of signals from spins with actual T_1 = 3 s, 4 s, 5 s and 6 s, calculated for the flip angle series (Equation (II-10)) using one assumed value for T_1. In (a), assumed values for T_1 are ∞ and 13 s. In (b), assumed values are 8 s and 5 s. The timing parameters used for the simulation are identical to the experimental parameters of Figure II-5. The scaling of I_{rel} is identical in both a and b.

The effect of using such a calculated flip angle series for different relaxation times is illustrated in Figure II-6, showing groups of curves representing the signal intensity as a function of the scan number. In each group, one fixed $T_{1,assumed}$ value is used for the calculation of the flip angles, and the resulting signal is plotted for spins with different $T_{1,actual}$ values. If $T_{1,assumed}$ is larger than $T_{1,actual}$, the signal is reduced in later scans, whereas in the opposite case, the signal increases. On the other hand, the larger $T_{1,assumed}$, the larger the signal of the first scan. After Fourier transformation, a large $T_{1,assumed}$ value will therefore lead to a broad peak with large integral, whereas a small $T_{1,assumed}$ value will lead to a narrow peak with small integral. In the latter case, however, the time domain signal is substantially different from zero in the last scan, leading to a peak shape resembling a sinc function, also known as a truncation artifact. This effect then needs to be counteracted with apodization. In practice, in order to maximize the signal-to-noise ratio obtainable from a sample with given initial polarization, it may be

advantageous to calculate the flip angle series using a $T_{1,assumed}$ value that is larger than the actual T_1 values of the molecule. Thereby, the reduction in signal intensity in later scans reinforces the apodization that would in any case be needed, and a larger initial signal can be obtained. Based on these considerations it appears that, while it may be beneficial to estimate T_1 relaxation times of the molecules under study for calculating optimal flip angles, the precise knowledge of those values is not required.

Polarization Levels

The final concentration of vanillin was determined by HPLC to be 0.9-1.0 mM for the [^{13}C,^{1}H]-HMQC-experiment and 4.2 mM for the [^{1}H,^{13}C]-HMQC-experiment. To estimate the levels of polarization, single scan 1D ^{1}H and ^{13}C spectra were acquired with the same parameters as the first scan of the [^{13}C,^{1}H]-HMQC-experiment (with π pulse on ^{1}H) and the [^{1}H,^{13}C]-HMQC-experiment, respectively. The small flip angle pulse was replaced with a $\pi/2$ pulse, and a 4.1 M vanillin sample in DMSO-d6 was used as a standard for this purpose. In the dataset presented in Figure II-2 ([^{13}C,^{1}H]-HSQC), we estimate a polarization level between 2% and 4% by comparison with the thermally acquired spectrum of the first transient, using the equations published elsewhere.[141] In the [^{1}H,^{13}C]-HSQC spectrum in Figure II-4, the polarization level was between 2% and 7% for all resonances. These polarization levels are in agreement with values that we have reported previously using the same instrumentation.[141]

Performance under Non-Stationary Conditions

The major mechanism of signal loss in ex-situ DNP is relaxation during sample injection; the signal gain afforded by the DNP process is effectively lost if the time required for sample injection and stabilization is more than three to four times the spin-lattice relaxation time T_1. In contrast, a major advantage of DNP enhanced NMR is the ability to measure time-resolved NMR spectra of chemical processes that occur after admixing of a second reactant to a DNP polarized sample.[142] To obtain a mixing dead time that is comparable to the high time resolution achievable in these experiments, it is necessary to measure an NMR spectrum as rapidly as possible after mixing of two sample components. Using a sample injector described elsewhere,[142] the spectra presented here were measured approximately 2.5 seconds after dissolution of the sample that has been polarized in the solid state, with a stabilization time of 200 ms. Rapid sample injection is however also concomitant with the need for measuring an NMR spectrum while residual fluid motion is still present in the NMR sample. Under these conditions, pulsed field gradients can lead to incomplete refocusing of coherences, and to attenuation of the observed signal. Indeed, a quantitative measurement of signal attenuation by pulsed field gradients is often used for the determination of diffusion coefficients by NMR.[161] The pulse sequence in Figure II-1 is optimized towards minimizing such undesired effects of pulsed field gradients, and the experiments presented appear to be quite robust when applied to non-stationary samples.

Conclusions

We have described a scheme that allows the acquisition of two-dimensional NMR spectra from a single DNP polarized sample. The present pulse sequence acquires the indirect spectral dimension sequentially, rather than distributed over space in the sample volume[139] or derived indirectly.[141] An advantage of this technique over indirectly derived chemical shift information lies in its capability of resolving overlapping chemical shifts through dispersion in a second dimension, albeit at the expense of spectral resolution. When compared to simultaneous sampling schemes, sequential acquisition as it is proposed here certainly requires a longer total experiment time (1-3 s). However, the present sequence is simpler to implement, and it is particularly robust with respect to experimental variations such as sample motion after rapid injection. For these reasons, sequential 2D spectroscopy of DNP polarized samples appears well suited for the routine structure determination of mass-limited samples of small molecules. In addition, it may also be useful for the NMR based investigation of non-equilibrium chemical processes in real-time.

CHAPTER III

QUANTITATIVE RATE DETERMINATION BY DNP ENHANCED NMR OF A DIELS-ALDER REACTION*

Emerging techniques for hyperpolarization of nuclear spins, foremost dynamic nuclear polarization (DNP), lend unprecedented sensitivity to nuclear magnetic resonance spectroscopy. Sufficient signal can be obtained from a single scan, and reactions even far from equilibrium can be studied in real-time. When following the progress of a reaction by nuclear magnetic resonance, however, spin relaxation occurs concomitantly with the reaction to alter resonance line intensities. Here, we present a model for accounting for spin-relaxation in such reactions studied by hyperpolarized NMR. The model takes into account auto- and cross-relaxation in dipole-dipole coupled spin systems, and is therefore applicable to NMR of hyperpolarized protons, the most abundant NMR-active nuclei. Applied to the Diels-Alder reaction of 1,4-dipheneylbutadiene (DPBD) with 4-phenyl-1,2,4-triazole-3,5-dione (PTD), reaction rates could be obtained accurately and reproducibly. Additional parameters available from the same experiment include relaxation rates of the reaction product, which may yield further information about the molecular properties of the product. The method presented is also compatible with an experiment where a single spin in the reactant is labeled in its spin-state by a selective radio-frequency pulse for subsequent tracking through the reaction, allowing the unambiguous identification of its position in the

* This chapter is reproduced with permission from Zeng, H. F., Y. Lee and C. Hilty (2010). "Quantitative Rate Determination by Dynamic Nuclear Polarization Enhanced NMR of a Diels-Alder Reaction." *Analytical Chemistry* **82**(21): 8897-8902. Copyright 2010 American Chemical Society.

product molecule. In this case, the chemical shift specificity of high-resolution NMR can allow for the simultaneous determination of reaction rates and mechanistic information in one experiment.

Introduction

Hyperpolarized NMR is gaining considerable interest for studying non-equilibrium chemical processes. The strong intensity of signals from hyperpolarized spin systems is sufficient to record an NMR spectrum in a single scan. Dynamic processes can then be followed in real-time, and potentially new information arising from the correlation of the chemical shifts from participating molecular species becomes available.

Many of these experiments use dynamic nuclear polarization (DNP)[162] as the hyperpolarization technique of choice, since this technique is capable of polarizing a variety of nuclei in almost any small molecule. DNP is usually carried out at low temperature (typically 1–77 K).[113, 115] With microwave irradiation of an electronic transition in a paramagnetic center, the high level of electron polarization is transferred to nuclear spins. For liquid state NMR, the polarized sample is rapidly thawed, and the NMR measurement is carried out before the spin system has relaxed.[115]

Proposed applications of this technique span the fields of chemistry and biomedicine. Golman et al. have used MRI for *in vivo* detection of the transformation of injected ^{13}C polarized pyruvate into alanine and lactate.[118] The metabolism in excised rat hearts has been studied by Merritt et al.[163] With ^{15}N enrichment, Sarkar et al. studied the hydrolysis of acetic choline through ^{15}N polarization, where polarization subsequently transferred to ^{1}H for sensitive detection.[143] Jensen et al. have used hyperpolarized NMR

for the detection of reaction intermediates with low population.[145] Our own group has determined the rates of enzyme catalysis by tracking reactant and product species using high-resolution ^{13}C NMR.[164] Mieville et al. have recently measured the kinetics of complexation of Y^{3+} with a ligand.[165] Similar experiments can further provide information on reaction mechanisms, if one spin of the reactant is "labeled" by selectively inverting its polarization. The reaction carries over this inverted polarization to the product, proving the transfer of the atom during the reaction.[144]

All of these techniques depend on the observation of the change in signal intensity as a function of time, due to the progressing reaction. At the same time, however, the polarization generated by DNP will decay to the non-polarized state with a relaxation time characteristic for each spin, usually in several seconds. Additionally, cross-relaxation effects may further play an important role in modulating signal intensities, as has been demonstrated by Merritt et al.[166] In some experiments, such effects may be reduced through isotope labeling (such as ^{2}H) or through the choice of special analytes that contain a spin which is isolated in space. However, in the general case of studying a chemical reaction, the molecules of interest are given, and it can also not be expected that isotope labeling would be readily applicable.

Here, we explore the effects of spin-relaxation on the signal intensities in reactions investigated by DNP-NMR, on the example of the Diels-Alder reaction of 1,4-dipheneylbutadiene (DPBD) with 4-phenyl-1,2,4-triazole-3,5-dione (PTD).[167] In this experiment, the signal intensities of protons were tracked. As a target nucleus, ^{1}H presents several advantages in that it is one of the most sensitive NMR active nuclei, is

present at 100% natural abundance, and is readily DNP polarized. Due to a high prevalence of ^{1}H in typical molecules, however, this nucleus is also prone to relatively fast auto- and cross-relaxation rates.[168] We present a general model for treating the effects of relaxation in the study of reactions with high sensitivity by DNP-NMR and show that by fitting the signal intensities of both reactant and product with a kinetic equation, reaction rate constants as well as relaxation rates can be obtained quantitatively.

Experimental Section

Dynamic Nuclear Polarization

The sample used for polarization consisted of 5 μL of 0.5M 1,4-dipheneylbutadiene (DPBD; Sigma-Aldrich, St. Louis, MO) in 85% tetrahydrofuran and 15% toluene with 15 mM of 2,2,6,6-Tetramethylpiperidine-1-oxyl (TEMPO; Sigma-Aldrich). Hyperpolarization took place in a HyperSense system (Oxford Instruments, Tubney Woods, UK), by irradiating a 100 mW power of 94.005 GHz (ω_e - ω_N) microwave frequency at a temperature of 1.4 K. After 30 min, the hyperpolarized sample was dissolved in 4 mL pre-heated acetonitrile, and automatically loaded into a 1 mL injection loop. The initial 450 μL of sample solution in the loop, which represents the part of the stream of solvent containing the highest analyte concentration, was injected into a 5 mm NMR tube that was preinstalled in the NMR spectrometer.[169] The injection took place by applying pressurized nitrogen gas (249 and 150 psi for forward and backpressure, respectively). For the experiments, where a reaction took place, 25 μL of 0.7 M 4-phenyl-1,2,4-triazole-3,5-dione (PTD; Sigma-Aldrich) solution in acetonitrile was

preloaded in the NMR tube before mixing with the polarized DPBD solution. The total required time to deliver the sample from the polarizer to the NMR tube was 1.8 s.

Since the sample is diluted with dissolution solvent during injection, it is desirable to independently determine the final sample concentration. The concentration of the unreacted PTD after dissolution was determined by UV-VIS spectrophotometry (BioSpec-mini, Shimadzu) at a wavelength of 530 nm. The concentration of the reaction product was measured by NMR spectroscopy. Using the present method for sample injection, homogeneous mixing of the two reactants has previously been confirmed, therefore the determined concentration accurately represents the reactant concentration during the reaction.[164]

NMR Spectroscopy

For each hyperpolarized sample, a series of ^{1}H spectra was acquired on a 400 MHz NMR spectrometer equipped with a broadband probe containing three pulsed field gradients (Bruker Biospin, Billerica, MA). All of the spectra were measured at a temperature of 27 ℃. For the experiments without selective inversion, the spectra were acquired using the pulse sequence (trigger – $[G_z - \alpha_x -$ acquire FID$]_{16}$). The resulting dataset consists of 16 transients, and the time delay between each transient was 0.4 s. Prior to each scan, a randomized pulsed field gradient G_z (25..35 G/cm, 1 ms) was applied to remove unwanted coherences present from the previous scan. The flip angle α of the excitation pulse was 17.0 °, and the pulse strength was 24 kHz. During each acquisition period, 4096 data points were acquired with an acquisition time of 365 ms. In the reference experiment with selective inversion (see below), the spectra were acquired

using the pulse sequence (trigger – shaped 180 – G_x – [G_z – α_x – acquire FID]$_{16}$). An IBURP2 shaped 180 degree pulse at the resonance frequency of H1 in DPBD (Figure III-1) with a duration of 50 ms, and a G_x pulsed field gradient (35 G/cm, 1 ms) were added. In the experiments where the reaction was carried out with selective inversion, the spectra were acquired using the pulse sequence (trigger – shaped 180 – G_x – shaped 90 – G_y – [G_z – α_x – acquire FID] $_{16}$). A EBURP2 shaped 90 ° pulse of 25 ms duration at the resonant frequency of H1' in the product molecule was added, followed by a G_y pulsed field gradient of 35 G/cm for a duration of 1 ms, to remove signal from reaction product accumulated during the time of sample mixing.[170]

Data Processing

The raw data were zero filled to 16384 complex data points, and an exponential window function with a line broadening of 2 Hz was applied before Fourier transform using the TOPSPIN 2.1 program (Bruker Biospin, Billerica, MA). Peak integration and curve fitting was performed by MATLAB (The MathWorks, Natick, MA). Analytical solutions to some of the differential equations described in the text were found using the program Mathematica (Wolfram Research, Champaign, IL).

Results and Discussion

Diels-Alder Reaction

In the Diels-Alder reaction of Figure III-1, a heterocyclic ring is formed by combining the reagents DPBD and PTD. For the NMR experiments, DPBD was hyperpolarized on its ^{1}H nuclei, and mixed with a non-polarized solution of PTD. The

consumption of reactant and generation of product were subsequently monitored by a series of small flip angle one-dimensional NMR spectra.

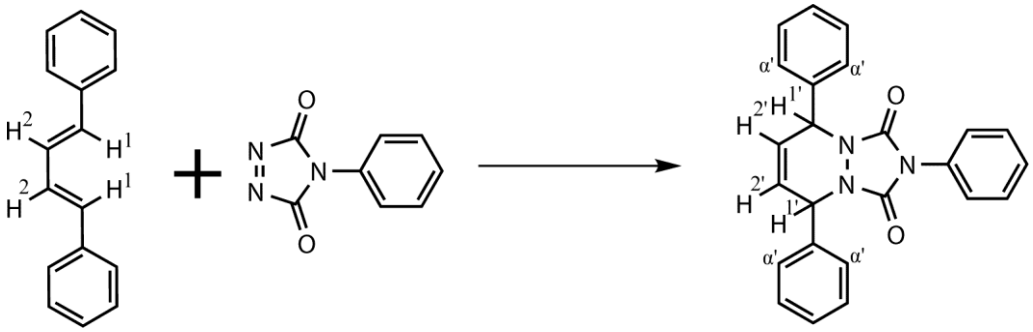

Figure III-1 : Reaction of DPBD with PTD in acetonitrile. The signal intensities of H1 and H1' were monitored in the NMR experiments.

Two well-resolved peaks, H1 in DPBD and H1' in the product, were chosen for quantitative analysis of the kinetics in this reaction. During the experimental time, the reaction carries over the polarization from the reactant to the product. As a result, the peak intensities of the reactant decrease, while the peak intensities of product initially increase, as shown in Figure III-2a. At the same time, the spins of interest interact through dipolar coupling with other proton spins in the molecules, foremost with those of the adjacent H2 and H2'. Finally, all of the signals decay because of their individual relaxation rates, and because of depletion of the initial polarization through the application of successive small flip angle pulses in the NMR experiment. In order to determine both the reaction and relaxation rates, allowing to separate the contribution of auto- and cross-relaxation in the product, the same reaction was repeated, applying a selective inversion to the spin of H1 in DPBD prior to the start of the reaction. As a result, the corresponding signals both in the reactant (H1) and in the product (H1') show

negative intensity (Figure III-2b). At the same time, the unaffected signal from H2' remains positive. The kinetic information about the reaction is accessible through the time-course of the peak intensities from Figure III-2, once separated from the effects of spin-relaxation.

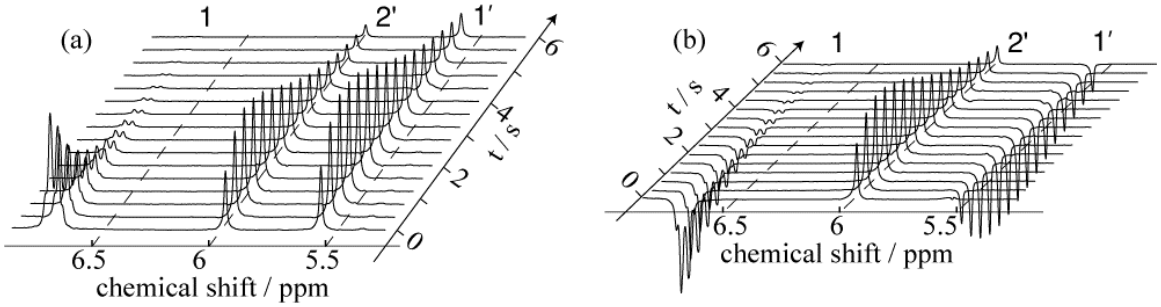

Figure III-2 : Stacked plots of the successively acquired spectra during the progress of the reaction. a) Spectra acquired using small flip angle pulses of a reaction mixture. b) Spectra acquired using small flip angle pulses of a reaction mixture, where initially a selective inversion was applied to H1 in DPBD. The three peaks from right to left are corresponding to H1, H2' and H1'.

General Model for Kinetics with Spin Relaxation

These experiments start with non-renewable initial hyperpolarization generated by the DNP process, which is several orders larger than the thermal polarization. By ignoring the thermal polarization, the initial hyperpolarization prior to the NMR experiment provides the only source for the observable signal in this system. To build a model for the time course of signal intensities, the differential equations for the signal intensities of each elementary step should take into account in both the reaction kinetics and the intrinsic spin relaxations. In a general kinetic model in Figure III-3, the signal flow from *S* to *Q* via *P*. The reaction rates r_1 and r_2 are determined by kinetics

mechanism, and they may contain factor of the concentrations not shown in the flow chart.

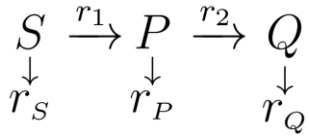

Figure III-3 : General kinetic model with relaxation. *S*, *P*, *Q*: molecular species; I_S, I_P, I_Q: signal intensities; r_S, r_P, r_Q: spin lattice relaxation rate; r_1, r_2: reaction rates. [*S*], [*P*], [*Q*]: concentrations.

The differential equations for the signal intensity of *P* is

$$\frac{dI_P}{dt} = r_1 \cdot \frac{I_S}{[S]} - r_2 \cdot \frac{I_P}{[P]} - r_P \cdot I_P \qquad \text{(III-1)}$$

Taking into account all the pathways for the signal inbound and outbound and also the loss due to relaxation, the differential equations for signal evolution are built.

Equations for the Signal Intensities

The quantitative analysis of the signal intensities from NMR data requires using a kinetic model of the reaction that includes the effects of spin-relaxation. While the same underlying principles apply as in a conventional NMR experiment, the boundary conditions are different. In a conventional experiment, relaxation drives the spin polarization back towards the level of thermal polarization after each scan. On the other hand, the DNP experiment starts with a large initial polarization, which is not renewable, and which decays towards the level of thermal polarization. Since the original polarization is much larger than thermal polarization, the latter can be neglected. As a

result, the only source of observable signals of the target spins stems from the hyperpolarized reactant.

The Diels-Alder reaction discussed here is a one-step second-order reaction; therefore the reaction rate can be described as $v = k\left[DPBD\right][PTD]$ Conditions were chosen such that after dissolution and mixing, [PTD] = 40 mM is sufficiently larger than [DPBD] = 2.7 mM, therefore a pseudo first order rate law can be used, with

$$v = k'[R] \tag{III-2}$$

$$k' \approx k\left[PTD\right]^0 \tag{III-3}$$

$$\begin{array}{ccc} R & \xrightarrow{k'} & P \\ \downarrow & & \downarrow \\ r_R & & r_P \end{array} \tag{III-4}$$

where R stands for reactant (DPBD) and P for product. Spin-relaxation, which occurs concomitantly with the reaction, is assumed to follow a single exponential decay with relaxation rates r_R and r_P for reactant and product, respectively. By combining the kinetic equation with spin relaxation terms, the differential equations for the longitudinal magnetization (polarization) of reactant and product become

$$\frac{dI_R(t)}{dt} = -(k' + r_R)I_R(t) \tag{III-5}$$

$$\frac{dI_P(t)}{dt} = -r_P I_P(t) + k' I_R(t) \tag{III-6}$$

The integration of these equations results in

$$I_R(t) = I_R^0 e^{-(k'+r_R)t} \tag{III-7}$$

$$I_P(t) = \frac{I_R^0 k'(e^{-r_P t} - e^{-(k'+r_R)t}) + I_P^0(k' + r_R - r_P)e^{-r_P t}}{k' + r_R - r_P} \quad \text{(III-8)}$$

Here, I_R^0 and I_P^0 are the longitudinal polarization of the reactant and product at the beginning of the data acquisition. In the experiment, a hard pulse with fixed small flip angle α was used to convert a portion of the longitudinal magnetization into observable transverse magnetization. By the influence of this small flip angle pulse, for each scan, *sin(α)* of the total longitudinal magnetization is used for detection, and *cos(α)* of the longitudinal magnetization is preserved for following scans. The fixed flip angle scheme introduces to the observed signal intensities an envelope function of $e^{-\lambda t}$, with $\lambda = \frac{\ln(cos\alpha)}{\Delta t}$, and Δt the time delay between scans. The experimental signal intensities *s* of the reactant and product then become:

$$s_R(t) = s_R^0 e^{-(k'+r_R+\lambda)t} \quad \text{(III-9)}$$

$$s_P(t) = \frac{s_R^0 k'(e^{-r_P t} - e^{-(k'+r_R)t}) + s_P^0(k' + r_R - r_P)e^{-r_P t}}{k' + r_R - r_P} e^{-\lambda t} \quad \text{(III-10)}$$

Equation (III-9) can be used for the determination of the pseudo first order reaction rate constant *k'* from experimental data, under the condition that *k*' is comparable to or larger than r_R and r_P.

Apparent Relaxation Rates Based on Auto- and Cross-Relaxation

The assumption that relaxation occurs as a single exponential is a priori true only for an isolated spin. In dipole-dipole coupled systems, cross relaxation should always be considered. In a two-spin system, if the thermal equilibrium polarization is ignored, the

evolution of the longitudinal magnetization of the two spins I_1 and I_2 due to relaxation can be written analogously to the Solomon equations[168] as

$$\frac{d}{dt}\begin{pmatrix} I_1 \\ I_2 \end{pmatrix} = -\begin{pmatrix} \rho_1 & \sigma_{12} \\ \sigma_{12} & \rho_2 \end{pmatrix}\begin{pmatrix} I_1 \\ I_2 \end{pmatrix} \qquad \text{(III-11)}$$

Here, the diagonal terms ρ_1 and ρ_2 are the auto-relaxation rates, which include the dipole-dipole relaxation (ρ_{12}) between the two spins and relaxation by other mechanisms (ρ^*), and the off-diagonal term σ_{12} is the cross relaxation rate. By solving this equation, the time evolution of the longitudinal polarization can be found as following:[168, 171-172]

$$I_1 = \frac{I_1^0 e^{-(\xi+\rho_1+\rho_2)t/2}((e^{\xi t}+1)\xi + (e^{\xi t}-1)(-\rho_1+\rho_2-2\kappa\sigma_{12}))}{2\xi} \qquad \text{(III-12)}$$

$$I_2 = \frac{I_2^0 e^{-(\xi+\rho_1+\rho_2)t/2}((e^{\xi t}+1)\xi + (e^{\xi t}-1)(\rho_1-\rho_2-2\sigma_{12}/\kappa))}{2\xi} \qquad \text{(III-13)}$$

Here, $\xi = \sqrt{(\rho_1-\rho_2)^2+4\sigma_{12}^2}$, $I_1{}^0$ and $I_2{}^0$ designate the initial longitudinal magnetization at t = 0, and $\kappa = I_2^0 / I_1^0$ is their ratio.

The apparent relaxation rates r_1 and r_2 are the derivative of the logarithm of the longitudinal magnetization over time. By Taylor expansion to first order in t,

$$r_1 = -\frac{dlnI_1}{dt} \approx \rho_1 + \kappa\sigma_{12} + \kappa\sigma_{12}(\rho_1-\rho_2+(\kappa-\frac{1}{\kappa})\sigma_{12})t \qquad \text{(III-14)}$$

$$r_2 = -\frac{dlnI_2}{dt} \approx \rho_2 + \frac{\sigma_{12}}{\kappa} + \frac{\sigma_{12}}{\kappa}(\rho_2-\rho_1-(\kappa-\frac{1}{\kappa})\sigma_{12})t \qquad \text{(III-15)}$$

The zero order term $\rho_1 + \kappa\sigma_{12}$ represents the initial relaxation rate.[173] When the time dependent part on the right-hand side of Equations (III-14) and (III-15) is small, the time dependence of the signal intensity can be approximated by an exponential curve with a

single parameter, the relaxation rate. Often, for small molecules, the main contribution to the relaxation is ρ^*. In this case, $\sigma_{12} \ll \rho_1$ and $|\rho_1 - \rho_2| < \rho_1$, and the above condition is satisfied if

The apparent relaxation rates are dependent both on the signal intensities of the dipole-dipole coupled spins, as well as on the signs of the relaxation terms. For small to middle sized molecules, $\sigma_{12} > 0$, and the cross relaxation contribution increases the apparent relaxation rate if all spins have the same sign of polarization. On the other hand, if the polarization of the spin of interest, I_1, is selectively inverted, the cross relaxation term will reduce the apparent relaxation rate. This property can be used to determine the cross-relaxation rates, which carry the structurally important information of the molecule, from experimental measurements of spin-relaxation with and without selective inversion, as described in the following.

If the initial magnetization for all spins are equal, *i.e.* $\kappa = 1$ in the non-inverted experiment, and $\kappa = -1$ with selective inversion, the apparent relaxation rates can be written as following:

$$\begin{cases} r = \rho_1 + \sigma_{12}(1 + (\rho_1 - \rho_2)t) & none \quad inverted \\ r^{\dagger} = \rho_1 - \sigma_{12}(1 + (\rho_1 - \rho_2)t) & selective\, inversion \end{cases} \tag{III-16}$$

The sum and difference of these rates then are

$$r - r^{\dagger} = 2\sigma_{12}(1 + (\rho_1 - \rho_2)t) \tag{III-17}$$

$$r + r^{\dagger} = 2\rho_1 \tag{III-18}$$

Equations (III-17) and (III-18) can be used for experimental determination of auto- and cross-relaxation rates, as described in the following section. If

$$\sigma_{12}t \ll 1 \text{ and } \left|\rho_1 - \rho_2\right|t \ll 1 \qquad \text{(III-19)}$$

the time-dependent part in Equations (III-14) – (III-17) is negligible, and the auto-relaxation rate $\rho_1 = ½ (r + r^{\dagger})$ and cross-relaxation rate $\sigma_{12} = ½ (r - r^{\dagger})$ can be obtained directly from the experimental measurements with and without selective inversion of the spin of interest.

More generally, when a spin is dipole-dipole coupled to multiple spins, a similar equation for the relaxation rate difference may be used,

$$r - r^{\dagger} = \sum_j 2\sigma_{1j}(1 + (\rho_1 - \rho_j)t) \qquad \text{(III-20)}$$

Comparison of NMR Data to the Model

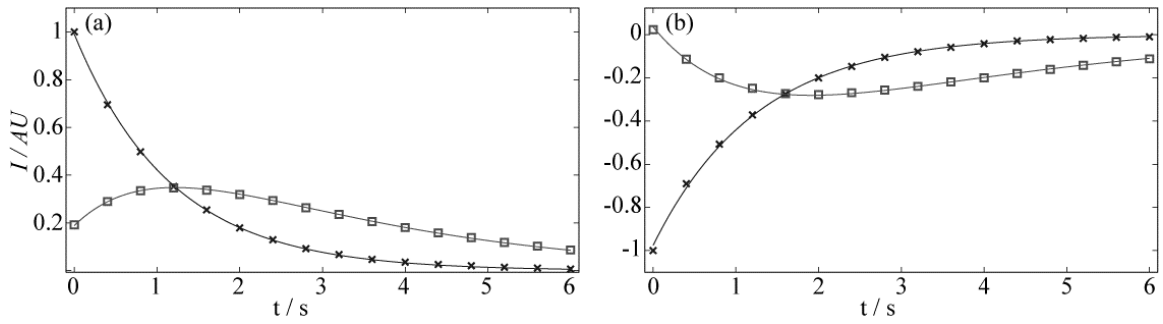

Figure III-4 : Fit of the H1(×) and H1' (□) signal intensities by Equations (III-9)-(III-10) simultaneously with initial signal intensities of reactant and product (s_R^0, s_P^0), pseudo first order reaction rate constant (k') and relaxation rate of product (r_P) as parameters, relaxation rate of reactant (r_R) was give by reference spectrum. a) Small flip-angle experiment (k'=0.419s^{-1}, r_P=0.312s^{-1}). b) Small flip angle experiment with selective inversion (k'=0.468s^{-1}, r_P=0.246s^{-1}).

Equations (III-9) and (III-10) were used to fit the experimental data obtained from the Diels-Alder reaction (Figure III-4). The fit parameters of primary interest are the pseudo first order reaction rate constant k' and the relaxation rate of the product species,

r_p. Additional parameters in the fit were the initial signal intensities of the reactant s_R^0 and the product s_P^0. The latter is required because the reaction started before the first acquisition of the NMR spectra due to the time required for sample mixing, resulting in a non-zero signal intensity of the product in the first spectrum. The curve fitting using the four specified parameters was carried out simultaneously to the two experimental curves for reactant and product intensities, respectively. It should be noted that the curve for the reactant intensity only depends on r_R and s_R^0, whereas the curve for product intensity depends on all four parameters. The remaining variables in Equations (III-9) and (III-10) were set to known values. The value for the parameter λ was calculated from the known small flip angle and the time between scans. The relaxation rates of the reactant, r_R = 0.322 s^{-1} and $r_R^\dagger$ = 0.215 s^{-1} (with selective inversion) were determined from separate reference experiments where hyperpolarized DPBD was injected into the NMR, but not mixed with the second reactant PTD (see Experimental Section). The rationale for using a known value for r_R, but not for r_P is that, by definition, the reactant is available for measurement of its relaxation rates. The product of the reaction would not always be available separately, or may be unstable, and therefore its relaxation rate should be determined from the reaction itself.

A possible error in the determination of absolute relaxation rates using a series of small flip angle measurements[131] could arise if residual turbulence carries hyperpolarized solution from outside of the active region of the NMR coil into the active region during the experiment. In this case, spins originally outside of the active region are not affected by pulses from preceding scans, resulting in a decay of the signal that is

too slow. An analytical expression for the maximum possible error is given in the supplementary materials. This effect can however be minimized by choosing suitable injection pressures.[174] Further cancellation of the effect is achieved through the calculation of rate differences both in the determination of cross relaxation rates and of reaction rates. The cross relaxation is derived from the difference between two relaxation rates, and the reaction rate constant is obtained from the fit of signal intensities of reactant and product, in which the relaxation rates from the reference experiments was used as input parameters.

Determination of Reaction Rate Constant

The pseudo first order reaction rate constants k' obtained from several datasets of the Diels-Alder reaction are shown in Table III-1. The fit reproduces the data with low root mean square deviations (*RMSD* values), further indicating that the simplifications made in the derivation of the equations are valid. The second order rate constant k can then be calculated using the known initial concentration of the second reactant (PTD), either by the amount preloaded in the NMR tube or determined after reaction.

Table III-1 : Rates determined from independent datasets of the Diels-Alder reaction. The first order rate constant k' was determined from the fit of the peak intensities of proton H1. The initial concentration of PTD, $[PTD]^0$ = [PTD] + [P] was used for determining the second order rate constant *k*. S.I. stands for selective inversion of the resonance of H1. The rate determined by UV/vis spectrophotometry, for reference, was $k = 11.7\ M^{-1}s^{-1}$.

	k' s^{-1}	[PTD] mM	[P] mM	*k* $M^{-1}s^{-1}$	*RMSD* %
Reaction	0.476	38.8	2.8	11.5	0.21
Reaction	0.471	37.5	2.8	11.7	0.15
Reaction	0.419	33.4	2.6	11.7	0.31
Reaction with S.I.	0.468	36.2	2.7	12.0	0.66
Reaction with S.I.	0.474	38.8	2.7	11.4	0.44

As can be seen from Table III-1, the reaction rates determined from different experiments, both with and without selective inversion, show good agreement. For the Diels-Alder reaction under the conditions used, the reaction rate averages to 11.7 ± 0.2 $M^{-1}s^{-1}$. This rate also agrees with a determination of the rate constant by UV/vis spectrophotometry.

Relaxation Rates of Product

The apparent relaxation rates of the reaction product that are obtained from the four-parameter fit of the reaction dataset in Figure III-4 are $r = 0.316\ s^{-1}$ and $r^{\dagger} = 0.255\ s^{-1}$ without and with selective inversion, respectively. These rates are in very good agreement with rates that were, for purposes of validation, measured independently from a hyperpolarized reference spectrum of the reaction product ($r = 0.291\ s^{-1}$ and $r^{\dagger} = 0.231\ s^{-1}$).

The apparent relaxation rates r and $r^{\dagger}$ contain contributions from various sources. Potentially more relevant information about the product molecule, such as distance information, is contained in the cross-relaxation rates. Using r and $r^{\dagger}$, the auto- and

cross-relaxation rates can be estimated from Equations (III-17) and (III-18). If neglecting the time dependent part in Equation (III-17), the calculated auto-relaxation rates are $\rho_{1'}$ = 0.286 s^{-1} and $\rho_{1'}$ = 0.261 s^{-1} from the four-parameter fit of the reaction data and from reference spectrum (for purposes of validation), respectively. The cross-relaxation rates are $\sigma_{1'2'}$ = 0.031 s^{-1} and $\sigma_{1'2'}$ = 0.030 s^{-1}, respectively.

However, here, $\left|\rho_{1'} - \rho_{2'}\right| t \approx 0.6$, and the second condition in Equation (III-19) is not strictly fulfilled. Applying the full Equation (III-17) requires knowledge of the auto-relaxation rates of the neby protons H2', Hα' (see Figure III-1). Here, $\rho_{1'}$ - $\rho_{2'}$ = -0.1 s^{-1} and $\rho_{1'}$ - $\rho_{\alpha'}$ = -0.1 s^{-1} were obtained from a hyperpolarized reference spectrum of the reaction product. Using the mid-point of the reaction time, t = 3.6 s, together with the apparent relaxation rates, the sum of cross-relaxation rates from H1' can be calculated to be 0.047 s^{-1}. Again for purposes of validation, the cross-relaxation rate of the reaction product was determined using conventional one-dimensional NOE experiments[175] (see Figure III-5 and Figure III-6). The sum of the cross relaxation rates of H1' from these experiments is 0.050 s^{-1}, which is in good agreement with the above rate determined from the hyperpolarized reaction experiment. Therefore, the hyperpolarized experiment of the reaction can not only yield a quantitative measurement of reaction kinetics, but also the nuclear cross-relaxation parameters, which are indicative of the structure of a product molecule. This information would be of particular importance if the reaction product is unstable, or is a reaction intermediate.

In addition to obtaining relaxation and reaction rates, the experiment with selective inversion is further fully compatible with the spin tracking experiment presented in,[144] which can reveal mechanistic information about the inverted site.

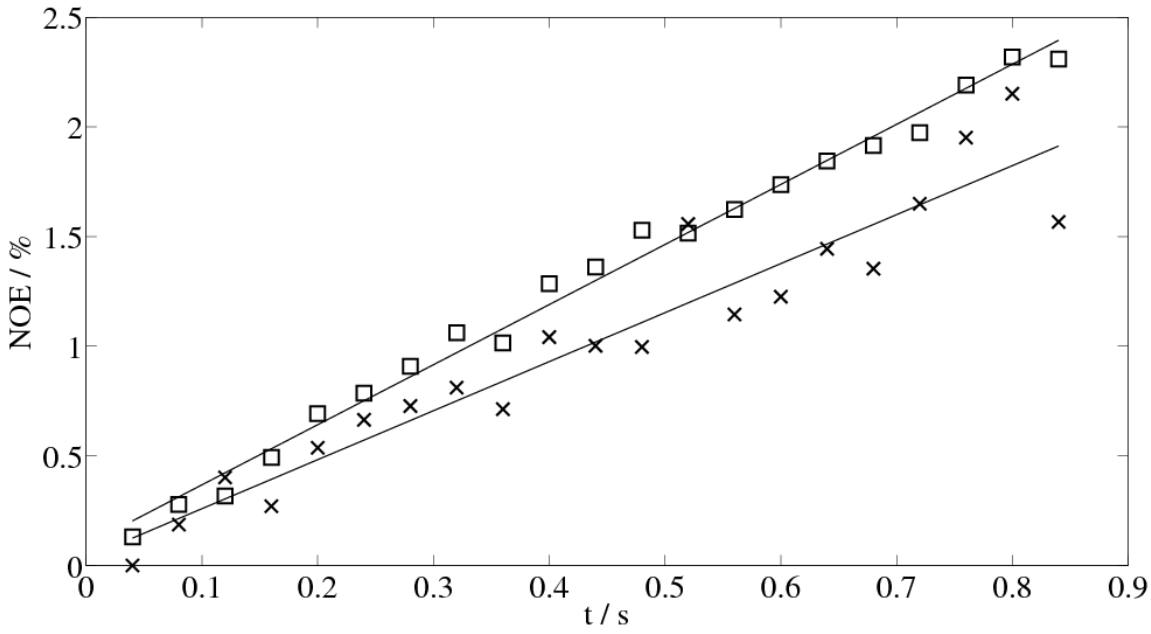

Figure III-5 : NOE buildup curves of proton H2'(□) and Hα'(×) from the cross relaxation with proton H1'. The cross relaxation rates are $0.029s^{-1}$ and $0.022s^{-1}$.

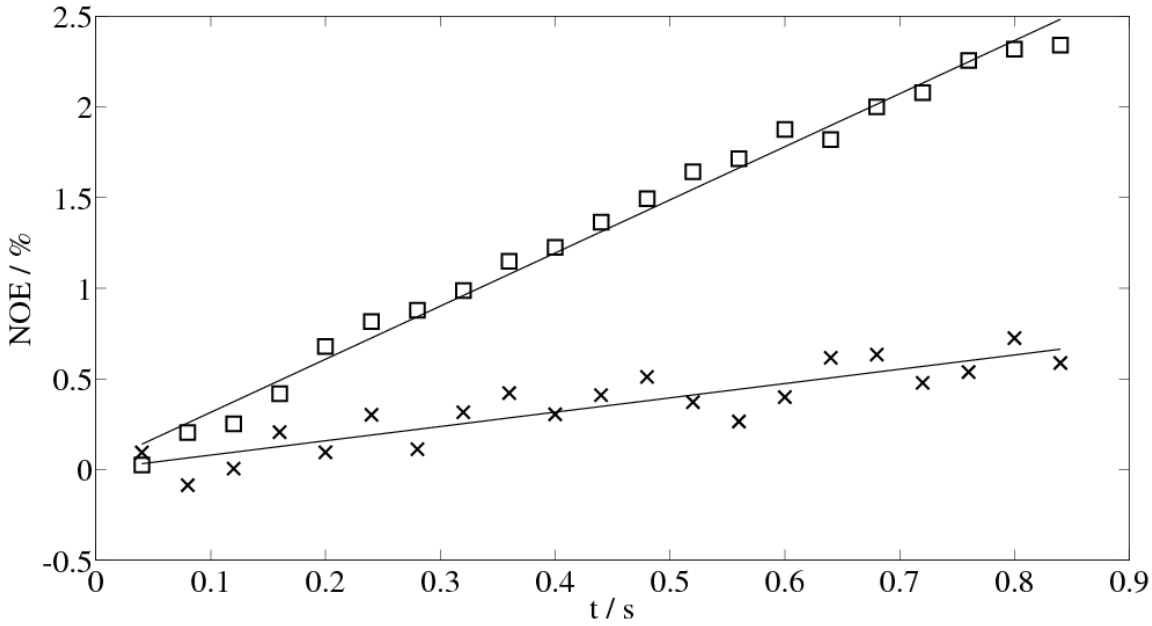

Figure III-6 : NOE buildup curves of proton H1'(□) and Hα'(×) from the cross relaxation with proton H2'. The cross relaxation rates are $0.027s^{-1}$ and $0.008s^{-1}$.

Analytical Expression for the Upper Limit of Error in Relaxation Rate due to Turbulence

In the DNP experiments, the hyperpolarized sample is injected into the NMR tube prior to the experiment. The injected sample volume is larger than the active volume of the coil. However, only the sample inside the coil experiences the radio frequency (rf) pulses. As the rf pulses convert a portion of the longitudinal magnetization into coherence for detection, the polarization of the sample inside the coil is depleted. This process is taken into account when using the integrated signal intensities for the calculation of relaxation rates. However, if the injection process generates sample motion that persists during the NMR measurement, fresh polarization from outside of the coil is introduced into the active region during the course of the experiment. This

increases the measured signal intensities, and can lead to seemingly decreased relaxation rates.

An upper limit for the error introduced by this effect can be estimated when considering the fast exchange limit, namely if the sample inside and outside of the coil would mix immediately. In the following, we present an analytical expression for this maximum possible error.

Consider that the volumes of sample inside and outside the coil are V_i and V_o. The flip angle of each of the rf pulses is α, the time delay between scans is Δt, and the spin-lattice relaxation rate is r. The longitudinal magnetization of sample both inside and outside of the coil just before the first scan is I_0. In the experiments measuring relaxation rates, the signal intensities of the 1st scan then are

$$s(0) = I_0 sin\alpha \tag{III-21}$$

The remaining longitudinal magnetization of the sample inside the rf coil is $I_0 cos\alpha$. Under instantaneous mixing with the sample outside of the rf coil (I_0 and V_o), the average longitudinal magnetization becomes $I_0 \frac{V_i cos\alpha + V_o}{V_i + V_o}$. With spin relaxation for Δt, the longitudinal magnetization before the second scan is

$$I(\Delta t) = I_0 e^{-r\Delta t} \frac{V_i cos\alpha + V_o}{V_i + V_o} \tag{III-22}$$

Similarly, the longitudinal magnetization before the k+1th scan is

$$I(\mathrm{k}\Delta t) = I_0 e^{-kr\Delta t} \left(\frac{V_i cos\alpha + V_o}{V_i + V_o} \right)^k \tag{III-23}$$

and the signal intensity of the k+1th scan

$$s(\mathrm{k}\Delta t) = I(\mathrm{k}\Delta t)\sin\alpha = I_0 \sin\alpha\, e^{-kr\Delta t}\left(\frac{V_i\cos\alpha + V_o}{V_i + V_o}\right)^k \qquad \text{(III-24)}$$

The signal decays exponentially with a rate of

$$r_d = r - ln\left(\frac{V_i\cos\alpha + V_o}{V_i + V_o}\right)/\Delta t \qquad \text{(III-25)}$$

If the sample motion is ignored, namely, V_o=0, the decay rate would be,

$$r_d' = r - \frac{ln(\cos\alpha)}{\Delta t} \qquad \text{(III-26)}$$

The difference is

$$r_d - r_d' = ln\left(\frac{(V_i + V_o)\cos\alpha}{V_i\cos\alpha + V_o}\right)/\Delta t \qquad \text{(III-27)}$$

Given the experimental parameters, V_i=200 μL, V_o=250 μL, $\alpha = 18°$, Δt=0.4 s, the sample movement would decreased the measured relaxation rate by a maximum of 0.07 s^{-1}.

Extension of Polarization Lifetime using Singlet States of Coupled Spins

The research accomplished in this chapter aimed at extracting the most information in the short life time of the hyperpolarization, which is typically several seconds for protons. An extension of the life time of hyperpolarization would increase the time window to observe the DNP polarized sample, allowing the measurement of slow chemical reactions.

The intramolecular dipole-dipole interaction is the main relaxation mechanism for ^{1}H in the present experiments, and is the main reason for the fast spin relaxation. One strategy to reduce the intramolecular dipole-dipole interaction would be deuteration of the molecule, but it requires non-trivial synthesis. Another is the use of long-lived spin states. Levitt et al. prepared a pair of spins in singlet state, showing up to 20 times longer lifetime than the normal T_1 relaxation time. [176-177]

In a symmetric two spin-1/2 system, the spin states can be represented in a basis consisting of a singlet state $|S_0\rangle = 1/\sqrt{2}\left(|\alpha\beta\rangle - |\beta\alpha\rangle\right)$, which is antisymmetric with respect to spin exchange operator, and three triplet states, $|T_1\rangle = |\alpha\alpha\rangle, |T_0\rangle = 1/\sqrt{2}\left(|\alpha\beta\rangle + |\beta\alpha\rangle\right)$ and $|T_{-1}\rangle = |\beta\beta\rangle$, which are symmetric. The singlet state cannot connect to the three triplet states by internal dipole interaction. As a result, it is preserved for a time longer than the usual T_1 relaxation time. By preparing DNP polarized small peptide in this long-lived state, the apparent decay rate of the protons on glycine residues was increased by 6 times.[178] Here, the extension of the lifetime of hyperpolarization in a small aromatic molecule is shown. p-chlorobenzaldehyde (pCBA), is a symmetric molecule with 4 protons (Figure III-7). Due to the symmetry, this molecule contains two equivalent pairs of spins (A, C) and (B, D). The coupling constants between the non-equivalent protons are $J_{AB} = J_{CD} = 8.2$ Hz and $J_{AD} = J_{CB} = 2.1$ Hz. The T_1 relaxation time of these two kinds of protons are both 4.4 s, as measured with hyperpolarized sample.[131]

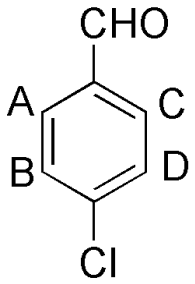

Figure III-7 : Structure of p-chlorobenzaldehyde (pCBA).

A two-spin system can be prepared in a singlet state by the pulse sequence element in a of Figure III-8, if the following conditions are met: (1) the two spins are isolated (*i.e.* there is no coupling with other spins); (2) the two spins are not equivalent, and there is scalar coupling *J* between the two spins.

The preservation of a singlet state in an external magnetic field requires that the external field does not break the symmetry, *i.e.*, the two spins are equivalent and have exactly the same precession frequency. Singlet states in inequivalent spin pairs can be preserved either by removing the magnetic field,[179] or by applying a continuous spin lock pulse,[177, 180] which eliminates the chemical shift difference between the spin pair (element b in Figure III-8).

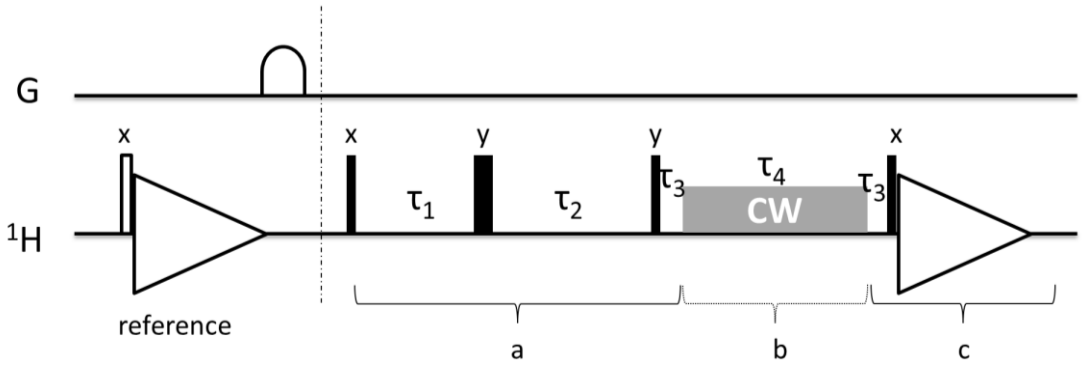

Figure III-8 : Pulse sequence for the experiment to measure singlet state life time. A reference 1D spectrum is acquired with small flip angle pulse. During the second scan, the spin system is kept in singlet state. a: preparation of singlet state; b: continuous wave irradiation for preservation of the singlet state; c: read out of singlet state. The open rectangle represents a 15˚ hard pulse. Narrow and wide black bars represent 90˚ and 180˚ pulses, respectively (γB_1 = 25 kHz). The phases of the pulses are indicated on the top. The delays are $\tau_1 = 1/(4J)$, $\tau_2 = 1/(4J) + 1/(2\Delta\omega)$, $\tau_3 = 1/(4\Delta\omega)$. During τ_4, a continuous wave (CW) irradiation at the center of the resonance of HA and HB with γB_1 = 5.0 kHz was applied.

Since the singlet state is not directly NMR observable, it is necessary to convert it into transverse magnetization for detection. In the experiment of Figure III-8, the polarization stored in the singlet state is read out using pulse sequence element c, which consists of a delay of τ_3 and a hard 90 ° pulse, followed by data acquisition. Different from the absorptive Lorentzian line shape in a conventional NMR spectrum, a dispersive line shape spectrum is observed, which is illustrated in Figure III-9.

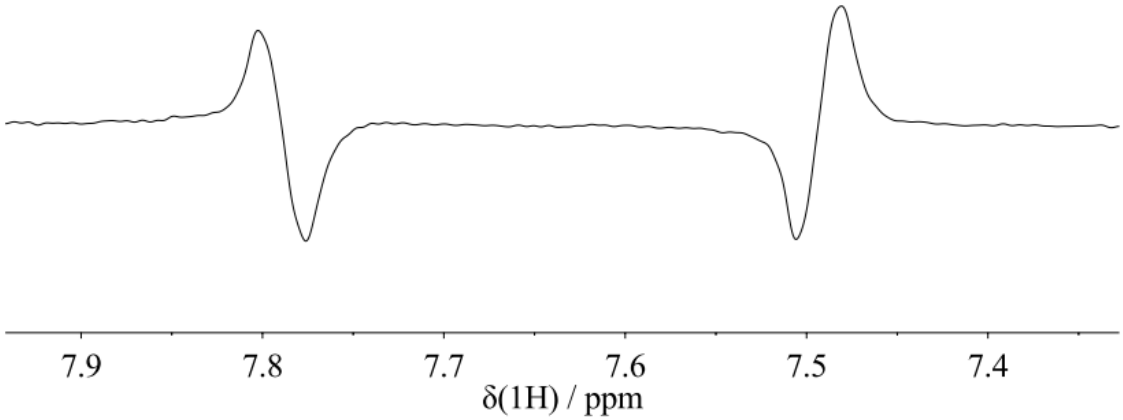

Figure III-9 : Typical dispersive line shape in singlet state experiments. 2 μL of 2 M p-chlorobenzaldehyde (pCBA) in CD_3CN with 15 mM TEMPO was polarized for 30 min and dissolved with acetonitrile, resulting in a final concentration of 4.4 mM pCBA. The spectrum was recorded using the pulse sequence illustrated in Figure III-8.

The lifetime of the hyperpolarized pCBA in the singlet state was determined by measuring the signal intensity after different storage times τ_4. The peak height after each storage time point was measured from a fresh DNP polarized sample. It was normalized relative to the peak height in the reference spectrum acquired with a small flip angle pulse, to compensate for any variation in polarization and concentrations between experiments.

In these experiments, the ^1H polarization of p-chlorobenzaldehyde (pCBA) was preserved in the singlet state for as long as 60s. The relative signal intensities were plotted and fitted with an exponential function (Figure III-10). The life time of the singlet state under the conditions used was 30 s, an approximately 7 fold extension compared to the T_1 relaxation time of 4.4 s. It may be possible to further extend the lifetime of the singlet state by removing the free radicals that are present in the solution due to the DNP process.[178]

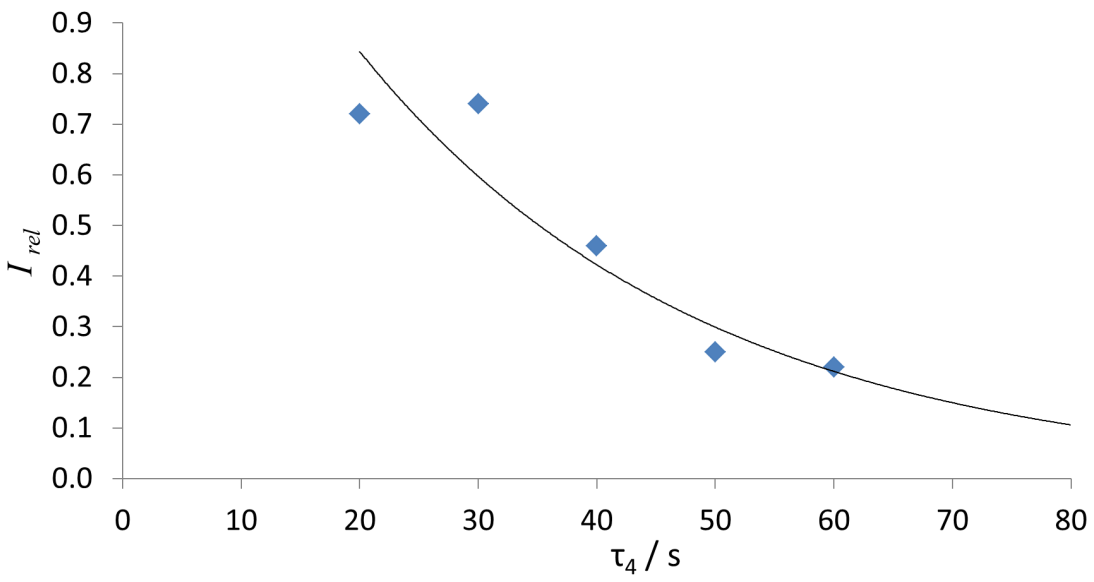

Figure III-10 : Relaxation of the singlet state. The spectrum was recorded with 4.4 mM DNP polarized p-chlorobenzaldehyde (pCBA) in acetonitrile using the pulse sequence illustrated in Figure III-8. The relative signal intensities are the peak height ratio between the singlet state spectra and the reference spectra. The signal intensities are fitted with an exponential function.

The extended lifetime of the hyperpolarization potentially expands the time window available to NMR experiments. Possible applications include studying slower reactions in a fashion similar to what is described in the previous parts of this chapter.

Conclusions

In the present work, DNP enhanced NMR allowed the monitoring of a Diels-Alder reaction in real-time. It was shown that using a fit to a model of expected signal intensities, the rate constant for a reaction can be determined quantitatively by this method. Most small molecules can fulfill the required assumptions for the relaxation behavior of the system under study, making the method generally applicable to a large number of reactions in chemistry and biochemistry. The experiments here were carried

out using the most abundant and highly sensitive NMR active nucleus, ^{1}H. It was shown that even in this case, it is possible to accurately separate the kinetic rate constants from the spin relaxation that occurs concomitantly to the reaction, if effects from auto- and cross-relaxation are considered. Apart from reaction rates, these relaxation rate constants can be obtained from the same data, yielding potentially additional information about the structure of the reaction product. The experimental scheme presented here, together with the theoretical framework concerning spin-relaxation and reaction allows for an efficient determination of rates and mechanism for reactions that complete within the time frame of spin relaxation, while making full use of the sensitivity gain afforded by DNP hyperpolarization. Furthermore, by preparing a spin pair in the singlet state, the spin relaxation rate can be reduced, potentially allowing the study of slower reactions.

CHAPTER IV

DNP ENHANCED NMR STUDY OF PROTEIN LIGAND BINDING*

Introduction

The protein-ligand interaction is fundamental in biological process. Biological function is often regulated by the ligand, which can act as an inhibitor for an enzyme, or as an agonist or antagonist for a receptor. Drug design usually starts with a lead compound that binds to the protein target related to the disease of interest. Understanding how a drug candidate interacts with the protein allows the optimization of its binding affinity and specificity.

High-resolution NMR spectroscopy plays an increasingly important role in studying protein-ligand interaction.[181-182] Various NMR methods have been developed, which work through measurement of parameters such as chemical shift, relaxation rates, NOE or diffusion. Depending on the type of experiment, ligand binding is detected by observation of signals from ligand or from protein. NMR is able to screen multiple ligands simultaneously,[183] if the primary interest lies in determining whether or not a ligand binds. Through the effect that chemical exchange between the free and bound forms of a ligand has on the NMR spectrum, it is possible to detect weak binding, with dissociation constants higher than 1 mM.[184-185] NMR can provide information about the

* Part of the material in this chapter is reproduced from a manuscript for Angewandte Chemie International Edition (accepted for publication), and from a manuscript to be submitted.

binding process at atomic resolution, which can be useful to optimize the structure of the ligand.

However, the low sensitivity of NMR is a limiting factor in the application to drug discovery, especially when the solubility of the ligand in water is low, or when it is difficult to express the protein in large amount. In this regard, providing several orders of magnitude of signal enhancement, dissolution DNP presents a significant opportunity for the study of protein ligand interaction. In this chapter, it will be demonstrated that the interaction of DNP polarized ligands with protein can be studied through the observation of ligand signals, as well as through polarization transfer from ligand to protein. Finally, a theoretical framework for describing polarization transfer between two competitively binding ligands will be presented.

Identification of Binding in Ligand Observed Experiments

DNP enhancement enables the detection of micro molar concentration of ligand, greatly expanding the scope of NMR study of protein ligand interaction. This technique has in the past most commonly been applied to ^{13}C nuclei, which often exhibit slow spin relaxation that reduces the loss of polarization prior to the NMR experiment, among many applications also allowing the detection of ligand binding.[186]

Here, we present experiments based on hyperpolarized fluorine, which are applicable to the identification of ligand binding, and in addition can be used for the quantitative determination of the dissociation constant K_D[187] of a ligand interacting with a protein. The use of fluorine is motivated by its importance in pharmaceuticals, where

these atoms impart specific properties pertaining to electronic structure, hydrophobicity, or metabolic stability.[188-189]

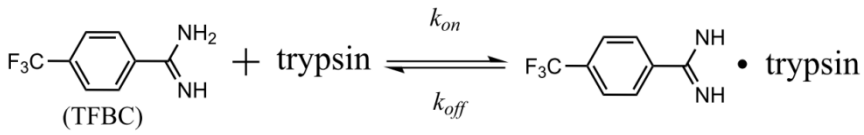

Figure IV-1 : Binding of 4-(trifluoromethyl)benzene-1-carboximidamide (TFBC) to trypsin.

4-(trifluoromethyl)benzene-1-carboximidamide hydrochloride dihydrate (TFBC) is a ligand to the serine protease trypsin (Figure IV-1). Figure IV-2 shows hyperpolarized ^{19}F spectra of TFBC together with sodium trifluoroacetate (TFA; used as internal reference). Comparing traces a) and c), recorded in the absence and presence of protein, respectively, indicates that binding can readily be observed both due to line broadening, peak height reduction and chemical shift change. Experimental variations unrelated to binding, such as small differences in sample volumes and polarization levels, are reflected in peak of the reference compound TFA, which does not bind to trypsin. By comparing ligand peak to sample peak, the binding of the ligand to the protein can be unambiguously detected. Hyperpolarization increased the signal of TFBC 800 fold as compared to conventional NMR in a 9.4 T magnet. Traces b) and d) in Figure IV-2 are experiments carried out closer to the limit of detection of the experimental setup, at concentrations of 1.1 μM TFBC and 10 μM protein.

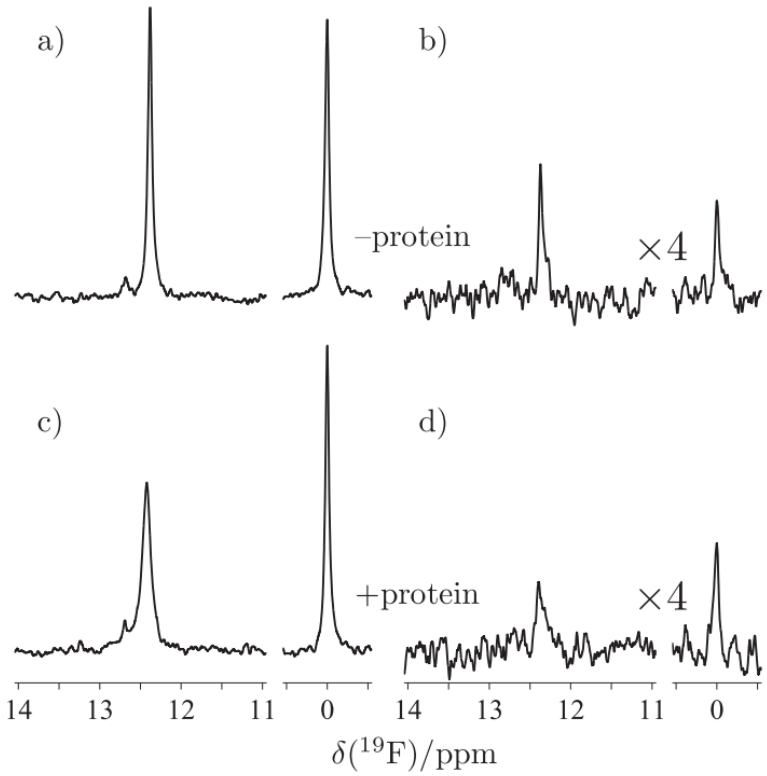

Figure IV-2 : Sections of spectra from samples containing TFBC (12.4 ppm) and TFA hyperpolarized on ^{19}F. 10.5 µM TFBC / 1.6 µM TFA a) in the absence of protein, and c) in the presence of 10 µM trypsin. 1.1 µM TFBC / 0.27 µM TFA b) in the absence of protein, and d) in the presence of 10 µM trypsin. All chemical shifts are referenced to TFA at 0 ppm. Spectra were recorded at 400 MHz with a conventional probe head, using a single excitation pulse.

The ability to record spectra at low ligand concentration is an important advantage of the hyperpolarized experiment both for detection of binding as well as for determination of the dissociation constant K_D, since a ratio ligand : protein < 1 : 1 can be reached even when using typically low protein concentration. In experiments for determining binding to a protein for large numbers of compounds, the detection of strongly binding ligands in slow exchange is then possible through observation of signal loss. In contrast, in conventional ligand observed NMR experiments that often use a 10 to 20 fold excess of ligand, binding in slow exchange gives rise to only a small reduction

in the overall signal, and its detection is unreliable. Furthermore, in screening applications, multiple ligands are often tested simultaneously, in a single protein sample. If more than one ligand binds to the protein competitively, the weaker binder may not be detected because the stronger binders occupy most of the binding sites of the protein.[190] This problem is also eliminated by using ligand concentrations smaller than protein concentration in these experiments.

In addition to the simple determination of binding or no binding, it is often of interest to quantify the strength of the ligand/protein interaction, which can be expressed in form of the dissociation constant K_D. From the equations describing the binding equilibrium, it is straight forward to find an expression for the fraction of bound ligand, p_b, under given experimental conditions

$$p_b = \frac{c_P + c_L + K_D - \sqrt{(c_P + c_L + K_D)^2 - 4c_P c_L}}{2c_L} \qquad \text{(IV-1)}$$

where c_P and c_L are protein and ligand concentrations, respectively.[187] In traditional NMR experiments for the determination of K_D, fast exchange between the bound and free form of the ligand is often assumed. In this case two readily observable spectral parameters, the line-width at half maximum $\nu_{1/2}$, as well as the change in chemical shift $\Delta\delta$, are proportional to p_b. A fit of one of these experimentally determined quantities to Equation (IV-1) can then be used to estimate the dissociation constant. In the hyperpolarized experiment presented here, the same approach is in principle viable. Since this method relies on the comparison of the line width between different stopped-flow sample injections,[169] the precision of the measurement can be greatly improved by

comparing line widths of the ligand under study to the non-binding reference, in order to remove the effect of variations in magnetic field inhomogeneity between experiments. The parameter of interest derived from the hyperpolarized experiment is then the change in line width in function of protein and ligand concentration,

$$\Delta\Delta\nu_{1/2}(c_P,c_L)=\left[\nu_{1/2}^{(\text{Ligand})}(c_P,c_L)-\nu_{1/2}^{(\text{Reference})}(c_P,c_L)\right]-\left[\nu_{1/2}^{(\text{Ligand})}(0,c_L)-\nu_{1/2}^{(\text{Reference})}(0,c_L)\right] \quad \text{(IV-2)}$$

This parameter can readily be fit to the proportionality relation $\Delta\Delta\nu_{1/2}(c_P,c_L)=p_b\cdot\Delta\Delta\nu_{1/2,\max}$, as shown in Figure IV-3. The fit uses two independent parameters; the dissociation constant K_D, and the maximum change in line width $\Delta\Delta\nu_{1/2,\max}$ that would be observed in the limit of very large protein concentration. These experiments were carried out with the protein/ligand titration along two orthogonal axes. The resulting two-dimensional surface fit indicated $\Delta\Delta\nu_{1/2,\max}$ = 303 Hz (with a 95% confidence interval between 196 Hz and 409 Hz), and K_D = 157 μM (with 95% confidence interval between 72 μM and 241 μM). Since the determination of the dissociation constant relies on the observation of broad signals, which concomitantly lowers the signal-to-noise ratio, the use of hyperpolarization is particularly beneficial for this application.

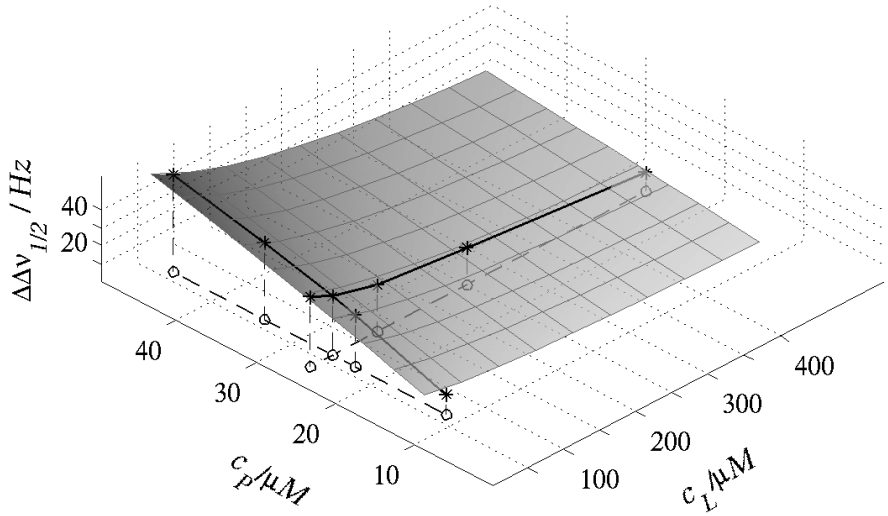

Figure IV-3 : Two-dimensional surface fit of Equation (IV-1) to the change in line width observed for varying concentrations of TFBC (ligand) and trypsin (protein).

As mentioned above, it is in principle also possible to determine K_D from the change in chemical shift instead of the change in line width. While both approaches are equivalent in the limit of fast exchange, there is an additional contribution to these parameters in the case of intermediate exchange rates. Figure IV-4 shows a simulation based on the Bloch equations for spin system evolution under the influence of chemical exchange.[159, 191] The parameters that were used are similar to those determined for trypsin/TFBC binding, and curves are plotted for several on-rates falling into the typical range near the diffusion limit.[187] It can be seen that in this case, the closest fit to the linear trend required for a good fit of K_D[192] is in the line width parameter for small values of p_b. The solutions to this problem clearly depend in a non-trivial way on the system parameters. Nevertheless, being based on the present experiments, the data in

Figure IV-4 appears illustrative of situations encountered in ligand binding studies. The consideration of the exchange contribution is not specific to the hyperpolarized experiment, but rather applies equally to the determination of dissociation constants by conventional NMR. However, in the hyperpolarized experiment, due to the enhanced sensitivity, the range of large p_b values becomes increasingly accessible, and the consideration of exchange effects can be more important. In the experiments of Figure IV-3, it is estimated that p_b, < 0.2, and therefore the change in line width is in the linear regime.

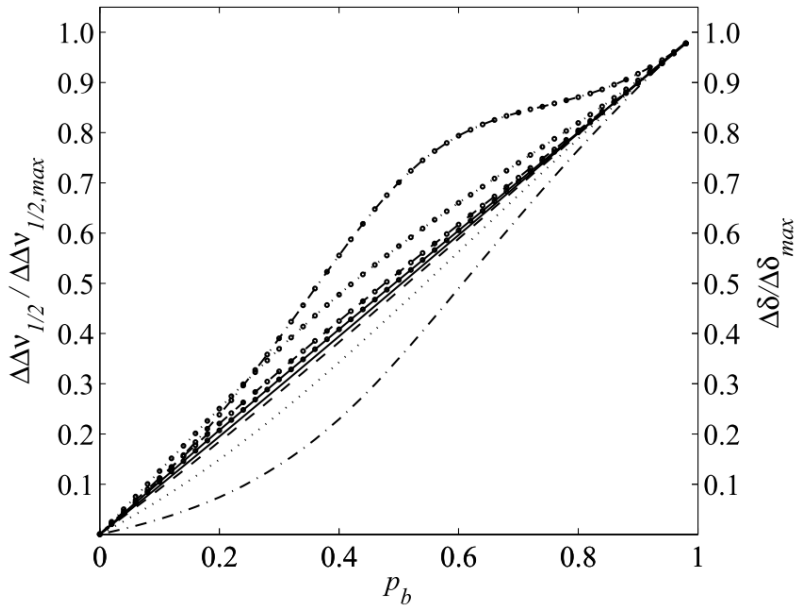

Figure IV-4 : Expected change in line width (curves above diagonal, with circle marker) and chemical shift (curves below diagonal), calculated for typical experimental conditions ($\Delta\Delta\nu_{1/2,max}$ = 300 Hz, $\Delta\delta_{max}$ = 300 Hz, K_D = 132 μM, k_{on}=10^7 (—·—), $3\cdot10^7$ (·····), 10^8 (------), $3\cdot10^8$ (——) $M^{-1}s^{-1}$.

In many respects, fluorine is an ideal target nucleus for the study of protein-ligand interactions by NMR. The high gyromagnetic ratio and 100% natural abundance of ^{19}F lead to a high signal. The chemical shift of ^{19}F is very sensitive to the local environment

of the nucleus, and to the change that occurs upon binding. The large chemical shift anisotropy of ^{19}F nuclei leads to strong line broadening at slow molecular tumbling, as *i.e.* upon binding to a protein with a long rotational correlation time.[190] Experimentally, NMR of hyperpolarized fluorine is enabled by rapid sample injection of the polarized aliquot, which counteracts the relatively short relaxation time and reduces the loss of the hyperpolarized signal prior to the NMR experiment.[169] Finally, a pharmaceutical typically contains only a small number of fluorine atoms, reducing signal overlap. Nevertheless, the same type of analysis is also applicable to the most abundant nucleus ^{1}H, which has similar NMR properties compared to ^{19}F.

In summary, here, the binding of a fluorinated ligand to trypsin as a target protein was investigated by hyperpolarized NMR. A titration of protein and ligand concentration further allowed the determination of the dissociation constant K_D. DNP hyperpolarization offers a promising route to the rapid and quantitative detection of ligand binding at low concentration, rendering also low-soluble ligands accessible to characterization by NMR. Reaching the concentration regime where a high fraction of bound ligand is present, robust detection of ligands is enabled, including strong binders with slow off-rates, which are not detected in conventional ligand observation experiments. Further, the range of accessible ligand to protein ratios is extended for determining accurate K_D values. On this basis, hyperpolarized NMR may lend itself for future inclusion into workflows for screening of protein/ligand interaction.

Polarization Transfer from Ligand to Protein

In structure-based drug design, the conformation of a ligand in the binding pocket of a protein plays a central role in the design of lead compounds. Traditionally, this information can be obtained by techniques such as crystallography, fluorescence resonance energy transfer, or NMR. In NMR, besides the determination of the entire structure of the protein-ligand complex,[159] it may be more convenient to selectively obtain structural information on the binding epitope by measurement of the transfer of magnetization between protein and ligand.[18, 193] In the saturation transfer difference (STD) experiment, the transfer of magnetization from protein to ligand is measured through the difference spectrum of the ligand with on and off resonance irradiation on the protein.[194] The signal intensity differences of the ligand are observable due to the fact that during the relatively long saturation time, the ligand binds to the protein multiple times, allowing the differences in signal intensity to accumulate. A larger difference in peak intensity means stronger interaction of the corresponding proton in the ligand with the protein. In some cases, the binding epitope of the ligand can even be reconstructed from the STD measured for each proton. A theoretical description of the STD experiment includes a treatment based on complete relaxation and conformational exchange matrices.[195] The result describes a useful method to calculate expected STD signals from hypothetical structures, correlation times, kinetic constants and concentrations of the ligand and the protein.

Apart from detection of binding and measurement of dissociation constants, it is of interest to obtain information about the binding pocket of the protein itself. Such

information would be provided by direct observation of signals from the protein. However, due to relatively broad signals observed from proteins, high concentrations are required for these experiments. Here, we propose to transfer a large polarization provided by DNP enhancement of the ligand to the protein, the signal of which in turn becomes enhanced. An additional benefit of this strategy lies in the expectation of selectivity towards enhancement of signals from spins in the binding pocket of the protein. A closer contact of a proton in the protein with the ligand results in a larger expected enhancement.

Model for Polarization Transfer from Ligand to Protein

To quantitatively understand the polarization transfer from the polarized ligand to the protein, we use a two-spin system to derive the analytical solution for signal intensity evolution in function of time. We consider a binding experiment of the ligand (*L*) to the protein (*P*),

$$L + P \underset{koff}{\overset{kon}{\rightleftarrows}} PL \qquad \text{(IV-3)}$$

To estimate the signal intensities observed in a NMR experiment, we use one spin for the ligand and the protein, respectively. Further, we assume that exchange is fast compared to chemical shift and compared to spin relaxation, and that consequently, the system is kinetically at equilibrium at all times.

The vector of signal intensities is

$$\vec{I} = \begin{pmatrix} I_L \\ I_{PL} \\ I_{LP} \\ I_P \end{pmatrix} \tag{IV-4}$$

Here, *L* is unbound ligand, *PL* is the protein when bound to ligand, *LP* is the ligand when bound to the protein, and *P* is unbound protein.

The relaxation matrix is given by

$$\boldsymbol{R} = \begin{pmatrix} \rho_L & 0 & 0 & 0 \\ 0 & \rho_{PL} & \sigma & 0 \\ 0 & \sigma & \rho_{LP} & 0 \\ 0 & 0 & 0 & \rho_P \end{pmatrix} \tag{IV-5}$$

The terms ρ are auto-relaxation rate constants for the respective species. σ is the cross-relaxation rate constant between the ligand and the protein.

The kinetic matrix[196] is

$$\boldsymbol{K} = \begin{pmatrix} k_{on}[\mathrm{P}] & 0 & -k_{off} & 0 \\ 0 & k_{off} & 0 & -k_{on}[\mathrm{L}] \\ -k_{on}[\mathrm{P}] & 0 & k_{off} & 0 \\ 0 & -k_{off} & 0 & k_{on}[\mathrm{L}] \end{pmatrix} \tag{IV-6}$$

Quantities in square brackets are concentrations, which are constant, since the system is kinetically in an equilibrium state. Using the above definitions, the time evolution of signal intensity is given by

$$\vec{I} = e^{-(\boldsymbol{K}+\boldsymbol{R})t}\,\vec{I}_0 \tag{IV-7}$$

Loosely following,[197-198] since exchange is on a faster time scale than spin relaxation, Equation (IV-7) can be simplified by finding a matrix $\boldsymbol{V}$ that diagonalizes $\boldsymbol{K}$. An explicit solution is

$$\boldsymbol{V} = \begin{pmatrix} 0 & \dfrac{k_{off}}{[\mathrm{P}]k_{on}} & 0 & -1 \\ \dfrac{[\mathrm{L}]k_{on}}{k_{off}} & 0 & -1 & 0 \\ 0 & 1 & 0 & 1 \\ 1 & 0 & 1 & 0 \end{pmatrix} \tag{IV-8}$$

Using Equation (IV-8), it is found that $\boldsymbol{K}$ has two eigenvalues that are equal to zero, such that

$$\boldsymbol{K}^{\dagger} = \boldsymbol{V}^{-1}\boldsymbol{K}\boldsymbol{V} = \begin{pmatrix} 0 & 0 & 0 & 0 \\ 0 & 0 & 0 & 0 \\ 0 & 0 & k_{off} + k_{on}[L] & 0 \\ 0 & 0 & 0 & k_{off} + k_{on}[P] \end{pmatrix} \tag{IV-9}$$

By the same transformation, $\boldsymbol{R}$ is not diagonalized:

$$\boldsymbol{R}^{\dagger} = \boldsymbol{V}^{-1}\boldsymbol{R}\boldsymbol{V} = \begin{pmatrix} \boldsymbol{R}_A & \boldsymbol{R}_B \\ \boldsymbol{R}_C & \boldsymbol{R}_D \end{pmatrix} \tag{IV-10}$$

in which $\boldsymbol{R}_A$, $\boldsymbol{R}_B$, $\boldsymbol{R}_C$ and $\boldsymbol{R}_D$ are 2×2 blocks.

Equation (IV-7) becomes

$$\vec{I} = e^{-(\boldsymbol{K}+\boldsymbol{R})t}\cdot\vec{I}_0 = \boldsymbol{V}\cdot e^{-\boldsymbol{V}^{-1}\cdot(\boldsymbol{K}+\boldsymbol{R})\cdot\boldsymbol{V}t}\cdot\boldsymbol{V}^{-1}\cdot\vec{I}_0 = \boldsymbol{V}\cdot e^{-(\boldsymbol{K}^{\dagger}+\boldsymbol{R}^{\dagger})t}\cdot\boldsymbol{V}^{-1}\cdot\vec{I}_0 \tag{IV-11}$$

The matrix exponential in Equation (IV-11) would be simplified by a second transformation that block diagonalizes $\boldsymbol{K}^{\dagger}+\boldsymbol{R}^{\dagger}$ to two 2×2 blocks. Analogous to the treatment in,[199] but with higher dimensionality, we consider $\boldsymbol{R}^{\dagger}$ as a small perturbation on $\boldsymbol{K}^{\dagger}$. As in perturbation theory,[199] we write

$$(\boldsymbol{K}^{\dagger}+\zeta\boldsymbol{R}^{\dagger})(\boldsymbol{E}+\zeta\boldsymbol{W}+\zeta^{2}\boldsymbol{W}'+\zeta^{3}\boldsymbol{W}''+...) = (\boldsymbol{E}+\zeta\boldsymbol{W}+\zeta^{2}\boldsymbol{W}'+\zeta^{3}\boldsymbol{W}''+...)(\boldsymbol{K}^{?}+\zeta\boldsymbol{D}+\zeta\ \boldsymbol{D}'+\zeta\ \boldsymbol{D}''+...) \quad \text{(IV-12)}$$

ζ is a parameter to keep track of the order, and the matrices $\boldsymbol{W}$ are the corrections to the eigenvectors of $\boldsymbol{K}^{\dagger}$. By definition, the matrices $\boldsymbol{D}$ are block diagonal, and the diagonal block elements of $\boldsymbol{W}$ are chosen to be 0. The first order correction is found by comparing the terms in ζ on both sides of Equation (IV-12).

$$\zeta(\boldsymbol{R}^{\dagger}+\boldsymbol{K}^{\dagger}\boldsymbol{W})=\zeta(\boldsymbol{W}\boldsymbol{K}^{\dagger}+\boldsymbol{D}) \quad \text{(IV-13)}$$

Writing every matrix in block form

$$\begin{pmatrix}\boldsymbol{R}_A & \boldsymbol{R}_B\\ \boldsymbol{R}_C & \boldsymbol{R}_D\end{pmatrix}+\begin{pmatrix}0 & 0\\ 0 & \boldsymbol{\Lambda}\end{pmatrix}\begin{pmatrix}0 & \boldsymbol{W}_A\\ \boldsymbol{W}_B & 0\end{pmatrix}=\begin{pmatrix}0 & \boldsymbol{W}_A\\ \boldsymbol{W}_B & 0\end{pmatrix}\begin{pmatrix}0 & 0\\ 0 & \boldsymbol{\Lambda}\end{pmatrix}+\begin{pmatrix}\boldsymbol{D}_A & 0\\ 0 & \boldsymbol{D}_B\end{pmatrix} \quad \text{(IV-14)}$$

The result shows that

$$\boldsymbol{D}_A=\boldsymbol{R}_A,\boldsymbol{D}_B=\boldsymbol{R}_D \quad \text{(IV-15)}$$

and

$$W_{Ai,j}=\boldsymbol{R}_{Bi,j}/\boldsymbol{\Lambda}_{j,j},\boldsymbol{W}_{Bi,j}=\boldsymbol{R}_{Ci,j}/\boldsymbol{\Lambda}_{i,i} \quad \text{(IV-16)(IV-17)}$$

If the elements in $\boldsymbol{\Lambda}$ are much larger than the elements of $\boldsymbol{R}$, the first order correction $\boldsymbol{W}$ to the eigenvectors is negligible. Therefore, to first order approximation of eigenvalues and zero order correction of eigenvectors,

$$exp(-(\boldsymbol{K}^{\dagger}+\boldsymbol{R}^{\dagger})t)\approx exp\left(-\left(\begin{array}{c|c}\boldsymbol{R}_A & 0\\ \hline 0 & \boldsymbol{\Lambda}+\boldsymbol{R}_D\end{array}\right)t\right)\approx exp\left(-\left(\begin{array}{c|c}\boldsymbol{R}_A & 0\\ \hline 0 & \boldsymbol{\Lambda}\end{array}\right)t\right) \quad \text{(IV-18)}$$

with

$$\boldsymbol{R}_A=(\boldsymbol{V}^{-1}\boldsymbol{R}\boldsymbol{V})_{1..2,1..2} \quad \text{(IV-19)}$$

the 2 × 2 matrix taken from the top left corner of $\boldsymbol{V}^{-1}\boldsymbol{R}\boldsymbol{V}$, then Equation (IV-7) becomes

$$\vec{I} \approx \boldsymbol{V} \cdot \left(\begin{array}{c|c} e^{-R_A t} & 0 \\ \hline 0 & e^{-\boldsymbol{\Lambda} t} \end{array} \right) \cdot \boldsymbol{V}^{-1} \cdot \vec{I}_0 \qquad \text{(IV-20)}$$

To calculate the NMR signal under fast exchange, it is necessary to sum the signals for the bound and free form of each species, since those appear at the same chemical shift. The summation can be accomplished by a transformation

$$\vec{J} = \boldsymbol{C} \cdot \vec{I} \qquad \text{(IV-21)}$$

with

$$\boldsymbol{C} = \begin{pmatrix} 1 & 0 & 1 & 0 \\ 0 & 1 & 0 & 1 \\ 0 & 0 & 1 & 0 \\ 0 & 0 & 0 & 1 \end{pmatrix} \qquad \text{(IV-22)}$$

and

$$\vec{J} = \begin{pmatrix} s_L \\ s_P \\ I_{LP} \\ I_P \end{pmatrix} \qquad \text{(IV-23)}$$

In *J*, only the first two elements are of interest, designating the NMR signal from the ligand 1 and the protein, respectively. The last two elements simply remain to complete the basis. Using Equation (IV-21),

$$\vec{J} \approx \boldsymbol{C} \cdot \boldsymbol{V} \cdot \left(\begin{array}{c|c} e^{-\boldsymbol{R}_A t} & 0 \\ \hline 0 & e^{-\boldsymbol{\Lambda} t} \end{array} \right) \cdot \boldsymbol{V}^{-1} \cdot \boldsymbol{C}^{-1} \cdot \vec{J}_0 \qquad \text{(IV-24)}$$

To calculate the matrix product in Equation (IV-24), it is convenient to write the constituents in block form:

$$\boldsymbol{C}\cdot\boldsymbol{V}=\left(\begin{array}{c|c}(\boldsymbol{CV})_{1..2,1..2} & 0\\ \hline (\boldsymbol{CV})_{3..4,1..2} & (\boldsymbol{CV})_{3..4,3..4}\end{array}\right) \tag{IV-25}$$

and

$$\boldsymbol{V}^{-1}\cdot\boldsymbol{C}^{-1}=\left(\begin{array}{c|c}(\boldsymbol{V}^{-1}\boldsymbol{C}^{-1})_{1..2,1..2} & 0\\ \hline (\boldsymbol{V}^{-1}\boldsymbol{C}^{-1})_{3..4,1..2} & (\boldsymbol{V}^{-1}\boldsymbol{C}^{-1})_{3..4,3..4}\end{array}\right) \tag{IV-26}$$

The property that the upper right block of 2×2 elements in Equations (IV-25) and (IV-26) is equal to zero appears non-trivial, but can be verified explicitly from Equations (IV-8) and (IV-22). Then,

$$\vec{J}\approx\left(\begin{array}{c|c}(\boldsymbol{CV})_{1..2,1..2}\cdot e^{-\boldsymbol{R}_A t}\cdot(\boldsymbol{V}^{-1}\boldsymbol{C}^{-1})_{1..2,1..2} & 0\\ \hline \cdots & \cdots\end{array}\right)\cdot\vec{J}_0 \tag{IV-27}$$

For obtaining the first two elements of $\vec{J}$, it is only necessary to consider the upper row of blocks in Equation (IV-27):

$$\vec{S}\approx(\boldsymbol{CV})_{1..2,1..2}\cdot e^{-\boldsymbol{R}_A t}\cdot(\boldsymbol{V}^{-1}\boldsymbol{C}^{-1})_{1..2,1..2}\cdot\vec{S}_0 \tag{IV-28}$$

with

$$\vec{S}=\begin{pmatrix}s_L\\ s_P\end{pmatrix} \tag{IV-29}$$

From Equations (IV-8) and (IV-22), it can further be found that in the basis that was used, fortuitously $\left((\boldsymbol{CV})_{1..2,1..2}\right)^{-1}=(\boldsymbol{V}^{-1}\boldsymbol{C}^{-1})_{1..2,1..2}$. In this case, Equation (IV-28) can be re-written as

$$\vec{S}\approx e^{-\boldsymbol{M}t}\cdot\vec{S}_0 \tag{IV-30}$$

with

$$\boldsymbol{M} = (\boldsymbol{CV})_{1..2,1..2} \cdot \boldsymbol{R}_A \cdot (\boldsymbol{V}^{-1}\boldsymbol{C}^{-1})_{1..2,1..2} \tag{IV-31}$$

The explicit form of $\boldsymbol{M}$ obtained using Equations (IV-8) and (IV-22) is

$$\boldsymbol{M} = \begin{pmatrix} \dfrac{k_{off}\rho_L + [\mathrm{P}]k_{on}\rho_{LP}}{k_{off} + [\mathrm{P}]k_{on}} & \dfrac{k_{off}\sigma}{k_{off} + [\mathrm{L}]k_{on}} \\ \dfrac{[\mathrm{P}]k_{on}\sigma}{k_{off} + [\mathrm{P}]k_{on}} & \dfrac{[\mathrm{L}]k_{on}\rho_P + k_{off}\rho_{PL}}{k_{off} + [\mathrm{L}]k_{on}} \end{pmatrix} \tag{IV-32}$$

Since the system is kinetically in the steady state,

$$k_{off}[\mathrm{PL}] = k_{on}[\mathrm{P}][\mathrm{L}] \tag{IV-33}$$

Consequently, *M* can be written in terms of concentrations

$$\boldsymbol{M} = \begin{pmatrix} \dfrac{[\mathrm{L1}]\rho_L + [\mathrm{PL}]\rho_{LP}}{[\mathrm{L1}] + [\mathrm{PL1}]} & \dfrac{[\mathrm{PL}]\sigma}{[\mathrm{P}] + [\mathrm{PL}]} \\ \dfrac{[\mathrm{PL}]\sigma}{[\mathrm{L}] + [\mathrm{PL}]} & \dfrac{[\mathrm{PL}]\rho_P + [\mathrm{P}]\rho_{PL}}{[\mathrm{P}] + [\mathrm{PL}]} \end{pmatrix} \tag{IV-34}$$

It may further be useful to define the parameters that describe the concentration fraction of species that are bound or unbound:

Fraction of the ligand bound to protein $$pb = \frac{[\mathrm{PL}]}{[\mathrm{PL}] + [\mathrm{L}]} \tag{IV-35}$$

Fraction of the ligand not bound to protein $$pf = \frac{[\mathrm{L}]}{[\mathrm{PL}] + [\mathrm{L}]} = 1 - pb \tag{IV-36}$$

Fraction of the protein bound to the ligand $$p_1 = \frac{[\mathrm{PL}]}{[\mathrm{P}] + [\mathrm{PL}]} \tag{IV-37}$$

Fraction of protein not bound to any ligand $$p = \frac{[\mathrm{P}]}{[\mathrm{P}] + [\mathrm{PL}]} = 1 - p_1 \tag{IV-38}$$

Then, Equation (IV-34) simplifies to

$$\boldsymbol{M} = \begin{pmatrix} pf\,\rho_L + pb\rho_{LP} & p_1\sigma_1 \\ pb_1\sigma_1 & p_1\rho_P + p\rho_{PL} \end{pmatrix} \tag{IV-39}$$

Equation (IV-39) can be written as

$$\boldsymbol{M} = \begin{pmatrix} r_L & \sigma^{**} \\ \sigma^{*} & r_{\mathrm{P}} \end{pmatrix} \tag{IV-40}$$

in which $r_L = pf \cdot \rho_{\mathrm{L}} + pb \cdot \rho_{\mathrm{LP}}$, $r_{\mathrm{P}} = p\rho_{\mathrm{P}} + p_1\rho_{\mathrm{PL}}$, as well as the off-diagonal elements $\sigma^{*} = pb \cdot \sigma$, $\sigma^{**} = p_1 \cdot \sigma$, are averages of auto relaxation rates ρ and cross relaxation rates σ, which are weighted with the concentration fractions of the corresponding species.

Additionally, since the hyperpolarization is much larger than the thermal polarization, the transferred magnetization for the whole buildup time is much smaller than the initial magnetization. In this case, the back-transfer of magnetization can be ignored, and then $\boldsymbol{M}$ becomes

$$\boldsymbol{M'} = \begin{pmatrix} r_L & 0 \\ \sigma^{*} & r_{\mathrm{P}} \end{pmatrix} \tag{IV-41}$$

In this form, $\boldsymbol{M'}$ is a triangular matrix. Since the hyperpolarization is much larger than the thermal polarization, the thermal polarization can be ignored. The initial polarization

$$\vec{s}_0 = \begin{pmatrix} s_{L,H} \\ 0 \end{pmatrix} \tag{IV-42}$$

The analytical solutions to Equation (IV-30) are considerably simplified, such that

$$s_{\mathrm{L}}(t) = s_{\mathrm{L,H}} \cdot e^{-r_L \cdot t} \tag{IV-43}$$

$$s_P(t) = \frac{(e^{-r_L \cdot t} - e^{-r_P \cdot t}) \cdot \sigma^{*} \cdot s_{\mathrm{L,H}}}{r_L - r_{\mathrm{P}}} \tag{IV-44}$$

In this treatment, r_L is the relaxation rate of the ligand in the presence of the protein, and r_P also includes the effects of spin diffusion in the protein.

Experimental Data

Experiments were performed to observe this polarization transfer from DNP polarized benzamidine to trypsin. An aliquot of 0.9 μL 400 mM benzamidine was hyperpolarized on protons, dissolved and injected into an NMR tube that was pre-loaded with 25 μL 1.5 mM trypsin. After a total delay of 1.5 s following mixing, a ^{1}H NMR spectrum was acquired (Figure IV-5). It can be seen that, compared with the spectrum of trypsin without hyperpolarized benzamidine, several peaks are enhanced. A maximum enhancement of ~9 fold was determined for the peak at 1.1 ppm.

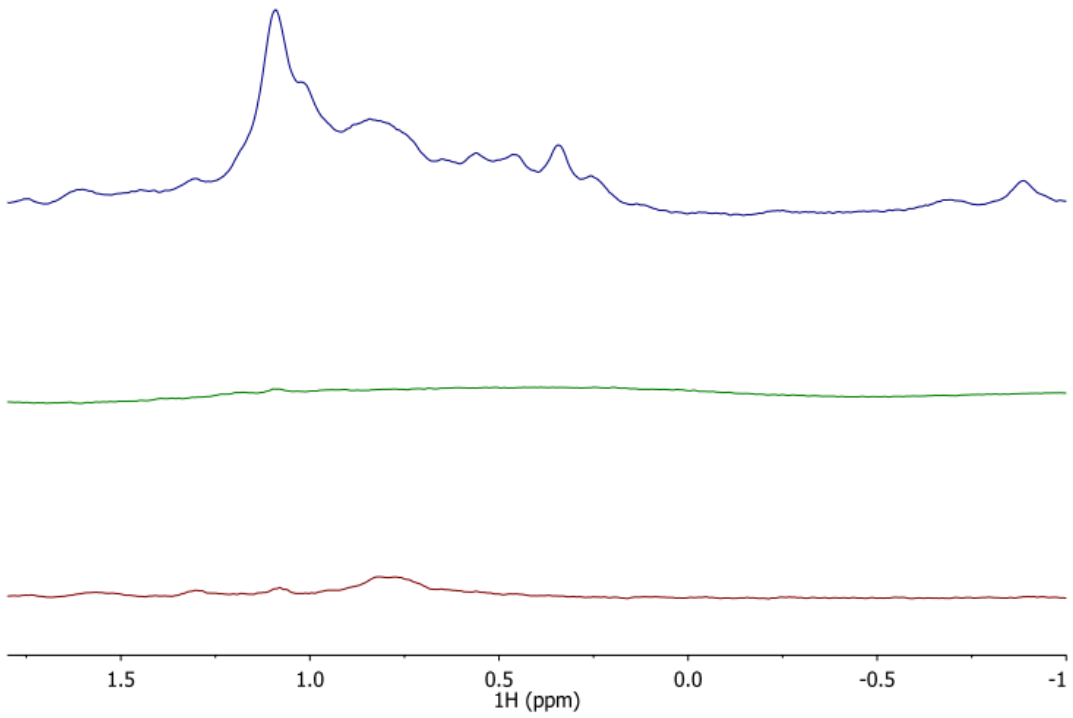

Figure IV-5 : ^{1}H spectra of trypsin. top: 80 μM trypsin with 320 μM polarized benzamidine; middle: 320 μM polarized benzamidine; bottom: 80 μM trypsin.

From Equation (IV-44), the signal intensity of the transferred polarization is related to the intermolecular cross relaxation rate. The cross relaxation rate is measuring the proximity of the ligand and the protein. In the present experiments, knowledge of the assignments of the selectively enhanced protein signals will potentially give additional information on the binding process.

Interligand Polarization Transfer

An interesting extension of the experiment described in the previous section lies in the transfer of the magnetization on the protein to another ligand in a second step. The protein is then still included in polarization flow, but the spectra are simplified because a

small molecule, the second ligand, is observed. Recently, the magnetization transfer between two competitively binding ligands mediated by the protein was used to determine the relative orientation of the two ligands in the binding pocket.[200-204] In these experiments, termed “Interligand Polarization Transfer for Pharmacophore Mapping” (INPHARMA), the magnetization of one ligand transfers to the protein in the initial binding step. Subsequently, it transfers to the other ligand in a second binding step. Correlations between ligand signals due to the transferred magnetization contain information on the relative orientation of these two ligands.[202, 204]

Since this process requires two intermolecular NOE transfer steps,[205] the transfer efficiency, and concomitantly, the sensitivity of this experiment is low. The signal enhancement provided by dissolution DNP can potentially compensate the low signal intensities. Starting with a first ligand that is DNP polarized, the protein mediated transfer of this hyperpolarization to the other ligand can be observed. The polarization transfer process in the DNP based experiment differs from that with thermal polarization in several aspects. Firstly, in the DNP experiment, the spin polarization is not at equilibrium. Secondly, a stronger than thermal polarization of the non-polarized ligand is observed, which allows neglecting thermal polarization. To better understand the experiment with DNP enhancement, a theoretical model of the polarization transfer process is presented here. Calculations of the transfer efficiencies for a protein/ligand system that includes protein kinase A are then preformed.[202]

Model for the Two-Step Intermolecular Polarization Transfer

To obtain the expression for the two-step intermolecular polarization transfer, we use a three-spin system to derive the analytical solution for signal intensity evolution in a competitive binding experiment. The derivation is an extension to the previously discussed one-step intermolecular polarization transfer.

We consider a competitive binding experiment of two ligands ($L1$ and $L2$) to a protein (P). For the polarization evolution, we use one spin in each species, and an assumption of fast exchange.

$$L1 + P \underset{koff\,1}{\overset{kon1}{\rightleftharpoons}} PL1 \tag{IV-45}$$

$$L2 + P \underset{koff\,2}{\overset{kon2}{\rightleftharpoons}} PL2 \tag{IV-46}$$

The vector of signal intensities extends to include 7 elements:

$$\vec{I} = \begin{pmatrix} I_{L1} \\ I_{L2} \\ I_{PL1} \\ I_{L1P} \\ I_{PL2} \\ I_{L2P} \\ I_{P} \end{pmatrix} \tag{IV-47}$$

Here, $L1$ is unbound ligand 1, $L2$ is unbound ligand 2, $PL1$ is the protein when bound to ligand 1, $L1P$ is ligand 1 when bound to protein, $PL2$ is protein when bound to ligand 2, $L2P$ is ligand 2 when bound to protein, and P is unbound protein.

The relaxation matrix becomes

$$\boldsymbol{R} = \begin{pmatrix} \rho_{L1} & 0 & 0 & 0 & 0 & 0 & 0 \\ 0 & \rho_{L2} & 0 & 0 & 0 & 0 & 0 \\ 0 & 0 & \rho_{PL1} & \sigma_1 & 0 & 0 & 0 \\ 0 & 0 & \sigma_1 & \rho_{L1P} & 0 & 0 & 0 \\ 0 & 0 & 0 & 0 & \rho_{PL2} & \sigma_2 & 0 \\ 0 & 0 & 0 & 0 & \sigma_2 & \rho_{L2P} & 0 \\ 0 & 0 & 0 & 0 & 0 & 0 & \rho_P \end{pmatrix} \quad \text{(IV-48)}$$

The terms ρ are auto-relaxation rate constants for the respective species. σ_1 is the cross-relaxation rate constant between ligand 1 and protein, and σ_2 the cross-relaxation rate constant between ligand 2 and protein.

The kinetic matrix is

$$\boldsymbol{K} = \begin{pmatrix} k_{on1}[\mathrm{P}] & 0 & 0 & -k_{off1} & 0 & 0 & 0 \\ 0 & k_{on2}[\mathrm{P}] & 0 & 0 & 0 & -k_{off2} & 0 \\ 0 & 0 & k_{off1} & 0 & 0 & 0 & -k_{on1}[\mathrm{L1}] \\ -k_{on1}[\mathrm{P}] & 0 & 0 & k_{off1} & 0 & 0 & 0 \\ 0 & 0 & 0 & 0 & k_{off2} & 0 & -k_{on2}[\mathrm{L2}] \\ 0 & -k_{on2}[\mathrm{P}] & 0 & 0 & 0 & k_{off2} & 0 \\ 0 & 0 & -k_{off1} & 0 & -k_{off2} & 0 & \left(k_{on1}[\mathrm{L1}] + k_{on2}[\mathrm{L2}]\right) \end{pmatrix} \quad \text{(IV-49)}$$

The time evolution of signal intensity is still given by Equation (IV-7). This equation is simplified in the same way as described above. The matrix $\boldsymbol{V}$, which diagonalizes $\boldsymbol{K}$, is

$$\boldsymbol{V} = \begin{pmatrix} 0 & 0 & \frac{koff_1}{[\mathrm{P}]kon_1} & -1 & 0 & 0 & 0 \\ 0 & \frac{koff_2}{[\mathrm{P}]kon_2} & 0 & 0 & -1 & 0 & 0 \\ \frac{[\mathrm{L1}]kon_1}{koff_1} & 0 & 0 & 0 & 0 & \frac{-a_1+b}{a_2-b} & \frac{-a_1-b}{a_2+b} \\ 0 & 0 & 1 & 1 & 0 & 0 & 0 \\ \frac{[\mathrm{L2}]kon_2}{koff_2} & 0 & 0 & 0 & 0 & \frac{-2[\mathrm{L2}]kon_2}{a_2-b} & \frac{-2[\mathrm{L2}]kon_2}{a_2+b} \\ 0 & 1 & 0 & 0 & 1 & 0 & 0 \\ 1 & 0 & 0 & 0 & 0 & 1 & 1 \end{pmatrix} \tag{IV-50}$$

with

$$a_1 = koff_1 - koff_2 + [\mathrm{L1}]kon_1 - [\mathrm{L2}]kon_2 \tag{IV-51}$$

$$a_2 = koff_1 - koff_2 + [\mathrm{L1}]kon_1 + [\mathrm{L2}]kon_2 \tag{IV-52}$$

$$b = \sqrt{(koff_1 + koff_2 + [\mathrm{L1}]kon_1 + [\mathrm{L2}]kon_2)^2 - 4([\mathrm{L1}]koff_2 kon_1 + koff_1(koff_2 + [\mathrm{L2}]kon_2))} \tag{IV-53}$$

It is found that $\boldsymbol{K}$ has three eigenvalues that are equal to zero, such that

$$\boldsymbol{K}^{\dagger} = \boldsymbol{V}^{-1}\boldsymbol{K}\boldsymbol{V} = \begin{pmatrix} 0 & & & & & & \\ & 0 & & & 0 & & \\ & & 0 & & & & \\ & & & \lambda_1 & & & \\ & & & & \lambda_2 & & \\ & 0 & & & & \lambda_3 & \\ & & & & & & \lambda_4 \end{pmatrix} = \begin{pmatrix} 0 & 0 \\ 0 & \boldsymbol{\Lambda} \end{pmatrix} \tag{IV-54}$$

By the same transformation, *R* is not diagonalized:

$$\boldsymbol{R}^{\dagger} = \boldsymbol{V}^{-1}\boldsymbol{R}\boldsymbol{V} = \begin{pmatrix} \boldsymbol{R}_A & \boldsymbol{R}_B \\ \boldsymbol{R}_C & \boldsymbol{R}_D \end{pmatrix} \tag{IV-55}$$

in which $\boldsymbol{R}_A$ is a 3×3 block, $\boldsymbol{R}_B$ a 3×4 block, $\boldsymbol{R}_C$ a 4×3 block, and $\boldsymbol{R}_D$ a 4×4 block. Using perturbation theory as above, and the summation matrix

$$\boldsymbol{C} = \begin{pmatrix} 1 & 0 & 0 & 1 & 0 & 0 & 0 \\ 0 & 1 & 0 & 0 & 0 & 1 & 0 \\ 0 & 0 & 1 & 0 & 1 & 0 & 1 \\ 0 & 0 & 0 & 1 & 0 & 0 & 0 \\ 0 & 0 & 0 & 0 & 1 & 0 & 0 \\ 0 & 0 & 0 & 0 & 0 & 1 & 0 \\ 0 & 0 & 1 & 0 & 0 & 0 & 0 \end{pmatrix}, \tag{IV-56}$$

the time evolution of

$$\vec{J} = \begin{pmatrix} s_{L1} \\ s_{L2} \\ s_P \\ I_{L1P} \\ I_{PL2} \\ I_{L2P} \\ I_{PL1} \end{pmatrix} \tag{IV-57}$$

is obtained. In *J*, only the first three elements are of interest, designating the NMR signal from ligand 1, ligand 2, and protein, respectively. The evolution of the signal intensities

$$\vec{S} = \begin{pmatrix} s_{L1} \\ s_{L2} \\ s_P \end{pmatrix} \tag{IV-58}$$

is then expressed by

$$\vec{S} \approx e^{-\boldsymbol{M}t} \cdot \vec{S}_0 \tag{IV-59}$$

with

$$\boldsymbol{M} = \begin{pmatrix} \dfrac{koff_1\rho_{L1} + [\mathrm{P}]kon_1\rho_{L1P}}{koff_1 + [\mathrm{P}]kon_1} & 0 & \dfrac{[\mathrm{L1}]kon_1koff_2\sigma_1}{[\mathrm{L1}]kon_1koff_2 + koff_1koff_2 + [\mathrm{L2}]kon_2koff_1} \\ 0 & \dfrac{koff_2\rho_{L2} + [\mathrm{P}]kon_2\rho_{L2P}}{koff_2 + [\mathrm{P}]kon_2} & \dfrac{[\mathrm{L2}]koff_1kon_2\sigma_2}{[\mathrm{L1}]kon_1koff_2 + koff_1koff_2 + [\mathrm{L2}]kon_2koff_1} \\ \dfrac{[\mathrm{P}]kon_1\sigma_1}{koff_1 + [\mathrm{P}]kon_1} & \dfrac{[\mathrm{P}]kon_2\sigma_2}{koff_2 + [\mathrm{P}]kon_2} & \dfrac{[\mathrm{L1}]kon_1koff_2\rho_{PL1} + koff_1koff_2\rho_P + [\mathrm{L2}]kon_2koff_1\rho_{PL2}}{[\mathrm{L1}]kon_1koff_2 + koff_1koff_2 + [\mathrm{L2}]kon_2koff_1} \end{pmatrix} \tag{IV-60}$$

Since the system is kinetically in the steady state,

$$koff_1[\mathrm{PL1}] = kon_1[\mathrm{P}][\mathrm{L1}] \tag{IV-61}$$

and

$$koff_2[\mathrm{PL2}] = kon_2[\mathrm{P}][\mathrm{L2}] \tag{IV-62}$$

Consequently, as above, $\boldsymbol{M}$ can be written in terms of concentrations

$$\boldsymbol{M} = \begin{pmatrix} \dfrac{[\mathrm{L1}]\rho_{L1} + [\mathrm{PL1}]\rho_{L1P}}{[\mathrm{L1}] + [\mathrm{PL1}]} & 0 & \dfrac{[\mathrm{PL1}]\sigma_1}{[\mathrm{P}] + [\mathrm{PL1}] + [\mathrm{PL2}]} \\ 0 & \dfrac{[\mathrm{L2}]\rho_{L2} + [\mathrm{PL2}]\rho_{L2P}}{[\mathrm{L2}] + [\mathrm{PL2}]} & \dfrac{[\mathrm{PL2}]\sigma_2}{[\mathrm{P}] + [\mathrm{PL1}] + [\mathrm{PL2}]} \\ \dfrac{[\mathrm{PL1}]\sigma_1}{[\mathrm{L1}] + [\mathrm{PL1}]} & \dfrac{[\mathrm{PL2}]\sigma_2}{[\mathrm{L2}] + [\mathrm{PL2}]} & \dfrac{[\mathrm{P}]\rho_P + [\mathrm{PL1}]\rho_{PL1} + [\mathrm{PL2}]\rho_{PL2}}{[\mathrm{P}] + [\mathrm{PL1}] + [\mathrm{PL2}]} \end{pmatrix} \tag{IV-63}$$

Defining the parameters that describe the concentration fractions of species that are bound or unbound:

Fraction of ligand 1 bound to protein $$pb_1 = \frac{[\mathrm{PL1}]}{[\mathrm{PL1}] + [\mathrm{L1}]} \tag{IV-64}$$

Fraction of ligand 1 not bound to protein $$pf_1 = \frac{[\mathrm{L1}]}{[\mathrm{PL1}] + [\mathrm{L1}]} = 1 - pb_1 \tag{IV-65}$$

Fraction of ligand 2 bound to protein $$pb_2 = \frac{[\mathrm{PL2}]}{[\mathrm{PL2}] + [\mathrm{L2}]} \tag{IV-66}$$

Fraction of ligand 2 not bound to protein $$pf_2 = \frac{[\mathrm{L2}]}{[\mathrm{PL2}] + [\mathrm{L2}]} = 1 - pb_2 \tag{IV-67}$$

Fraction of protein bound to ligand 1 $$p_1 = \frac{[\mathrm{PL1}]}{[\mathrm{P}]+[\mathrm{PL1}]+[\mathrm{PL2}]} \quad \text{(IV-68)}$$

Fraction of protein bound to ligand 2 $$p_2 = \frac{[\mathrm{PL2}]}{[\mathrm{P}]+[\mathrm{PL1}]+[\mathrm{PL2}]} \quad \text{(IV-69)}$$

Fraction of protein not bound to any ligand $$p = \frac{[\mathrm{P}]}{[\mathrm{P}]+[\mathrm{PL1}]+[\mathrm{PL2}]} = 1 - p_1 - p_2 \quad \text{(IV-70)}$$

Then, Equation (IV-63) simplifies to

$$\boldsymbol{M} = \begin{pmatrix} pf_1\rho_{L1} + pb_1\rho_{L1P} & 0 & p_1\sigma_1 \\ 0 & pf_2\rho_{L2} + pb_2\rho_{L2P} & p_2\sigma_2 \\ pb_1\sigma_1 & pb_2\sigma_2 & p\rho_P + p_1\rho_{PL1} + p_2\rho_{PL2} \end{pmatrix} \quad \text{(IV-71)}$$

Equation (IV-71) can be written as

$$\boldsymbol{M} = \begin{pmatrix} r_1 & \sigma_1^{**} & 0 \\ \sigma_1^{*} & r_\mathrm{P} & \sigma_2^{*} \\ 0 & \sigma_2^{**} & r_2 \end{pmatrix} \quad \text{(IV-72)}$$

in which $r_1 = pf_1\rho_{\mathrm{L1}} + pb_1\rho_{\mathrm{L1P}}$, $r_2 = pf_2\rho_{\mathrm{L2}} + pb_2\rho_{\mathrm{L2P}}$, $r_\mathrm{P} = p\rho_\mathrm{P} + p_1\rho_{\mathrm{PL1}} + p_2\rho_{\mathrm{PL2}}$, as well as the off-diagonal elements $\sigma_1^{*} = pb_1\sigma_1$, $\sigma_1^{**} = p_1\sigma_1$, $\sigma_2^{*} = pb_2\sigma_2$, $\sigma_2^{**} = p_2\sigma_2$, are averages of auto relaxation rates ρ and cross relaxation rates σ, which are weighted with the concentration fractions of the corresponding species.

From Equation (IV-71), it can be seen most clearly that the evolution of NMR signal in Equation (IV-59) is governed by rate constants, which consist of the auto- and cross-relaxation rates of the individual species weighted by the corresponding concentration fractions.

Binding Kinetics

If the signal from ligand L_1 is hyperpolarized, whereas the polarization of the protein P and ligand L_2 are from Boltzmann magnetization, initial conditions are

$$\vec{I}(0) = \begin{pmatrix} I_{\mathrm{L1,H}} \\ I_{\mathrm{L2,B}} \\ I_{\mathrm{P,B}} \end{pmatrix} \tag{IV-73}$$

According to Equation (IV-59), the signal evolution is

$$\vec{I}(t) = \begin{pmatrix} I_{\mathrm{L1}}(t) \\ I_{\mathrm{L2}}(t) \\ I_{\mathrm{P}}(t) \end{pmatrix} = e^{-\boldsymbol{M}\cdot t} \cdot \vec{I}(0) \tag{IV-74}$$

Additionally, since the hyperpolarization is much larger than the thermal polarization, the back-transfer of magnetization can again be ignored. Then, $\boldsymbol{M}$ becomes

$$\boldsymbol{M}' = \begin{pmatrix} r_1 & 0 & 0 \\ 0 & r_2 & \sigma_2^{**} \\ \sigma_1^{*} & 0 & r_{\mathrm{P}} \end{pmatrix} \tag{IV-75}$$

This matrix simplified to a 2×2 matrix in Equation (IV-41) if the second ligand does not exist.

In this form, and the analytical solutions to Equation (IV-74) are considerably simplified, such that

$$I_{\mathrm{L1}}(t) = I_{\mathrm{L1,H}} \cdot \exp(-r_1 \cdot t) \tag{IV-76}$$

$$I_{\mathrm{L2}}(t) = -\frac{(r_1 - r_2)\cdot\exp(-r_{\mathrm{P}}\cdot t) + (r_2 - r_{\mathrm{P}})\cdot\exp(-r_1\cdot t) + (r_{\mathrm{P}} - r_1)\cdot\exp(-r_2\cdot t)}{(r_1 - r_2)\cdot(r_2 - r_{\mathrm{P}})\cdot(r_{\mathrm{P}} - r_1)}\sigma_1^{*}\cdot\sigma_2^{**}\cdot I_{\mathrm{L1,H}} \tag{IV-77}$$

Equations (IV-76) and (IV-77) are valid in the absence of radio-frequency pulses. For experimental measurement of I_{L1} and I_{L2}, however, it is desirable to obtain the buildup of signal from a single hyperpolarized sample. This can be achieved by applying a series of small flip angle pulses to the sample, each followed by data acquisition. A RF pulse with flip angle α converts a fraction $\sin(\alpha)$ of the total longitudinal magnetization

into a coherence for detection. A fraction $\beta=cos(\alpha)$ of the longitudinal magnetization is preserved for following scans. Additionally, in the dissolution DNP experiment, depending on the conditions for sample injection prior to the NMR experiment, mixing between the sample inside and outside the active coil region can result in a factor β' that is larger than β.[206] The experimental signal intensities of the k^{th} scan then become:

$$s_{\mathrm{L1}}^{k} = I_{\mathrm{L1,H}} \cdot \exp(-r_1 \cdot t) \cdot \prod_{i}^{k-1} \beta_i^{'} \cdot sin\alpha \tag{IV-78}$$

$$s_{\mathrm{L2}}^{k} = -\frac{(r_1 - r_2)\exp(-r_{\mathrm{P}}t) + (r_2 - r_{\mathrm{P}})\exp(-r_1 t) + (r_{\mathrm{P}} - r_1)\exp(-r_2 t)}{(r_1 - r_2)\cdot(r_2 - r_{\mathrm{P}})\cdot(r_{\mathrm{P}} - r_1)} \sigma_1^{*}\sigma_2^{**} I_{\mathrm{L1,H}} \prod_{i}^{k-1} \beta_i^{'} sin\alpha \tag{IV-79}$$

where β_i' is the fraction of polarization lost in scan i. The additional terms containing α and β, which are introduced due to the experiment, cancel if considering the relative signal intensity

$$s_{\mathrm{L2,rel}} = s_{\mathrm{L2}} / s_{\mathrm{L1}} \tag{IV-80}$$

If Equation (IV-80) is expanded for small times t, a quadratic dependence

$$s_{\mathrm{L2,rel}} = \frac{1}{2}\sigma_1^{*} \cdot \sigma_2^{**} \cdot t^2 = \frac{1}{2} pb_1 \cdot p_2 \cdot \sigma_1 \cdot \sigma_2 \cdot t^2 \tag{IV-81}$$

is found. Further, in the limit that $r_{\mathrm{P}} >> r_1$, r_2 and $r_1 \approx r_2$, Equation (IV-81) can be simplified to

$$s_{\mathrm{L2,rel}} = \frac{\sigma_1^{*} \cdot \sigma_2^{**} \cdot t}{r_{\mathrm{P}}} = \frac{pb_1 \cdot p_2 \cdot \sigma_1 \cdot \sigma_2 \, t}{p\rho_{\mathrm{P}} + p_1\rho_{\mathrm{PL1}} + p_2\rho_{\mathrm{PL2}}} \tag{IV-82}$$

predicting a linear dependence of the signal on time, which also holds for longer times.

Equations (IV-81) and (IV-82) illustrate that the transferred signal is proportional to the product of both cross relaxation rates. Since the cross relaxation rates depend on the distances of the proton in a ligand to the protons in the protein, a more efficient transfer indicates a closer contact. For Equation (IV-82), it should be noted that, since r_1 and r_2 are averages of bound and free relaxation rates, the condition $r_1 \approx r_2$ would be fulfilled if the fraction of bound state is similar for ligand 1 and ligand 2.

Simulation of Transferred Polarization

In order to test the feasibility of this experiment, as well as validate the simplified equations, numerical calculations were carried out using Equations (IV-48)(IV-49)(IV-7) ("7×7 matrix"), as well as using Equations(IV-72) and (IV-74) ("3×3 matrix"). These simulations are compared with results from Equations (IV-76) and (IV-77) (equation). For the simulations, experimental parameters close to those expected for the two ligands 3-(4-Pyridyl)indazole and 5-benzyl-2,5-dihydrothiazol-2-amine binding to protein kinase A were chosen.[202]

The primary parameters used in the simulations were:

Total concentrations – c_{L1} = 448 μM, c_{L2} = 329 μM, c_P = 19 μM

Kinetic parameters for the binding of ligand 1 or 2 to protein – $kon_1 = kon_2 = 1 \times 10^8$ M^{-1} s^{-1} = 100 μM^{-1} s^{-1}, $koff_1$ = 300 s^{-1}, $koff_2$ = 400 s^{-1}.

Auto relaxation rates of protein and protein bound ligands – $\rho_P = \rho_{PL1} = \rho_{PL2} = \rho_{L1P} = \rho_{L2P}$ = 8 s^{-1}

Auto relaxation rates of free ligands – ρ_1 = 0.25 s^{-1}, ρ_2 = 0.25 s^{-1}

Cross relaxation rates between ligand 1 or 2 and protein – $\sigma_1 = \sigma_2$ = -1.4 s^{-1}

The derived parameters are:

Equilibrium concentrations – [L1] = 436 μM, [L2] = 322 μM, [PL1] = 12.2 μM, [PL2] = 6.75 μM, [P] = 0.0838 μM

Dissociation constants for binding of ligand 1 and 2 to protein – K_{D1} = 3 μM, K_{D2} = 4 μM

Fractions of free and bound ligand – pb_1 = 0.027, pb_2 = 0.021, pf_1 = 0.97, pf_2 = 0.98

Fractions of free and bound protein – p = 0.0044, p_1 = 0.64, p_2 = 0.36

Apparent auto relaxation rates for ligand and protein – r_1 = 0.46 s^{-1}, r_2 = 0.41 s^{-1}, r_P =8 s^{-1}

Apparent cross relaxation rates between ligand 1 or 2 and protein – σ_1^* = -0.038 s^{-1}, σ_1^{**} = -0.90 s^{-1}, σ_2^* = -0.029 s^{-1}, σ_2^{**} = -0.50 s^{-1}

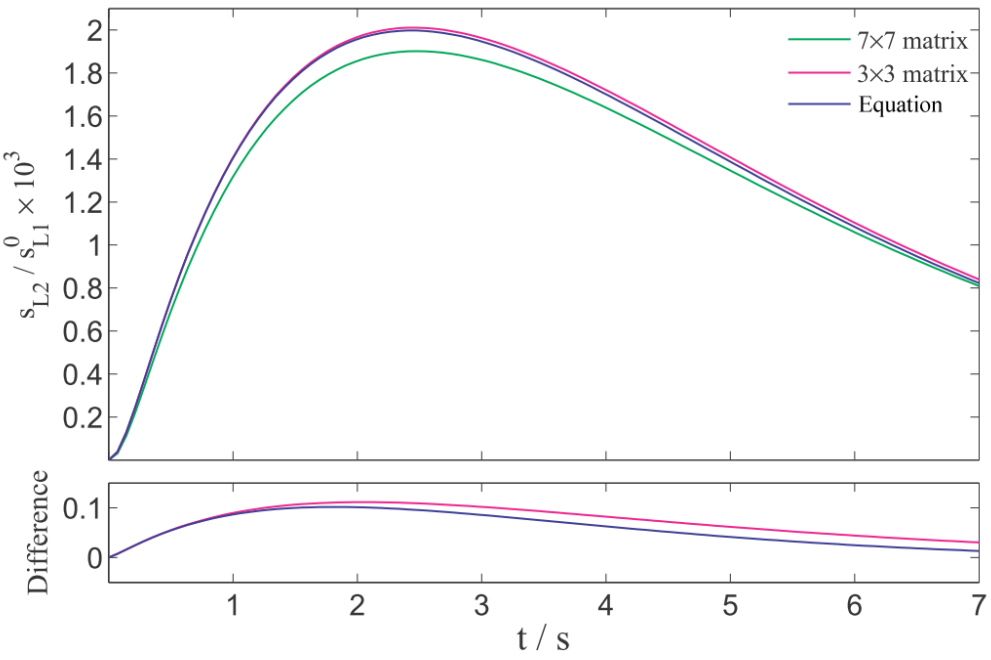

Figure IV-6 : Simulated signal intensities of L_2 with the 7×7 evolution matrix, 3×3 evolution matrix and Equation IV-77. In the 7×7 evolution matrix method, $s_{L1} = I_{L1} + I_{L1P}$, $s_{L2} = I_{L2} + I_{L2P}$. The lower panel shows the difference from the 7×7 evolution matrix method.

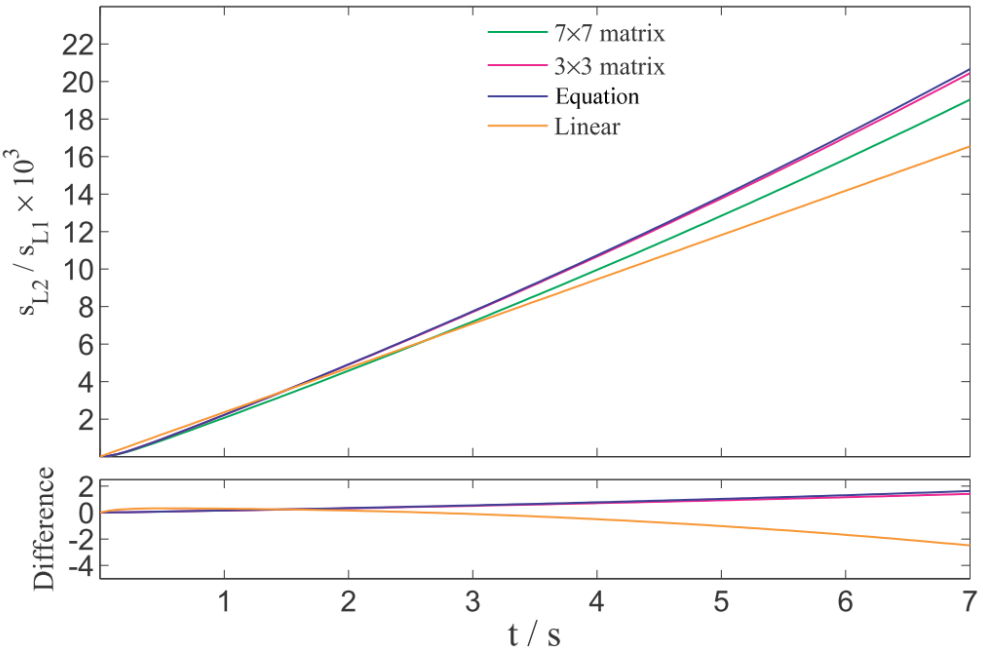

Figure IV-7 : Simulated signal intensities of L_2 relative to the signal intensity of L_1 with the 7×7 evolution matrix, 3×3 evolution matrix, and Equations IV-76 and IV-77. The lower panel shows the difference from the calculation using the 7×7 evolution matrix.

From Figure IV-6 and Figure IV-7, it can be seen that the simulated signal intensities by different methods are very close, validating the simplification in deriving the equations.

In order to illustrate that the treatments of the dynamic system by the seven-dimensional and three-dimensional matrix equations are equivalent under fast kinetics, Figure IV-8 and Figure IV-9 show simulations using the same parameters as above, except with all kinetic constants increased by 100 fold.

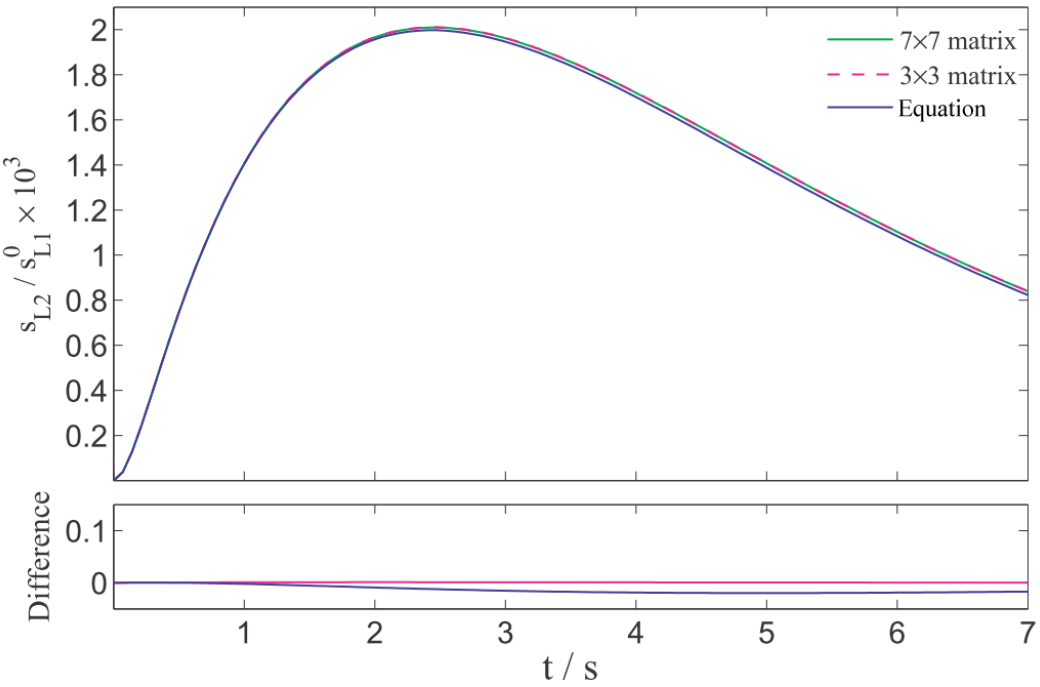

Figure IV-8 : Same plot as in Figure IV-6, except that all kinetic parameters are increased 100-fold.

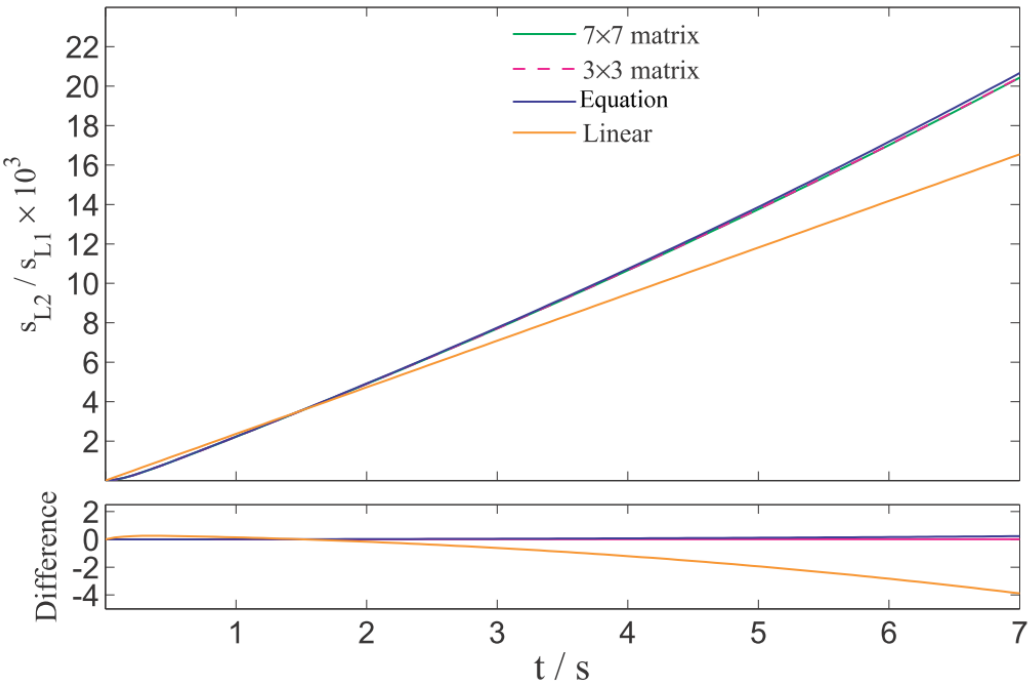

Figure IV-9 : Same plot as in Figure IV-7, except that all kinetic parameters are increased 100-fold.

Comparing Figure IV-8 and Figure IV-9 with Figure IV-6 and Figure IV-7, with faster kinetics, the differences between the 7×7 evolution matrix, 3×3 evolution matrix, and Equations IV-76 and IV-77 are smaller, validating the fast exchange assumption.

Conclusions

In summary, methods for the study of protein-ligand interactions by DNP enhanced NMR have been discussed. Using ^{19}F polarized TFBC, the binding of this ligand to the protease trypsin was detected by observation of line width and chemical shift changes. The dissociation constant was determined by a titration of ligand concentration. In these ligand detected experiments, the signal enhancement provided by DNP polarization enables the use of low ligand concentration, which provides for reliable detection of binding even in the limit of slow exchange.

Potentially, additional information is available from protein detected experiments. A model for describing the transfer of polarization from a hyperpolarized ligand to a protein was developed. Experimentally, when ^{1}H polarized benzamidine was mixed with trypsin, the proton signal of trypsin was selectively enhanced. Presumably, the resonances showing greatest enhancement stem from sites in or near the binding pocket. Further experiments to assign these enhanced peaks would provide additional information on the structure of the binding motif.

In the case of two competitively binding ligands, the observation of protein mediated interligand polarization transfer presents an alternative strategy for characterizing the binding process. A model to describe an experiment starting with a

large hyperpolarization on one ligand, which is transferred to a second ligand, was derived. The magnitude of the buildup rate for magnetization of the receiving ligand is a function of the contact between individual spins on the receiving ligand and the protein, and has the potential to provide structural information on the binding epitope.

CHAPTER V

GENERAL CONCLUSIONS

Dissolution DNP, by converting electron to nuclear spin polarization at lower than liquid helium temperature, affords several orders of magnitude in signal enhancement for liquid state NMR. This versatile technique enables polarization of various nuclei, including ^{1}H, ^{13}C, ^{15}N and ^{19}F, and works efficiently in most small molecules. The high signal intensity obtained in NMR spectra of DNP polarized substances enables to carry out traditionally insensitive NMR experiments, to study mass-limited or insoluble compounds at low concentration, and to work with molecules without isotope enrichment. Additionally, tracking of spin hyperpolarization in non-equilibrium processes can yield unique information on mechanisms and dynamics. Still, challenges remain for dissolution DNP enhanced NMR. The generation of hyperpolarization is a one-time process, and the hyperpolarization decays with a characteristic spin-lattice relaxation time constant. Secondly, in spin-tracking experiments, the quantitative signal intensities of the chemical species are both dependent on the relaxation process and kinetics. In this dissertation, methodologies have been developed to overcome some of these limitations in applying dissolution DNP to the study of molecules and chemical processes. In particular, the effects of spin relaxation have been discussed.

A scheme to acquire HMQC spectra from a single DNP polarized sample was developed. In this experiment, a series of variable small flip angle pulses utilize a portion of the hyperpolarization in each scan, while the remaining hyperpolarization is preserved as longitudinal magnetization for future scans. The indirect spectral dimension

is acquired sequentially, similar to a conventional HMQC pulse sequence. To evenly distribute the hyperpolarization over multiple scans, the spin relaxation is taken into account in the design of the small flip angle series. The resulting pulse sequence is robust and easy to implement. Its applicability was demonstrated using analytes of sub-millimolar concentration at natural abundance of ^{13}C, corresponding to less than ~10 μM of NMR active species.

By removing the need for signal averaging, DNP enables the investigation of non-equilibrium chemical processes by NMR with a time resolution given by the NMR acquisition time of each scan, on the order of 100 ms. The use of DNP enhanced ^{1}H NMR for the study of chemical reactions was demonstrated with a Diels-Alder reaction. ^{1}H is the most sensitive nucleus, highly abundant and readily polarizable. However, it is prone to fast spin lattice relaxation and cross relaxation, due to dipolar interactions with neighboring protons. A model to describe the signal evolution of the chemical species, which takes into account the kinetics, as well as auto- and cross- relaxation, was derived. From a fit of this model to the experimentally observed evolution of signal intensities, the rate constant for the Diels Alder reaction and the auto- and cross- relaxation rates of spins in the reaction product were determined quantitatively. This experimental scheme and theoretical framework outlines an approach that can be used to determine the kinetics of reactions completed within the time frame of spin relaxation. In order to overcome the limitation imposed by the fast relaxation of ^{1}H, the ^{1}H spins can be kept in the singlet state, which is unaffected by the main relaxation mechanism of dipole-dipole interaction. A singlet state prepared in DNP polarized p-chlorobenzaldehyde showed a

decay time constant about 7 times a long as the spin-lattice relaxation time, illustrating the potential of using the singlet state for extending the time window of this type of experiment.

Just as reaction kinetics and spin relaxation drive the evolution of polarization in a non-equilibrium process, chemical exchange and intermolecular NOEs determine its distribution under chemical equilibrium. This effect provides information about protein ligand interaction, which is often needed for drug discovery. Experiments were presented to determine whether a ligand binds to the protein. Using DNP polarized fluorinated small molecules, the line width and chemical shift change upon addition of protein was observed. The dissociation constant could be determined by titration of the ligand concentration. In addition to the determination of binding, information about the binding epitope can potentially be obtained from polarization transfer between ligand and protein. A model describing this polarization transfer was presented. In an experiment, where DNP polarized benzamidine was mixed with trypsin, signals of the protein were enhanced through intermolecular cross relaxation. Finally, the model describing polarization transfer was extended to include protein mediated polarization transfer between two competitively binding ligands. The results indicate that the buildup rate of polarization for each proton on the receiving ligand is proportional to the intermolecular cross relaxation rate with the protein. This cross-relaxation rate potentially contains structural information.

The work presented in this dissertation is intended to illustrate some of the powerful applications of dissolution DNP based NMR. Benefitting from the high signal intensities,

the evolution polarization, both in chemical reactions and at equilibrium, is studied with a time resolution that equals the single scan NMR acquisition time. The effects of kinetics, spin relaxation, chemical exchange and intermolecular NOEs were investigated experimentally and theoretically, showing that their quantitative interpretation can yield a variety of information on the underlying chemical processes.

REFERENCES

1. Ernst, R. R. *Angew. Chem. Int. Ed.* **1992**, *31*, 805-823.
2. Carver, T. R., Slichter, C. P. *Phys. Rev.* **1953**, *92*, 212-213.
3. Carver, T. R., Slichter, C. P. *Phys. Rev.* **1956**, *102*, 975-980.
4. Sattler, M., Schleucher, J., Griesinger, C. *Prog. Nucl. Mag. Res. Sp.* **1999**, *34*, 93-158.
5. Battiste, J. L., Wagner, G. *Biochemistry* **2000**, *39*, 5355-5365.
6. Prestegard, J. H., Al-Hashimi, H. M., Tolman, J. R. *Q. Rev. Biophys.* **2000**, *33*, 371-424.
7. Gardner, K. H., Kay, L. E. *Annu. Rev. Bioph. Biom.* **1998**, *27*, 357-406.
8. Bifulco, G., Dambruoso, P., Gomez-Paloma, L., Riccio, R. *Chem. Rev.* **2007**, *107*, 3744-3779.
9. Derome, A. E. *Nat. Prod. Rep.* **1989**, *6*, 111-141.
10. Exarchou, V., Krucker, M., van Beek, T. A., Vervoort, J., Gerothanassis, I. P., Albert, K. *Magn. Reson. Chem.* **2005**, *43*, 681-687.
11. Fukushi, E. *Biosci. Biotechnol., Biochem.* **2006**, *70*, 1803-1812.
12. Rizzo, V., Pinciroli, V. *J. Pharm. Biomed. Anal.* **2005**, *38*, 851-857.
13. Zuccaccia, C., Stahl, N. G., Macchioni, A., Chen, M. C., Roberts, J. A., Marks, T. J. *J. Am. Chem. Soc.* **2004**, *126*, 1448-1464.
14. Bax, A., Grzesiek, S. *Acc. Chem. Res.* **1993**, *26*, 131-138.
15. Meyer, B., Peters, T. *Angew. Chem. Int. Ed.* **2003**, *42*, 864-890.

16. Otting, G. *Prog. Nucl. Mag. Res. Sp.* **1997**, *31*, 259-285.
17. Searle, M. S. *Prog. Nucl. Mag. Res. Sp.* **1993**, *25*, 403-480.
18. Pellecchia, M., Sem, D. S., Wuthrich, K. *Nat. Rev. Drug Discovery* **2002**, *1*, 211-219.
19. Watts, A. *Nat. Rev. Drug Discovery* **2005**, *4*, 555-568.
20. Peng, J. W., Moore, J., Abdul-Manan, N. *Prog. Nucl. Mag. Res. Sp.* **2004**, *44*, 225-256.
21. Stockman, B. J., Dalvit, C. *Prog. Nucl. Mag. Res. Sp.* **2002**, *41*, 187-231.
22. Fujiwara, T., Ramamoorthy, A. *Annu. R. NMR S.* **2006**, *58*, 155-175.
23. Bhattacharya, A. *Nature* **2010**, *463*, 605-606.
24. McQuarrie, D. A., Simon, J. D., *Physical Chemistry, a Molecular Approach*. University Science Books: 1997.
25. Hore, P. J., Broadhurst, R. W. *Prog. Nucl. Mag. Res. Sp.* **1993**, *25*, 345-402.
26. Goez, M. *Annu. R. NMR S.* **2009**, *66*, 77-147.
27. Hayashi, H., *Introduction to Dynamic Spin Chemistry: Magnetic Field Effects upon Chemical and Biochemical Reactions*. World Scientific Publishing Company: 2004.
28. Kaptein, R., Dijkstra, K., Nicolay, K. *Nature* **1978**, *274*, 293-294.
29. Roth, H. D., Manion, M. L. *J. Am. Chem. Soc.* **1975**, *97*, 6886-6888.
30. Dietliker, K., Broillet, S., Heltrung, B., Rzadek, P., Rist, G., Wirz, J., Neshchadin, D., Gescheidt, G. *Helv. Chim. Acta* **2006**, *89*, 2211-2225.
31. Petrova, S. S., Kruppa, A. I., Leshina, T. V. *Chem. Phys. Lett.* **2004**, *385*, 40-44.

32. Eckert, G., Goez, M. *J. Am. Chem. Soc.* **1994**, *116*, 11999-12009.

33. Eckert, G., Goez, M. *J. Inform. Rec.* **1996**, *22*, 561-565.

34. Eckert, G., Goez, M. *J. Am. Chem. Soc.* **1999**, *121*, 2274-2280.

35. Eckert, G., Goez, M., Kunze, A., Muller, U. *J. Inform. Rec.* **1996**, *22*, 413-416.

36. Goez, M., Eckert, G. *J. Am. Chem. Soc.* **1996**, *118*, 140-154.

37. Goez, M., Eckert, G. *Phys. Chem. Chem. Phys.* **2006**, *8*, 5294-5303.

38. Goez, M., Zubarev, V., Eckert, G. *J. Am. Chem. Soc.* **1998**, *120*, 5347-5348.

39. Walker, T. G., Happer, W. *Rev. Mod. Phys.* **1997**, *69*, 629-642.

40. Navon, G., Song, Y. Q., Room, T., Appelt, S., Taylor, R. E., Pines, A. *Science* **1996**, *271*, 1848-1851.

41. Moller, H. E., Chen, X. J., Saam, B., Hagspiel, K. D., Johnson, G. A., Altes, T. A., de Lange, E. E., Kauczor, H. U. *Magn. Reson. Med.* **2002**, *47*, 1029-1051.

42. Bifone, A., Song, Y. Q., Seydoux, R., Taylor, R. E., Goodson, B. M., Pietrass, T., Budinger, T. F., Navon, G., Pines, A. *Proc. Natl. Acad. Sci. U.S.A.* **1996**, *93*, 12932-12936.

43. Albert, M. S., Cates, G. D., Driehuys, B., Happer, W., Saam, B., Springer, C. S., Wishnia, A. *Nature* **1994**, *370*, 199-201.

44. Spence, M. M., Rubin, S. M., Dimitrov, I. E., Ruiz, E. J., Wemmer, D. E., Pines, A., Yao, S. Q., Tian, F., Schultz, P. G. *Proc. Natl. Acad. Sci. U.S.A.* **2001**, *98*, 10654-10657.

45. Cherubini, A., Bifone, A. *Prog. Nucl. Mag. Res. Sp.* **2003**, *42*, 1-30.

46. Fitzgerald, R. J., Sauer, K. L., Happer, W. *Chem. Phys. Lett.* **1998**, *284*, 87-92.

47. Song, Y. Q. *Concepts Magn. Reson.* **2000**, *12*, 6-20.

48. Sozzani, P., Comotti, A., Simonutti, R., Meersmann, T., Logan, J. W., Pines, A. *Angew. Chem. Int. Ed.* **2000**, *39*, 2695-2698.

49. Room, T., Appelt, S., Seydoux, R., Hahn, E. L., Pines, A. *Phys. Rev. B* **1997**, *55*, 11604-11610.

50. Haake, M., Pines, A., Reimer, J. A., Seydoux, R. *J. Am. Chem. Soc.* **1997**, *119*, 11711-11712.

51. Xu, Y., Tang, P. *BBA-Biomemberanes* **1997**, *1323*, 154-162.

52. Dubois, L., Da Silva, P., Landon, C., Huber, J. G., Ponchet, M., Vovelle, F., Berthault, P., Desvaux, H. *J. Am. Chem. Soc.* **2004**, *126*, 15738-15746.

53. Landon, C., Berthault, P., Vovelle, F., Desvaux, H. *Protein Sci.* **2001**, *10*, 762-770.

54. Natterer, J., Bargon, J. *Prog. Nucl. Mag. Res. Sp.* **1997**, *31*, 293-315.

55. Bowers, C. R., Weitekamp, D. P. *J. Am. Chem. Soc.* **1987**, *109*, 5541-5542.

56. Eisenschmid, T. C., Kirss, R. U., Deutsch, P. P., Hommeltoft, S. I., Eisenberg, R., Bargon, J., Lawler, R. G., Balch, A. L. *J. Am. Chem. Soc.* **1987**, *109*, 8089-8091.

57. Pravica, M. G., Weitekamp, D. P. *Chem. Phys. Lett.* **1988**, *145*, 255-258.

58. Duckett, S. B., Sleigh, C. J. *Prog. Nucl. Mag. Res. Sp.* **1999**, *34*, 71-92.

59. Adams, R. W., Aguilar, J. A., Atkinson, K. D., Cowley, M. J., Elliott, P. I. P., Duckett, S. B., Green, G. G. R., Khazal, I. G., Lopez-Serrano, J., Williamson, D. C. *Science* **2009**, *323*, 1708-1711.

60. Duckett, S. B., Wood, N. J. *Coord. Chem. Rev.* **2008**, *252*, 2278-2291.

61. Bouchard, L. S., Burt, S. R., Anwar, M. S., Kovtunov, K. V., Koptyug, I. V., Pines, A. *Science* **2008**, *319*, 442-445.

62. Goldman, M., Johannesson, H. *C.R. Phys.* **2005**, *6*, 575-581.

63. Goldman, M., Johannesson, H., Axelsson, O., Karlsson, M. *C.R. Chim.* **2006**, *9*, 357-363.

64. Golman, K., Olsson, L. E., Axelsson, O., Mansson, S., Karlsson, M., Petersson, J. S. *Brit. J. Radiol.* **2003**, *76*, S118-S127.

65. Abragam, A., Goldman, M. *Rep. Prog. Phys.* **1978**, *41*, 395-467.

66. Overhauser, A. W. *Phys. Rev.* **1953**, *92*, 411-415.

67. Hofer, P., Parigi, G., Luchinat, C., Carl, P., Guthausen, G., Reese, M., Carlomagno, T., Griesinger, C., Bennati, M. *J. Am. Chem. Soc.* **2008**, *130*, 3254-3255.

68. Armstrong, B. D., Han, S. *J. Chem. Phys.* **2007**, *127*, 104508.

69. Prandolini, M. J., Denysenkov, V. P., Gafurov, M., Endeward, B., Prisner, T. F. *J. Am. Chem. Soc.* **2009**, *131*, 6090-6092.

70. Loening, N. M., Rosay, M., Weis, V., Griffin, R. G. *J. Am. Chem. Soc.* **2002**, *124*, 8808-8809.

71. Hu, K. N., Debelouchina, G. T., Smith, A. A., Griffin, R. G. *J. Chem. Phys.* **2011**, *134*.

72. Kan-Nian, H. Polarizing agents for high-frequency Dynamic Nuclear Polarization : Development and Applications. Thesis (Ph. D.), Massachusetts Institute of Technology, Dept. of Chemistry, 2006.

73. Barnes, A. B., De Paepe, G., van der Wel, P. C. A., Hu, K. N., Joo, C. G., Bajaj, V. S., Mak-Jurkauskas, M. L., Sirigiri, J. R., Herzfeld, J., Temkin, R. J., Griffin, R. G. *Appl. Magn. Reson.* **2008**, *34*, 237-263.

74. Hwang, C. F., Hill, D. A. *Phys. Rev. Lett.* **1967**, *19*, 1011-1013.

75. Hwang, C. F., Hill, D. A. *Phys. Rev. Lett.* **1967**, *18*, 110-112.

76. Wollan, D. S. *Phys. Rev. B* **1976**, *13*, 3671-3685.

77. Wind, R. A., Duijvestijn, M. J., Vanderlugt, C., Manenschijn, A., Vriend, J. *Prog. Nucl. Mag. Res. Sp.* **1985**, *17*, 33-67.

78. Farrar, C. T., Hall, D. A., Gerfen, G. J., Inati, S. J., Griffin, R. G. *J. Chem. Phys.* **2001**, *114*, 4922-4933.

79. Lumata, L., Jindal, A. K., Merritt, M. E., Malloy, C. R., Sherry, A. D., Kovacs, Z. *J. Am. Chem. Soc.* **2011**, *133*, 8673-8680.

80. Singel, D. J., Seidel, H., Kendrick, R. D., Yannoni, C. S. *J. Magn. Reson.* **1989**, *81*, 145-161.

81. Stocklein, W., Seidel, H., Singel, D., Kendrick, R. D., Yannoni, C. S. *Chem. Phys. Lett.* **1987**, *141*, 277-282.

82. Afeworki, M., Mckay, R. A., Schaefer, J. *Macromolecules* **1992**, *25*, 4084-4091.

83. Afeworki, M., Schaefer, J. *Macromolecules* **1992**, *25*, 4097-4099.

84. Afeworki, M., Vega, S., Schaefer, J. *Macromolecules* **1992**, *25*, 4100-4105.

85. Hall, D. A., Maus, D. C., Gerfen, G. J., Inati, S. J., Becerra, L. R., Dahlquist, F. W., Griffin, R. G. *Science* **1997**, *276*, 930-932.

86. Bajaj, V. S., Farrar, C. T., Hornstein, M. K., Mastovsky, I., Vieregg, J., Bryant, J., Elena, B., Kreischer, K. E., Temkin, R. J., Griffin, R. G. *J. Magn. Reson.* **2003**, *160*, 85-90.

87. Bajaj, V. S., Hornstein, M. K., Kreischer, K. E., Sirigiri, J. R., Woskov, P. P., Mak-Jurkauskas, M. L., Herzfeld, J., Temkin, R. J., Griffin, R. G. *J. Magn. Reson.* **2007**, *189*, 251-279.

88. Torrezan, A. C., Han, S. T., Mastovsky, I., Shapiro, M. A., Sirigiri, J. R., Temkin, R. J., Barnes, A. B., Griffin, R. G. *IEEE Trans. Plasma Sci.* **2010**, *38*, 1150-1159.

89. Gerfen, G. J., Becerra, L. R., Hall, D. A., Griffin, R. G., Temkin, R. J., Singel, D. J. *J. Chem. Phys.* **1995**, *102*, 9494-9497.

90. Hornstein, M. K., Bajaj, V. S., Griffin, R. G., Kreischer, K. E., Mastovsky, I., Shapiro, M. A., Sirigiri, J. R., Temkin, R. J., Woskov, P. P. *Conference Digest of the 2004 Joint 29th International Conference on Infrared and Millimeter Waves and 12th International Conference on Terahertz Electronics* **2004**, 147-148.

91. Torrezan, A. C., Shapiro, M. A., Sirigiri, J. R., Temkin, R. J., Griffin, R. G. *IEEE T. Electron Dev.* **2011**, *58*, 2777-2783.

92. Denysenkov, V. P., Prandolini, M. J., Krahn, A., Gafurov, M., Endeward, B., Prisner, T. F. *Appl. Magn. Reson.* **2008**, *34*, 289-299.

93. Woskov, P. P., Bajaj, V. S., Hornstein, M. K., Temkin, R. J., Griffin, R. G. *IEEE Trans. Microwave Theory Tech.* **2005**, *53*, 1863-1869.

94. Woskov, P. P., Hornstein, M. K., Temkin, R. J., Bajaj, V. S., Griffin, R. G., presented in part at IRMMW-THz2005: The Joint 30th International Conference on Infrared and Millimeter Waves and 13th International Conference on Terahertz Electronics, Vols 1 and 2, 2005.

95. Hu, K. N., Yu, H. H., Swager, T. M., Griffin, R. G. *J. Am. Chem. Soc.* **2004**, *126*, 10844-10845.

96. Song, C. S., Hu, K. N., Joo, C. G., Swager, T. M., Griffin, R. G. *J. Am. Chem. Soc.* **2006**, *128*, 11385-11390.

97. Hu, K. N., Song, C., Yu, H. H., Swager, T. M., Griffin, R. G. *J. Chem. Phys.* **2008**, *128*, 052302.

98. Matsuki, Y., Maly, T., Ouari, O., Karoui, H., Le Moigne, F., Rizzato, E., Lyubenova, S., Herzfeld, J., Prisner, T., Tordo, P., Griffin, R. G. *Angew. Chem. Int. Ed.* **2009**, *48*, 4996-5000.

99. Hu, K. N., Bajaj, V. S., Rosay, M., Griffin, R. G. *J. Chem. Phys.* **2007**, *126*.

100. Maly, T., Debelouchina, G. T., Bajaj, V. S., Hu, K. N., Joo, C. G., Mak-Jurkauskas, M. L., Sirigiri, J. R., van der Wel, P. C. A., Herzfeld, J., Temkin, R. J., Griffin, R. G. *J. Chem. Phys.* **2008**, *128*.

101. Rosay, M., Lansing, J. C., Haddad, K. C., Bachovchin, W. W., Herzfeld, J., Temkin, R. J., Griffin, R. G. *J. Am. Chem. Soc.* **2003**, *125*, 13626-13627.

102. Rosay, M., Zeri, A. C., Astrof, N. S., Opella, S. J., Herzfeld, J., Griffin, R. G. *J. Am. Chem. Soc.* **2001**, *123*, 1010-1011.

103. van der Wel, P. C. A., Hu, K. N., Lewandowski, J., Griffin, R. G. *J. Am. Chem. Soc.* **2006**, *128*, 10840-10846.

104. Rosay, M., Weis, V., Kreischer, K. E., Temkin, R. J., Griffin, R. G. *J. Am. Chem. Soc.* **2002**, *124*, 3214-3215.

105. Mullerwarmuth, W., Meisegresch, K. *Adv. Magn. Reson.* **1983**, *11*, 1-45.

106. Hausser, K. H., Stehlik, D., Waugh, J. S., *Dynamic Nuclear Polarization in Liquids*. Academic Press, Inc. : New York, 1968; Vol. 3.

107. Mueller-Warmuth, W., Meise-Gresch, K., Waugh, J. S., *Molecular Motions and Interactions as Studied by Dynamic Nuclear Polarization (DNP) in Free Radical Solutions*. Academic Press, Inc. : New York, 1983; Vol. 11.

108. Armstrong, B. D., Han, S. G. *J. Am. Chem. Soc.* **2009**, *131*, 4641-4647.

109. Pavlova, A., McCarney, E. R., Peterson, D. W., Dahlquist, F. W., Lew, J., Han, S. *Phys. Chem. Chem. Phys.* **2009**, *11*, 6833-6839.

110. Lingwood, M. D., Siaw, T. A., Sailasuta, N., Ross, B. D., Bhattacharya, P., Han, S. G. *J. Magn. Reson.* **2010**, *205*, 247-254.

111. Reese, M., Turke, M. T., Tkach, I., Parigi, G., Luchinat, C., Marquardsen, T., Tavernier, A., Hofer, P., Engelke, F., Griesinger, C., Bennati, M. *J. Am. Chem. Soc.* **2009**, *131*, 15086-15087.

112. Krahn, A., Lottmann, P., Marquardsen, T., Tavernier, A., Turke, M. T., Reese, M., Leonov, A., Bennati, M., Hoefer, P., Engelke, F., Griesinger, C. *Phys. Chem. Chem. Phys.* **2010**, *12*, 5830-5840.

113. Joo, C. G., Hu, K. N., Bryant, J. A., Griffin, R. G. *J. Am. Chem. Soc.* **2006**, *128*, 9428-9432.

114. Joo, C. G., Casey, A., Turner, C. J., Griffin, R. G. *J. Am. Chem. Soc.* **2009**, *131*, 12-13.

115. Ardenkjaer-Larsen, J. H., Fridlund, B., Gram, A., Hansson, G., Hansson, L., Lerche, M. H., Servin, R., Thaning, M., Golman, K. *Proc. Natl. Acad. Sci. U.S.A.* **2003**, *100*, 10158-10163.

116. McDermott, A. E., Polenova, T., *Solid State NMR Studies of Biopolymers*. John Wiley & Sons: Chichester, West Sussex, 2010.

117. Bowen, S., Hilty, C. *Phys. Chem. Chem. Phys.* **2010**, *12*, 5766-5770.

118. Golman, K., in't Zandt, R., Lerche, M., Pehrson, R., Ardenkjaer-Larsen, J. H. *Cancer Res.* **2006**, *66*, 10855-10860.

119. Day, S. E., Kettunen, M. I., Gallagher, F. A., Hu, D. E., Lerche, M., Wolber, J., Golman, K., Ardenkjaer-Larsen, J. H., Brindle, K. M. *Nat. Med.* **2007**, *13*, 1382-1387.

120. Golman, K., Ardenaer-Larsen, J. H., Petersson, J. S., Mansson, S., Leunbach, I. *Proc. Natl. Acad. Sci. U.S.A.* **2003**, *100*, 10435-10439.

121. Golman, K., in't Zandt, R., Thaning, M. *Proc. Natl. Acad. Sci. U.S.A.* **2006**, *103*, 11270-11275.

122. Mayer, D., Yen, Y. F., Tropp, J., Pfefferbaum, A., Hurd, R. E., Spielman, D. M. *Magn. Reson. Med.* **2009**, *62*, 557-564.

123. Albers, M. J., Bok, R., Chen, A. P., Cunningham, C. H., Zierhut, M. L., Zhang, V. Y., Kohler, S. J., Tropp, J., Hurd, R. E., Yen, Y. F., Nelson, S. J., Vigneron, D. B., Kurhanewicz, J. *Cancer Res.* **2008**, *68*, 8607-8615.

124. Larson, P. E. Z., Bok, R., Kerr, A. B., Lustig, M., Hu, S., Chen, A. P., Nelson, S. J., Pauly, J. M., Kurhanewicz, J., Vigneron, D. B. *Magn. Reson. Med.* **2010**, *63*, 582-591.

125. Lupo, J. M., Chen, A. P., Zierhut, M. L., Bok, R. A., Cunningham, C. H., Kurhanewicz, J., Vigneron, D. B., Nelson, S. J. *Magn. Reson. Imaging* **2010**, *28*, 153-162.

126. Zierhut, M. L., Yen, Y. F., Chen, A. P., Bok, R., Albers, M. J., Zhang, V., Tropp, J., Park, I., Vigneron, D. B., Kurhanewicz, J., Hurd, R. E., Nelson, S. J. *J. Magn. Reson.* **2010**, *202*, 85-92.

127. Gallagher, F. A., Kettunen, M. I., Day, S. E., Hu, D. E., Ardenkjaer-Larsen, J. H., in't Zandt, R., Jensen, P. R., Karlsson, M., Golman, K., Lerche, M. H., Brindle, K. M. *Nature* **2008**, *453*, 940-943.

128. Merritt, M. E., Harrison, C., Kovacs, Z., Kshirsagar, P., Malloy, C. R., Sherry, A. D. *J. Am. Chem. Soc.* **2007**, *129*, 12942-12943.

129. Jindal, A. K., Merritt, M. E., Suh, E. H., Malloy, C. R., Sherry, A. D., Kovacs, Z. *J. Am. Chem. Soc.* **2010**, *132*, 1784-1785.

130. Gabellieri, C., Reynolds, S., Lavie, A., Payne, G. S., Leach, M. O., Eykyn, T. R. *J. Am. Chem. Soc.* **2008**, *130*, 4598-4599.

131. Day, I. J., Mitchell, J. C., Snowden, M. J., Davis, A. L. *J. Magn. Reson.* **2007**, *187*, 216-224.

132. Kurdzesau, F., van den Brandt, B., Comment, A., Hautle, P., Jannin, S., van der Klink, J. J., Konter, J. A. *J. Phys. D: Appl. Phys.* **2008**, *41*.

133. Wilson, D. M., Hurd, R. E., Keshari, K., Van Criekinge, M., Chen, A. P., Nelson, S. J., Vigneron, D. B., Kurhanewicz, J. *Proc. Natl. Acad. Sci. U.S.A.* **2009**, *106*, 5503-5507.

134. Day, I. J., Mitchell, J. C., Snowden, M. J., Davis, A. L. *Appl. Magn. Reson.* **2008**, *34*, 453-460.

135. Bowen, S., Sekar, G., Hilty, C. *NMR Biomed.* **2011**, *24*, 1016-1022.

136. Ragavan, M., Chen, H. Y., Sekar, G., Hilty, C. *Anal. Chem.* **2011**, *83*, 6054-6059.

137. Frydman, L., Scherf, T., Lupulescu, A. *Proc. Natl. Acad. Sci. U.S.A.* **2002**, *99*, 15858-15862.

138. Frydman, L. *C.R. Chim.* **2006**, *9*, 336-345.

139. Frydman, L., Blazina, D. *Nat. Phys.* **2007**, *3*, 415-419.

140. Mishkovsky, M., Frydman, L. *Chemphyschem* **2008**, *9*, 2340-2348.

141. Bowen, S., Zeng, H., Hilty, C. *Anal. Chem.* **2008**, *80*, 5794-5798.

142. Bowen, S., Hilty, C. *Angew. Chem. Int. Ed.* **2008**, *47*, 5235-5237.

143. Sarkar, R., Comment, A., Vasos, P. R., Jannin, S., Gruetter, R., Bodenhausen, G., Hall, H., Kirik, D., Denisov, V. P. *J. Am. Chem. Soc.* **2009**, *131*, 16014-16015.

144. Bowen, S., Hilty, C. *Anal. Chem.* **2009**, *81*, 4543-4547.

145. Jensen, P. R., Meier, S., Ardenkjaer-Larsen, J. H., Duus, J. O., Karlsson, M., Lerche, M. H. *Chem. Commun.* **2009**, 5168-5170.

146. Day, S. E., Kettunen, M. I., Gallagher, F. A., Hu, D. E., Lerche, M., Wolber, J., Golman, K., Ardenkjaer-Larsen, J. H., Brindle, K. M. *Nat. Med.* **2007**, *13*, 1382-1387.

147. Merritt, M. E., Harrison, C., Storey, C., Jeffrey, F. M., Sherry, A. D., Malloy, C. R. *Proc. Natl. Acad. Sci. U.S.A.* **2007**, *104*, 19773-19777.

148. Gabellieri, C., Reynolds, S., Lavie, A., Payne, G. S., Leach, M. O., Eykyn, T. R. *J. Am. Chem. Soc.* **2008**, *130*, 4598-4599.

149. Zhao, L., Mulkern, R., Tseng, C. H., Williamson, D., Patz, S., Kraft, R., Walsworth, R. L., Jolesz, F. A., Albert, M. S. *J. Magn. Reson., Ser. B* **1996**, *113*, 179-183.

150. Mishkovsky, M., Frydman, L. *ChemPhysChem* **2008**, *9*, 2340-2348.

151. Bax, A., Griffey, R. H., Hawkins, B. L. *J. Magn. Reson.* **1983**, *55*, 301-315.

152. Willker, W., Leibfritz, D., Kerssebaum, R., Bermel, W. *Magn. Reson. Chem.* **1993**, *31*, 287-292.

153. Keeler, J., Neuhaus, D. *J. Magn. Reson.* **1985**, *63*, 454-472.

154. Bodenhausen, G., Kogler, H., Ernst, R. R. *J. Magn. Reson.* **1984**, *58*, 370-388.

155. Shaka, A. J., Barker, P. B., Freeman, R. *J. Magn. Reson.* **1985**, *64*, 547-552.

156. Shaka, A. J., Freeman, R. *J. Magn. Reson.* **1983**, *55*, 487-493.

157. Mandal, P. K., Majumdar, A. *Concepts Magn. Reson. A* **2004**, *20A*, 1-23.

158. Moskau, D. *Concepts Magn. Reson.* **2002**, *15*, 164-176.

159. Cavanagh, J., Fairbrother, W. J., Palmer, A. G., Skelton, N. J., *Protein NMR Spectroscopy: Principles And Practice*. Academic Press, Inc. : San Diego, 1996; p 587.

160. Ernst, R. R., Bodenhausen, G., Wokaun, A., *Principles of Nuclear Magnetic Resonance in One and Two Dimensions*. Oxford University Press: New York, 1986; p 102, 333-335.

161. Stejskal, E. O. *J. Chem. Phys.* **1965**, *43*, 3597-3603.

162. Abragam, A., *The Principles of Nuclear Magnetism*. Clarendon Press, Oxford: 1961.

163. Merritt, M. E., Harrison, C., Storey, C., Jeffrey, F. M., Sherry, A. D., Malloy, C. R. *Proc. Natl. Acad. Sci. U.S.A.* **2007**, *104*, 19773-19777.

164. Bowen, S., Hilty, C. *Angew. Chem. Int. Ed.* **2008**, *47*, 5235-5237.

165. Mieville, P., Jannin, S., Helm, L., Bodenhausen, G. *J. Am. Chem. Soc.* **2010**, *132*, 5006-5007.

166. Merritt, M. E., Harrison, C., Mander, W., Malloy, C. R., Sherry, A. D. *J. Magn. Reson.* **2007**, *189*, 280-285.

167. Burrage, M. E., Cookson, R. C., Gupte, S. S., Stevens, D. R. *J. Chem. Soc., Perkin Trans. 2* **1975**, 1325-1334.

168. Solomon, I. *Phys. Rev.* **1955**, *99*, 559-565.

169. Bowen, S., Hilty, C. *Phys. Chem. Chem. Phys.* **2010**, *12*, 5766-5770.

170. Geen, H., Freeman, R. *J. Magn. Reson.* **1991**, *93*, 93-141.

171. Gaggelli, E., Valensin, G., Kushnir, T., Navon, G. *Magn. Reson. Chem.* **1992**, *30*, 461-465.

172. Freeman, R., Hill, H. D. W., Tomlinso, B. L., Hall, L. D. *J. Chem. Phys.* **1974**, *61*, 4466-4473.

173. Liu, M., Farrant, R. D., Lindon, J. C. *Magn. Reson. Chem.* **1992**, *30*, 173-176.

174. Chen, H. Y., Lee, Y., Bowen, S., Hilty, C. *J. Magn. Reson.* **2011**, *208*, 204-209.

175. Stott, K., Keeler, J., Van, Q. N., Shaka, A. J. *J. Magn. Reson.* **1997**, *125*, 302-324.

176. Carravetta, M., Johannessen, O. G., Levitt, M. H. *Phys. Rev. Lett.* **2004**, *92*, 153003.

177. Carravetta, M., Levitt, M. H. *J. Am. Chem. Soc.* **2004**, *126*, 6228-6229.

178. Vasos, P. R., Comment, A., Sarkar, R., Ahuja, P., Jannin, S., Ansermet, J. P., Konter, J. A., Hautle, P., van den Brandt, B., Bodenhausen, G. *Proc. Natl. Acad. Sci. U.S.A.* **2009**, *106*, 18469-18473.

179. Carravetta, M., Johannessen, O. G., Levitt, M. H. *Phys. Rev. Lett.* **2004**, *92*, -.

180. Pilelo, G., Concistre, M., Carravetta, M., Levitt, M. H. *J. Magn. Reson.* **2006**, *182*, 353-357.

181. Pellecchia, M., Sem, D. S., Wüthrich, K. *Nat. Rev. Drug Discovery* **2002**, *1*, 211-219.

182. Meyer, B., Peters, T. *Angew. Chem. Int. Ed.* **2003**, *42*, 864-890.

183. Dalvit, C., Fagerness, P. E., Hadden, D. T. A., Sarver, R. W., Stockman, B. J. *J. Am. Chem. Soc.* **2003**, *125*, 7696-7703.

184. Fielding, L. *Tetrahedron* **2000**, *56*, 6151-6170.

185. Hajduk, P. J., Meadows, R. P., Fesik, S. W. *Q. Rev. Biophys.* **1999**, *32*, 211-240.

186. Lerche, M. H., Meier, S., Jensen, P. R., Baumann, H., Petersen, B. O., Karlsson, M., Duus, J. O., Ardenkjaer-Larsen, J. H. *J. Magn. Reson.* **2010**, *203*, 52-56.

187. Fielding, L. *Prog. Nucl. Magn. Reson. Sp.* **2007**, *51*, 219-242.

188. Ismail, F. M. D. *J. Fluorine Chem.* **2002**, *118*, 27-33.

189. Müller, K., Faeh, C., Diederich, F. *Science* **2007**, *317*, 1881-1886.

190. Dalvit, C. *Prog. Nucl. Mag. Res. Sp.* **2007**, *51*, 243-271.

191. Ernst, R. R., Bodenhausen, G., Wokaun, A., *Principles of Nuclear Magnetic Resonance in One and Two Dimensions* Clarendon Press: Oxford, 1990; p 610.

192. Feeney, J., Batchelor, J. G., Albrand, J. P., Roberts, G. C. K. *J. Magn. Reson.* **1979**, *33*, 519-529.

193. Hajduk, P. J., Meadows, R. P., Fesik, S. W. *Q. Rev. Biophys.* **1999**, *32*, 211-240.

194. Mayer, M., Meyer, B. *J. Am. Chem. Soc.* **2001**, *123*, 6108-6117.

195. Krishna, N. R., Jayalakshmi, V. *Prog. Nucl. Mag. Res. Sp.* **2006**, *49*, 1-25.

196. Moseley, H. N. B., Curto, E. V., Krishna, N. R. *J. Magn. Reson., Ser. B* **1995**, *108*, 243-261.

197. Moseley, H. N. B., Curto, E. V., Krishna, N. R. *J. Magn. Reson. B* **1995**, *108*, 243-261.

198. Zimmerman, J. R., Brittin, W. E. *J. Phys. Chem.* **1957**, *61*, 1328-1333.

199. Auletta, G., Fortunato, M., Parisi, G., *Quantum Mechanics*. Cambridge University Press: Cambridge, UK ; New York, 2009; p 724.

200. Sánchez-Pedregal, V. M., Reese, M., Meiler, J., Blommers, M. J. J., Griesinger, C., Carlomagno, T. *Angew. Chem. Int. Ed.* **2005**, *44*, 4172-4175.

201. Reese, M., Sánchez-Pedregal, V. M., Kubicek, K., Meiler, J., Blommers, M. J. J., Griesinger, C., Carlomagno, T. *Angew. Chem. Int. Ed.* **2007**, *46*, 1864-1868.

202. Orts, J., Tuma, J., Reese, M., Grimm, S. K., Monecke, P., Bartoschek, S., Schiffer, A., Wendt, K. U., Griesinger, C., Carlomagno, T. *Angew. Chem. Int. Ed.* **2008**, *47*, 7736-7740.

203. Orts, J., Griesinger, C., Carlomagno, T. *J. Magn. Reson.* **2009**, *200*, 64-73.

204. Bartoschek, S., Klabunde, T., Defossa, E., Dietrich, V., Stengelin, S., Griesinger, C., Carlomagno, T., Focken, I., Wendt, K. U. *Angew. Chem. Int. Ed.* **2010**, *49*, 1426-1429.

205. Ni, F. *Prog. Nucl. Mag. Res. Sp.* **1994**, *26*, 517-606.

206. Zeng, H., Lee, Y., Hilty, C. *Anal. Chem.* **2010**, *82*, 8897-8902.

APPENDIX

POLARIZATION CONDITIONS IN DISSOLUTION DNP EXPERIMENTS

Each section of the present dissertation contains detailed experimental information. Here, a summary of experimental techniques is provided for reference. DNP experiments were carried out using an Oxford HyperSense DNP polarizer and a Bruker Avance III 400 MHz NMR spectrometer (Figure V-1).

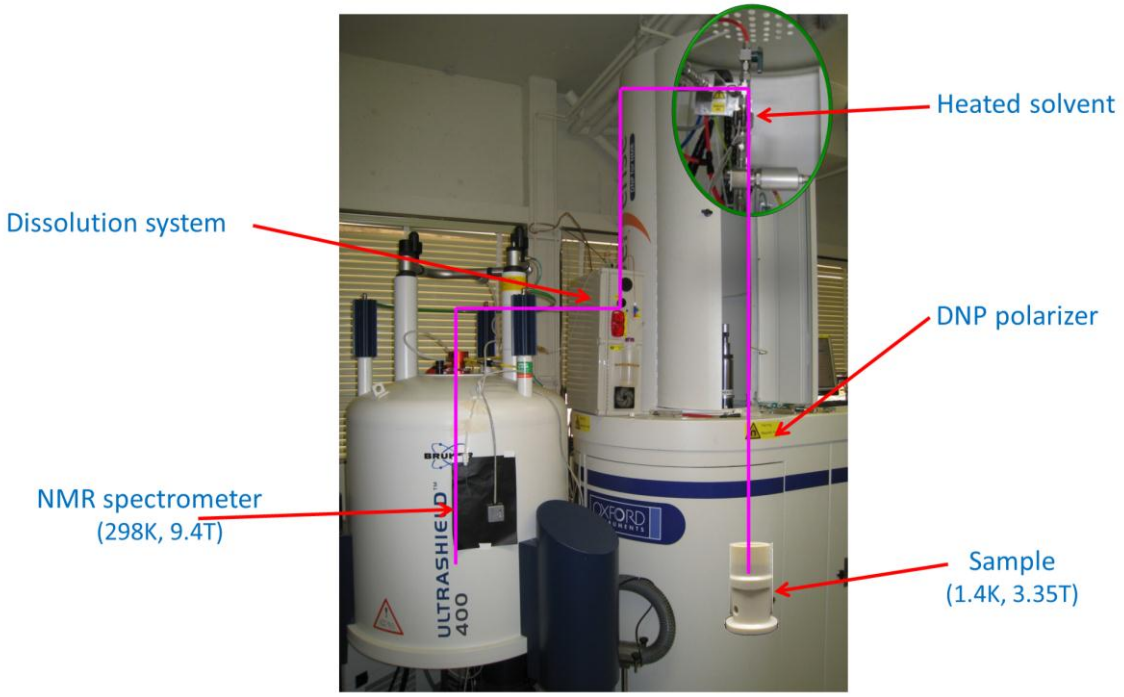

Figure V-1 : Experimental setup for dissolution DNP experiments.

In a typical dissolution DNP experiment, the sample is composed of target molecules, stable free radical and solvent. In the present thesis, the trityl radicals are used to polarize nuclei with low gyromagnetic ratio, such as ^{13}C and ^{15}N, and the

derivatives of TEMPO radicals are used to polarize high gyromagnetic ratio nuclei such as ^{1}H and ^{19}F. Another consideration in choosing free radicals is the desired solubility in the solution. For example, the OX63 radical is used in aqueous system and the α,γ-bisdiphenylene-β-phenylallyl (BDPA) is used in organic solvent system (for structures of these radicals, refer to Figure I-2).

The solvent is chosen to prevent crystallization of the sample when solidified at low temperature, to ensure homogeneous distribution of the free radical and the target molecules. Solvent for DNP polarization under aqueous conditions typically consisted of a mixture of dimethyl sulfoxide (DMSO) or ethylene glycol with water. On the other hand, organic liquids often freeze into an amorphous glass by themselves, in which case a separate solvent is not required. In other cases, an organic solvent mixture may be used.

Since the solvent also becomes hyperpolarized, it should further be chosen to avoid interference with the NMR signals of interest. In the ideal case, the solvent does not contain the type of nucleus to be observed. For example, a deuterated solvent may be used to polarize ^{1}H. It is also possible to choose solvents that do not have signals overlapping with the molecules to be studies, in which case the strong signal from the polarized solvent can be selectively suppressed during the NMR experiment. Typical sample volumes used were between 1 μL for ^{1}H samples and 20 μL for natural abundance ^{13}C samples. Due to the small volume of the aliquots for DNP polarization, a high sample concentration is desired.

For polarization, the sample is cooled to a temperature below 1.4 K, by evaporation of liquid helium. The magnetic field is 3.35 T and the corresponding ESR frequency is

~94 GHz. The optimal microwave frequency is dependent on the targeted nuclei and the free radical.

After completion of the polarization process, the sample is dissolved and transferred to the NMR spectrometer.[117] Dissolution solvent is heated to a vapor pressure of 10 bar. This heated solvent quickly thaws the polarized sample and warms it to room temperature. Since the volume of the dissolution solvent is larger than the polarized sample, the dissolution solvent is the major component of the final sample for NMR measurement. After transfer of the sample, the NMR experiment is triggered automatically. In order to obtain a narrow line width in the resulting spectra, the spectrometer is pre-shimmed using a test sample under similar conditions.

^{1}H Polarization

For aqueous systems, the polarization solvent typically was chosen to be a mixture of 80/20 (v/v) ratio of DMSO-d6 and D_2O. 15 mM of 4-Hydroxy-2,2,6,6-tetramethylpiperidine-1-oxyl (TEMPOL) free radical was added to provide the free electron center. For ^{1}H polarization, 100 mW of microwave power was applied for typically 30 min. Using this method, vanillin and benzyl-1,3-thiazol-2-amine were polarized.

For organic systems, a mixture of two organic solvents may be required for glass forming. In the polarization of 1,4-dipheneylbutadiene, a mixture of 85% tetrahydrofuran and 15% toluene was used. 15 mM of 2,2,6,6-Tetramethylpiperidine-1-oxyl (TEMPO) was added as free electron center.

^{13}C Polarization

For aqueous systems, DMSO and water mixtures were used as glass forming reagents. 15 mM tris[8-carboxy-2,2,6,6-tetramethylbenzo[1,2-d:4,5-d′]-bis(1,3)dithiol-4-yl]methyl sodium salt (Finland radical) or tris[8-carboxyl-2,2,6,6-tetra[2-(1-hydroxyethyl)]-benzo(1,2-d:4,5-d)bis(1,3)dithiole-4-yl]methyl sodium salt (OX63 radical) was used to provide free electron centers. The microwave power was 60 mW, the polarization time was usually longer than 2 h.

^{19}F Polarization

For aqueous systems, a glass forming mixture of DMSO and water was chosen. 15 mM TEMPOL was added as radical. 100 mW microwave power was applied for 40 min.

VITA

Name Haifeng Zeng

Address Department of Chemistry, Texas A&M University

Mail Stop 3255

College Station, TX 77843

Email zenghaifeng@gmail.com

Education Ph.D., Chemistry, Texas A&M University, TX, 2012

B.S., Chemistry, Peking University, Beijing, China, 2006